Tribological behavior of Cd and Al coatings on steel substrates

Priyadarshi Behera

Department of Mining and Materials Engineering

McGill University, Montreal

June 2017

A thesis submitted to McGill University in partial fulfillment of the requirements for the degree of Doctor of Philosophy

Contents

Abstract

Sacrificial Cd and Al coating on steel substrate are subjected to sliding contact in industrial and aerospace application, making it necessary to evaluate the tribological and wear properties of the coating and the substrate. Low hydrogen embrittling (LHE Cd), Ion Vapor deposited (IVD) Al and Electrodeposited Al are studied for the modification of the friction and wear on AISI 1018 steel substrate. A coating thickness of 10-25 µm is deposited on steel substrate and evaluated for change in average, instantaneous coefficient of friction and its effect on mitigating substrate wear.

Carcinogenic properties of Cd metal and cyanide plating bath used for coating faces environmental and work hazardous regulations. Al coating, which are also sacrificial to steel substrate can be a viable replacement for Cd coating. The difference in chemical structure, hardness and plating procedure between Cd and Al can lead to different tribological properties. The surface morphology of the coatings studied by SEM has more porosity present for Cd as compared to IVD and electrodeposited Al. The cross-section of the coating has more through thickness cracks present for Cd and IVD Al coating as compared to electrodeposited Al.

The steel substrate and coatings were subjected to linearly reciprocating sliding test with a steel countersphere (blind test) and a sapphire countersphere (custom built *in situ* tribometer). The instantaneous friction coefficient is recorded at a sampling rate of 800 Hz with a spatial resolution of 20 µm to generate triboscopic image, which is correlated with the morphological changes associated with the third body evolution. The relative humidity during the test was varied from dry air (RH 0) to 60% (RH 60) with an intermediate step of 30% (RH 30) at 23 °C to study the change in third body morphology. Third body evolution at the contact interface for coatings are studied by *in situ* test and correlated with the friction coefficient using triboscopy method. The change in friction coefficient with change in relative humidity is studied by statistical frequency distribution of instantaneous friction coefficient features identified from triboscopic image.

Combining different tribometry method, third body morphology change was correlated with changes in friction coefficient. The change in transfer film and wear track morphology is associated with signature change in instantaneous coefficient of friction change. Tribological evaluation of uncoated low carbon steel with a 440C steel countersphere (blind test) is evaluated

as reference study. SEM analysis of the wear track at varying relative humidity is carried out to observe the change in third body morphology. The average coefficient of friction for cold-rolled steel and grit blast steel at steady state is similar at same relative humidity. With increase in relative humidity, the average coefficient of friction decreases. The wear debris formation for both cold-rolled and grit blast steel decreases with increase in humidity. The friction coefficient of steel substrate is modified with application of Cd and Al coating. With increase in relative humidity, the number of steady state friction coefficient regimes increases for Cd coated steel. At lower humidity, the fluctuation in average coefficient of friction for IVD Al coating is observed to be more frequent, which decreases with increase in relative humidity as compared to electrodeposited Al coating. This change in average coefficient of friction is associated with difference in wear debris morphology with change in relative humidity.

The wear rate of steel substrate with and without Cd and Al coating were studied and correlated with the change in relative humidity. The presence of coating and difference in third body morphology with change in relative humidity, compared to uncoated steel modifies the wear rate of substrate. The wear rate of steel substrate decreases with increase in relative humidity. LHE Cd has a beneficial effect in reducing the wear rate of steel substrate, whereas Al coatings increases the substrate wear at low humidity.

Résumé

Le revêtement sacrificiel de Cd et Al sur un substrat en acier est soumis à un contact glissant dans une application industrielle et aérospatiale, ce qui nécessite d'évaluer les propriétés tribologiques et d'usure du revêtement et du substrat. Du Cd fragilisé par hydrogène (LHE Cd), des dépôts de vapeur d'ions d'Al (IVD) et de l'Al électrodéposé sont étudiés pour la modification du frottement et de l'usure sur le substrat en acier AISI 1018. Une épaisseur de revêtement de 10 à 25 μm est déposée sur un substrat en acier et évaluée pour modifier le coefficient de frottement moyen et instantané et son effet sur l'atténuation de l'usure du substrat.

Les propriétés cancérogènes du Cd métallique et du bain de cyanure utilisés pour le revêtement font face à des réglementations environnementales et sur le travail dangereux. Le revêtement d'Al, qui est également sacrificiel sur le substrat en acier, peut être un remplacement viable pour le revêtement de Cd. La différence dans la structure chimique, la dureté et la procédure de placage entre le Cd et l'Al peut conduire à différentes propriétés tribologiques. La morphologie de surface des revêtements, étudiés par SEM, montre plus de porosité pour le Cd que pour le dépôt de vapeur d'ions d'Al (IVD) et l'Al électrodéposé. La section transversale du revêtement montre plus de fissures d'épaisseur pour le revêtement de Cd et le dépôt de vapeur d'ions d'Al que l'Al électrodéposé.

Le substrat et les revêtements en acier ont été soumis à un test de glissement linéairement alternatif avec une contre-sphère en acier (test aveugle) et une contre-sphère de saphir (tribomètre in situ intégré sur mesure). Le coefficient de frottement instantané fut enregistré à une fréquence d'échantillonnage de 800 Hz avec une résolution spatiale de 20 μm pour générer une image triboscopique, corrélée aux changements morphologiques associés à l'évolution du troisième corps. L'humidité relative pendant le test a varié d'air sec (HR 0) à 60% (HR 60) avec une étape intermédiaire de 30% (HR 30) à 23 °C pour étudier la modification de la morphologie du troisième corps. L'évolution du troisième corps à l'interface de contact pour les revêtements fut étudiée par un test in situ et corrélée avec le coefficient de frottement selon la méthode de la triboscopie. La variation du coefficient de frottement avec variation de l'humidité relative est étudiée par la

répartition statistique des fréquences de coefficients de frottement instantanés identifiés à partir de l'image triboscopique.

En combinant différentes méthodes de tribométrie, le changement de morphologie du troisième corps était corrélé aux changements du coefficient de frottement. Le changement de la pellicule de transfert et de la morphologie de la trace d'usure est associé à un changement de signature dans le changement instantané du coefficient de frottement. L'évaluation tribologique de l'acier à faible teneur en carbone non revêtu avec une contre-sphère en acier 440C (test aveugle) est évaluée comme référence. L'analyse SEM de la piste d'usure à une humidité relative variable est effectuée pour observer la modification de la morphologie du troisième corps. Le coefficient de frottement moyen en régime permanent pour l'acier laminé à froid et l'acier sablé avec des particules est similaire à la même humidité relative. Avec une augmentation de l'humidité relative, le coefficient de friction moyen diminue. La formation de débris d'usure pour l'acier laminé à froid et l'acier sablé avec des particules diminue avec l'augmentation de l'humidité. Le coefficient de frottement du substrat en acier est modifié avec l'application du revêtement Cd et Al. Avec une augmentation de l'humidité relative, le nombre de régimes de coefficient de frottement en régime permanent augmente pour l'acier revêtu de Cd. À une humidité faible, les fluctuations du coefficient de frottement moyen pour le revêtement par dépôt de vapeur d'ions d'Al (IVD) sont fréquents, ce qui diminue avec l'augmentation de l'humidité relative comparé au revêtement Al électrodéposé. Cette variation du coefficient de frottement moyen est associée à la différence de morphologie des débris d'usure avec un changement de l'humidité relative.

Le taux d'usure du substrat avec et sans revêtement Cd et Al a été étudié et corrélé avec la variation de l'humidité relative. La présence de revêtement et la différence dans la morphologie du troisième corps avec variation de l'humidité relative, par rapport à l'acier non revêtu, modifie le taux d'usure du substrat. Le taux d'usure du substrat en acier diminue avec l'augmentation de l'humidité relative. Le Cd fragilisé par hydrogène (LHE Cd) a un effet bénéfique pour réduire le taux d'usure du substrat en acier, tandis que les revêtements d'Al augmentent l'usure du substrat à faible humidité.

Acknowledgements

This work was completed with the support and guidance of many people for which I am deeply grateful. Firstly, I would like to thank my research supervisor Prof. Richard R. Chromik for his help, support, insightful research discussion and providing me the opportunity to study at McGill University. I also thank my co-supervisor Prof. Stephen Yue for his guidance and feedback.

I would also like to thank Salim Brahimi for swiftly managing the research program, arranging constant update and feedback from the industrial sponsors and also with his feedback from an industrial point of view. Special thanks to Ranjan Roy for helping me with FTIR characterization. I would also like to thank our department staff especially Ms. Barbara Hanley who helped with any problems or questions during my work.

Special thanks to my vibrant SECTL research and hot deformation lab group members for their support to shape this project. The technical support at McGill university is one of the best staff who helped me with their prompt and swift work to support my research.

I would like to thank my funding agencies without which the project would not have been possible. I would first like to acknowledge McGill Engineering Doctoral Award (MEDA) and other named fellowship to support my studies. Further acknowledgement is due to Natural Sciences and Engineering Research Council (NSERC) and other industrial sponsors i.e, Boeing, Pratt and Whitney Canada, Canadian Fastener Institute, Heroux Devtek Canada and Safran for providing samples and research fund.

Last but not the least I would like to thank my family for their constant moral support and motivation they provided during my research work. Special thanks to my friends at Montreal including Sriraman, Aroba, Lisa, Yinyin, Sima, Vamsi, Akash, Sourav, Riya, Saikat, Bikram, Amrita, Tuhin, Pratik, Aditi; it would not have been possible to finish this memorable journey without you guys.

Preface and Contribution of Authors

This thesis work consists of research done over a timeframe of September 2012 to May 2017, during which the author was a PhD candidate under the supervision of Prof. Richard R. Chromik and Prof. Stephen Yue at McGill University. The thesis is presented as a collection of manuscripts, aside from Chapter 4 which presents a baseline study of the properties of steel substrates used in this work. Chapters 5 through 8 are all manuscript style and are published (Ch. 5) or to be submitted (Chs. 6 – 8) in a peer reviewed journal. The detailed contribution of each co-author is listed below.

- **Chapter 4**: Tribological behaviour of 1018 low carbon steel at different relative humidity

  This chapter provides a reference study for substrate steel and is not intended for publication. All of the experimental work and writing of this chapter was conducted by P. Behera. R.R. Chromik supervised the research.

- **Chapter 5**: Combining *in situ* tribometry and triboscopy to understand third body behavior of a Cd coating, *Surf. Topogr. Metrol. Prop.*, vol. 5, no. 1, p. 14001, 2017.

  P. Behera performed the *in situ* and blind sliding test, writing the manuscript including analysis. K. R. Sriraman helped in designing the experiment and editing the manuscript. R.R. Chromik and S. Yue edited the manuscript and supervised the research.

- **Chapter 6**: Effect of relative humidity on third bodies evolution of LHE Cd coating

  P. Behera performed sliding test and writing the manuscript including analysis. L. Lee and K. R. Sriraman helped in designing the experiments and editing the manuscript. R.R. Chromik and S. Yue edited the manuscript and supervised the research.

- **Chapter 7**: Effect of relative Humidity on Tribological Behavior of IVD and Electrodeposited Al Coating

P. Behera performed the *in situ*, blind sliding test and writing the manuscript including analysis. L. Lee and K. R. Sriraman helped in designing the experiments and editing the manuscript. R.R. Chromik and S. Yue edited the manuscript and supervised the research.

- **Chapter 8**: Influence of Cd and Al coating on wear rate modification of steel substrate

  P. Behera performed the stripe test and writing the manuscript including analysis. R.R. Chromik and S. Yue edited the manuscript and supervised the research.

Chapter 1

1. Introduction

Metallic surfaces in sliding contact are an integral part of industrial applications. Often the selection of certain materials for their bulk properties are not sufficient and require additional surface engineering to accomplish other physical and mechanical requirements. For example, application of sacrificial coatings on steel substrate can improve the corrosion resistance in addition to high specific strength of base material. In specific to aerospace application, the materials that are used should have high strength in a limited space, leading to sliding contact between components. Sacrificial metal coatings applied on substrate material can modify the friction coefficient and wear due to sliding.

Cd coatings are used as sacrificial coatings on steel substrate from last five decades. But due to health hazards associated with Cd metal and plating procedure, there is a need to develop and evaluate alternate coatings. Al coatings have reduction potential close to that of Cd coating, making it a leading candidate for Cd replacement. Newer methods of Al deposition like Ion Vapor Deposition (IVD) and electrodeposition in non-aqueous media are being used to replace Cd coating. Though Cd is used from a long period, the open literature available for the coatings are limited. Thus, the viability of Al coating in replacing Cd coating is studied during sliding contact at similar tribological conditions. In addition to sliding contact, the effect of relative humidity typical to aerospace application is also studied.

The use of high strength steel in fastener and landing gear with coatings [1]–[17] can modify the tribological properties of substrate material [18]–[21]. Chemically or mechanically altered layer different from the two sliding first bodies formed at the interface (defined as third bodies [22]) can significantly modify the friction and wear. Formation of third bodies at the contact interface due to application of metallic soft coatings can modify the velocity accommodation mechanism [23]. The study of these metallic third bodies and its effect on the modification of friction and wear of the substrate material can help in better understanding the dynamic nature at the contact interface.

The objective of this thesis is to understand the effect of Cd and Al coatings on modification of friction and wear of steel substrate at varying relative humidity by *in situ* and triboscopy method. The approach here is to study the tribological behavior of steel substrate at varying relative humidity as a reference material, and to compare the effectiveness of Cd and Al coating on the modification of friction and wear. The manufacturing difference between two coating process for Al will be evaluated for its difference in tribological properties and compared with friction and wear of steel substrate and Cd coating. Both Cd and Al are soft coatings as compared to the steel substrate, this lower hardness of the coating as compared to substrate material will modify the tribological behavior of the substrate. *In situ* [24]–[28] and tribosocopy [29]–[32] methods were previously used with other characterization method like on-line tribometry and electric contact resistance to understand the third body evolution at the interface, but these two techniques were never combined before to understand the change in coefficient of friction with change in third body morphology. Thus, in this work, tribosocpoy method is studied in detail and correlated with the *in situ* tribometry for changes in friction coefficient and third bodies for coatings.

Most of the thesis consists of understanding the features identified from triboscopic image with friction coefficient evolution and third body morphology at varying relative humidity. For Cd and Al coating, due to the formation of transfer film; *in situ* method is combined with triboscopic image to better understand the change in third morphology. Blind test is also done to correlate the features identified from triboscopic image with wear track morphology by SEM and surface profiling. This study helped in correlating the change in third body morphology on wear track with friction coefficient.

The last part of the thesis consists of wear rate measurement of the steel substrate, and its modification with Cd and Al coating. The wear rate of the steel substrate and the coating is measured at similar normal load to evaluate the change in substrate wear. The wear rate of the un-coated steel substrate and coatings are evaluated and compared at varying relative humidity.

1.1 Organization of thesis

The thesis work is categorised into ten chapters. This section focuses on providing an overview and outline of the thesis.

Chapter 2 consists of literature review providing a brief overview of the tribological behavior of coating and steel substrate. Third body formation and its effect on velocity accommodation mechanism. Previous work done *in situ* method and triboscopy relevant to the scope of this thesis work.

Chapter 3 briefly discusses the experimental steps followed for sample preparation, characterization equipment used. Detailed description of the custom built tribometer, parameters used to set up the experiments and no. of tests done for each experiment.

Chapter 4 consists of basic tribological studies on steel substrate, effect of grit-blasting on evolution of friction coefficient at varying relative humidity and its correlation with wear track morphology.

Chapter 5 presents a combination of analysis from *in situ* tribometry and triboscopy method for LHE Cd coating. This chapter mostly focus on detecting instantaneous coefficient of friction variation with change in third body morphology. Spectral analysis of similar features identified from the triboscopic image is done to correlate different counterspheres.

Chapter 6 consists of studying the effect of relative humidity in modifying the tribological behavior of LHE Cd coating. Triboscopic method in combination with SEM analysis of wear track and transfer film will be correlated with features identified from the triboscopic image. Spectral analysis of the features identified at different relative humidity will be compared.

Chapter 7 consists of comparing different type of Al coatings and its effect on the formation of transfer film. Correlation of transfer film morphology is done with the triboscopic image by *in situ* studies. Steel countersphere is used to study the effect of relative humidity on the tribological behavior of the two types of coating.

Chapter 8 presents measurement of wear volume and wear rate of as-received steel substrate and grit-blast steel substrate at varying relative humidity. Influence of Cd and Al coating on modification of steel substrate wear rate is studied at varying relative humidity.

Chapter 9 will summarize the work with concluding remarks and recommendations for future work.

Chapter 2

2. Literature Review

2.1 General Tribology

Tribology is a term derived from Greek using the root of the word "τριβω" and the suffix "λογια", combining to mean the study of rubbing or sliding between two bodies [33]. The general terms associated with tribology is friction and wear. Friction is the force that resists sliding of interface at the contact region when two bodies are in relative motion [34]. Most common term used in tribology is coefficient of friction (μ), generally abbreviated as CoF, which is the ratio of tangential friction force (F_t) to that of applied normal load (F_N) during sliding (see Equation 2.1)

$$\mu = \frac{F_t}{F_N} \tag{2.1}$$

Wear is the removal of material form either or both first bodies during sliding contact. The wear mechanism can be divided into different types i.e, adhesive, abrasive, fatigue, impact, chemical, fretting wear [35]. The different types of wear can occur in combination or in singularity depending on the tribological parameters such as normal load, sliding velocity, ambient atmosphere, temperature etc. The elementary way of quantifying wear can be done using Archard's law [36] (Equation 2.2), where ν is wear volume, F_N is normal load, d is sliding distance, H is surface hardness of the material that is removed and k is wear coefficient dependent on the probability of wear particle formed during asperity contact [35]

$$v = \frac{kF_N d}{H} \tag{2.2}$$

Archard law is based on shearing of the welded junction by adhesion at the contacting asperities, producing a wear particle. However, the wear particle might not be ejected out from the contact region, can be present at the sliding interface for few cycles or recirculated at the contact region. Siniawaski et al. [37] proposed a different way of quantifying abrasive wear (Equation 2.3)

$$A(n) = \frac{V(n)}{d} = A_1 n^{\beta} \tag{2.3}$$

where A(n) is the abrasion rate for n cycles, V(n) is the volume of the material removed, d is the total sliding distance, A_1 is the volume of material removed normalised by sliding distance and β is the cycle dependant abrasion rate. The value of β commonly lies between -1 to 0 for abrasion rate decreasing with time, β = -1is associated with no abrasiveness after first sliding cycle, β = 0 corresponds to constant abrasion rate and β > 0 corresponds to increase in abrasion rate with time. This method of comparing the β parameter proved to be a good study for wear between different systems. The formation of abrasive particles at the contact interface can modify the friction coefficient. This formation of abrasive particles at the contact interface can also be called as third bodies [22], accommodating the velocity difference between two sliding bodies first bodies.

2.1.1 Third Body, Velocity Accommodation and Tribological Circuit

Berthier proposed formation of third bodies at the interface, which is defined as chemically or mechanically altered layer different from the two first bodies whose main function is to transmit the load, accommodate difference in relative motion between the first bodies, separating the first bodies [22]. Berthier et al. [23] further divided the third bodies into screens and bulk, accommodating the velocity difference at five different sites i.e S_1- S_5 and four different accommodation modes i.e, elastic deformation, breaking, shearing and/or rolling as shown in Figure 2.1.

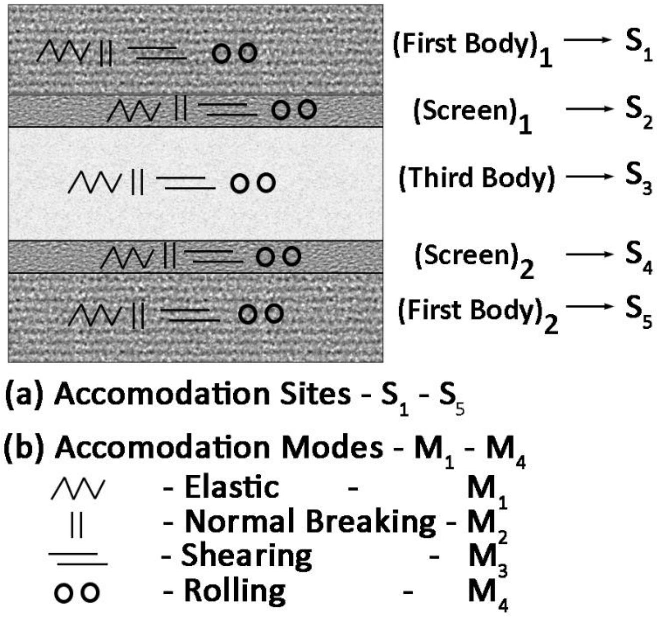

Figure 2.1 Velocity accommodation mechanism by third bodies as proposed by Berthier et al. [23]

The flow of third bodies at the contact region during sliding between first bodies can be classified into five different types, encompassing the "tribological circuit" as shown in Figure 2.2, proposed by Berthier [22]. The detachment of materials from the first bodies to form third body is called as source flow (Q_s). The movement of third bodies across the interface is called as internal flow (Q_i). Third bodies ejected out from the contact region are called ejection flow (Q_e). The ejection flow can be reintroduced into the contact region leading to recirculation flow (Q_r) or can be permanently removed from the tribological circuit, called as wear flow (Q_w).

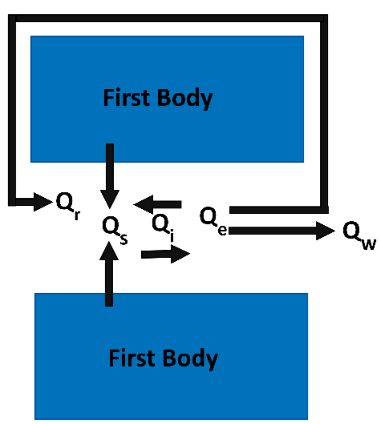

Figure 2.2 Tribological Circuit by Berthier [22]

2.2 Tribology of Coatings

The application of thin metallic coatings on bulk substrate can modify the contact mechanics at the sliding interface, altering the friction and wear properties with considerable effect from the substrate. The presence of this thin layer of coatings changes the Von Mises stresses which varies with thickness of the coating applied as shown in Figure 2.3, leading to modification of tribological behavior as studied by Sainsot et al. [38].

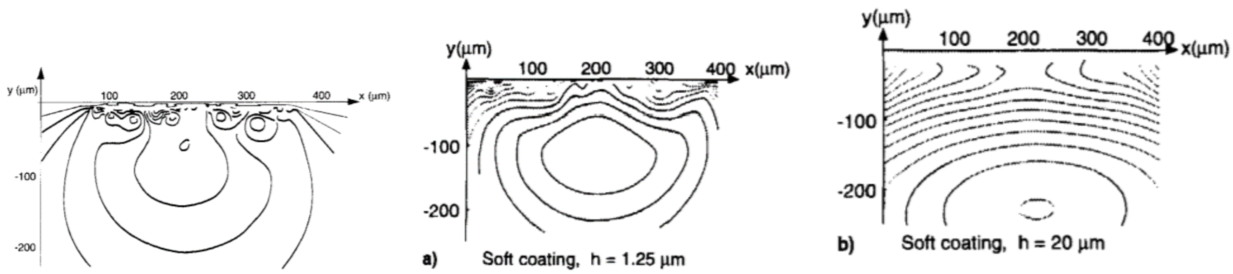

Figure 2.3 Von Mises stresses of uncoated and coated soft coatings [38]

In addition to change in pressure distribution at the interface, the presence of coating at the contact interface also modifies the velocity accommodation mechanism observed for bulk first bodies without coating (shown in Figure 2.1). In addition to 20 velocity accommodation mechanism acting at the contact interface (Figure 2.1), the application of coatings can add the velocity accommodation sites between micron thickness film formed at the top of the interface, interface between substrate and coating and within the coating (shown as point 4, 5 and 6 in Figure 2.4 (b)). The increase in number of sites subsequently affects the friction coefficient and wear, making the velocity accommodation mechanism more complex [23], [39]. The shear strength, fracture toughness of the coating has an considerable effect in velocity accommodation mechanism in sites 3,4 and 5 (shown in Figure 2.4 (b) table). The importance of different sites and mechanism accommodating the velocity difference between the two first bodies is shown in Figure 2.4 (b) table.

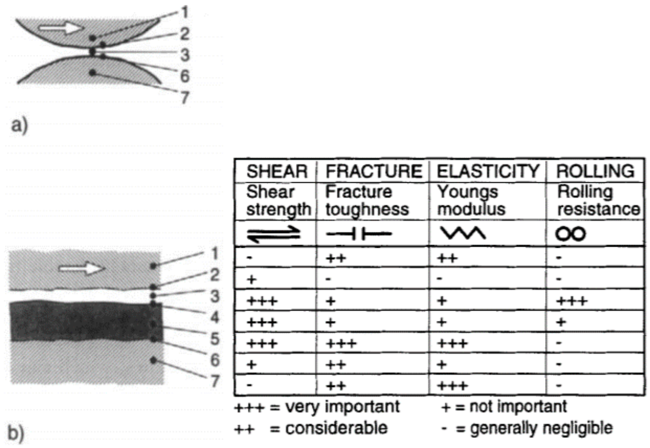

SHEAR	FRACTURE	ELASTICITY	ROLLING
Shear strength	Fracture toughness	Youngs modulus	Rolling resistance
-	++	++	-
+	-	-	-
+++	+	+	+++
+++	+	+	+
+++	+++	+++	-
+	++	+	-
-	++	+++	-

Figure 2.4 Velocity accommodation in (a) uncoated and (b) coated sliding contact and their influence on friction and wear [39]

2.3 Tribometry Methods

In this study, a pin-on-disk or ball-on-flat tribometer is used to measure the coefficient of friction and wear. This method employed for current study helped in attaining some flexibility to observe the evolution of friction coefficient by using steel countersphere and sapphire countersphere (transparent countersphere for *in situ* studies) with the same equipment.

2.3.1 Pin-on-disk Tribometry

The tribological tests done to evaluate the coefficient of friction and wear of material depends on various characteristics and parameters [40] like temperature, ambient atmosphere, sliding velocity, track length, normal load etc. The change in one of these parameters can modify the third body formation at the contact interface. The criticality in simulating a result applicable for industrial application is difficult from laboratory test, but a comparative result for different materials with the same tribometer setup can help in co-relation of tribological behavior. The American Society of Lubrication engineers (ASLE) defines 234 test rigs which is categorised into 12 types according to their geometry [40]. Pin-on-disk tribometry method is the most conventional tribometer used in laboratory scale evaluation of friction and wear but the repeatability and reproducibility of the data should be done critically considering all the parameters. The most common pin-on-disk tribometer setup are shown in Figure 2.5. Replacing the pin from the linearly reciprocating pin-on-flat with a ball will be called as ball-on flat linearly reciprocating tribometer commonly used for coatings tribological studies [41], [42].

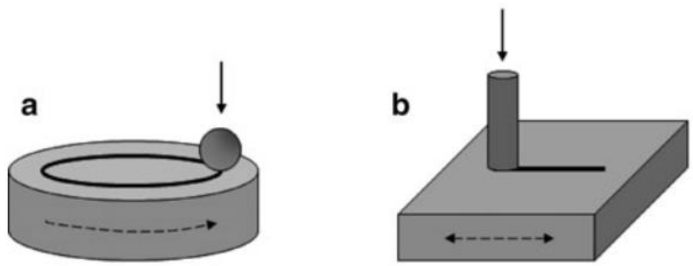

Figure 2.5 Common pin-on-disk tribometer configurations (a) rotating ball-on-disk, (b) linearly reciprocating pin-on-flat [43]

2.3.1.1 Hertzian Stress for ball-on-disk tribometer

Hertzian theory [44] is used to calculate the pressure and radius of the contact area when two smooth and non-conforming elastic half spheres are in contact. Using Hertzian theory, stress at the contact region can be calculated to apply appropriate normal load before the start of the test. The contact radius (a) between sphere and a plane in contact is shown in Equation 2.5

$$a = \left(\frac{3F_n R}{4E_r}\right)^{1/3} \tag{2.5}$$

Where R is calculated as shown in Equation 2.6

$$\frac{1}{R} = \frac{1}{R_1} + \frac{1}{R_2} \tag{2.6}$$

R_1 – Radii of sphere 1, R_2 – Radii of sphere 2 (considering $1/R_2$ as negligible due to flat surface)

E_r is the reduced modulus calculated as shown in Equation 2.7

$$\frac{1}{E_r} = \frac{1-\nu_1^2}{E_1} + \frac{1-\nu_2^2}{E_2} \tag{2.7}$$

E_1 and E_2 are the modulus of sphere and flat

ν_1 and ν_2 are the Poisson's ratio of the sphere and flat

F_n is the normal load

R is the equivalent radius of sphere

The average Hertzian contact stress (P_{avg}) between two elastic half spheres in contact can be calculated by Equation 2.8

$$P_{avg} = \frac{F_n}{\pi a^2} \tag{2.8}$$

The maximum Hertzian contact stress (P_{max}) can be calculated from average Hertzian contact stress from Equation 2.9

$$P_{max} = \frac{3}{2}\, P_{avg} \tag{2.9}$$

Hertzian contact stress is often used as a test parameter characterizing the initial elastic contact before sliding (i.e. the initial Hertzian contact stress, IHCS). This is because sliding induces plastic deformation, wear of the two bodies in contact and the formation of third bodies. All of these processes will modify the contact conditions making the IHCS no longer a good estimate of the stress conditions during sliding.

2.3.1.2 Blind Test

Third body [22] proposed by Godet [45] was first studied via imaging at the contact surface for appearance of morphologically different particles as compared to the first body by post test analysis. The formation of third body at the interface can modify the friction coefficient evolution, making the study of third bodies essential. The formation of third bodies at the interface is mostly investigated after the tribological test is finished, this method provides a flexibility in understanding the evolution of friction coefficient by performing chemical analysis and detailed imaging (FIB, SEM, TEM) of the third bodies by separating the first bodies. Opaque counterspheres used in linearly reciprocating ball-on-disk tribometer is commonly described as "blind test" (440C steel countersphere used for this thesis work) due to concealment of interface, requiring a post-experiment morphological and chemical analysis by separating first bodies.

2.3.1.3 *In situ* Tribometry

Real time study of third body morphology at the interface can help in better understanding of dynamic nature at the sliding contact region. The study of the third body and how they relate to the coefficient of friction can be done using *in situ* tribometry method. *In situ* tribometry involves investigation of the third bodies formed at the interface by using a transparent countersphere coupled with a microscope. Typically, *in situ* method is coupled with other characterization techniques to better understand the dynamic behavior of the third bodies. Sawyer et al. [46] consolidated different methods that can be combined with *in situ* method to study third bodies as shown in Table 2-1 .

Table 2-1 Techniques and limitation that can be coupled with in situ method [46]

Technique	Measurement	Spatial Resolution	Limitations
Optical microscopy	Tribofilm formation and motion, contact size	~ 1 μm	One counterface must be optically transparent.
Interferometry (contact)	Contact separation	~ 1 μm	One counterface must be optically transparent.
Interferometry (wear track)	Wear	~ 1 μm	Index of refraction or reflectivity changes can distort results.
Raman microscopy	Composition/chemistry, film thickness	~ 1 μm	One counterface must be optically transparent.
ATR-FTIR spectroscopy	Chemical bonding	mm to cm (width of crystal)	One counterface must be IR-transparent.
TEM + EELS + AFM/ nanoindentation	Microstructural transformation, interfacial film formation composition, chemistry	0.1 nm	Interface region must be electron-transparent; vacuum environment
SEM/EDX	Surface morphology, composition	10 nm	Contact charging, contamination in low vacuum environments
SEM + FIB	Cross section of sliding surfaces w/o separation	0.1 nm	Potential beam damage from FIB sectioning
SFA + x-ray diffraction or neutron relativity	Structure	μm's	Requires synchrotron access
AFM	Friction, surface topography, contact stiffness, wear	~ 1 nm	Difficult to ascertain contact size, chemistry
AES	Composition	10 nm	Cannot probe inside contact zone
XPS	Composition, chemical state	10s of μm	Cannot probe inside contact zone
Contact resistance	Coating thickness, damage, interfacial film formation		

For evaluation of tribological behavior by *in situ* method, either of the two first bodies can be transparent. Use of transparent flat sample will significantly reduce the flexibility in using engineering materials, making selection of transparent counterface as a general choice for unlubricated metallic samples. Using a transparent countersphere for *in situ* tribometry [23], [47] (shown in Figure 2.6), third body and the environmental factors can be correlated with friction coefficient.

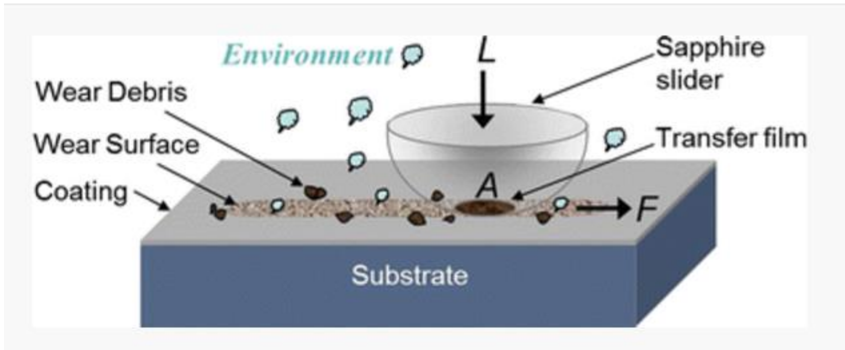

Figure 2.6 Schematic of in situ tribology using sapphire countersphere to study the evolution third bodies [24], [47]

In situ studies on metallic coatings can be utilised to understand the transfer film morphology and its effect on the friction coefficient. Shockley et al. [27] observed dynamic nature of third bodies due to plastic flow, formation and healing of holes by adhesion and scoring marks for cold sprayed Al coatings by *in situ* tribometry. Using *in situ* method, Descartes et al. [48] also observed the rheology and activated flows of third bodies at the contact interface for $MoS_{1.6}$ coatings. Dvorak et al. [49] combined the visual investigation of third bodies at the interface by combing a transparent countershphere with chemical analysis of the third bodies using Raman spectroscopy to observe formation of MoS_2 at the contact interface during sliding test of Pb-Mo-S coating. Singer et al. [50] further studied the real-time evolution (*in situ*) of third bodies with varying relative humidity for Pb-Mo-S coating showing a patchy transfer film in dry air, which changed to unstable debris transfer film with decrease in humidity and again changed to patchy transfer film with increase in humidity confirming the change in third body morphology with change in tribological parameters. There are various other studies done using *in situ* tribometry methods to evaluate third bodies and its effect on friction coefficient [24]–[26], [51], [52].

2.3.2 Triboscopy

Recording the instantaneous coefficient of friction with respect to track position instead of generating the average coefficient of friction over a cycle can provide significant information about the formation of third bodies and its circulation at the interface. Sensors which can simultaneously measure the track position and the coefficient of friction with high frequency can be used to generate spatial and temporal evolution of instantaneous coefficient of friction for creating a triboscopic map of the full test [29]. Triboscopy method proposed by Belin [29] uses a numerical imager to produce the data recorded for the full test as shown in Figure 2.7.

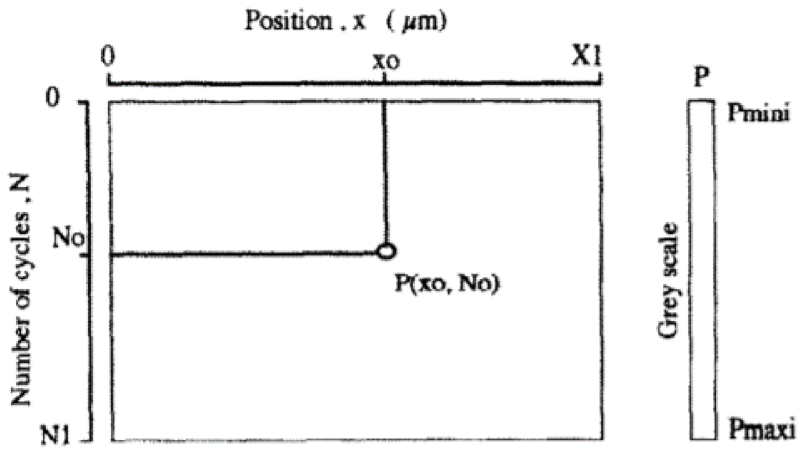

Figure 2.7 Triboscopic Image generated after the tribological test as proposed by Belin [29]

Belin et al. [30] proposed the concept of "Triboscopy" by generating a numerical image (instantaneous coefficient of friction plotted with cycle number and track position) when a sphere is rubbed against a flat specimen in reciprocating motion with a constant load, this method is coupled with electrical contact resistance to further understand the wear of the polymer coated surface as shown in Figure 2.8. The coupling of this method helped in understanding the initial ploughing of the soft coating, formation of wear debris and emergence of surface asperities at the contact region with respect to the surface roughness of the substrate. Further using this method, Belin et al. [30] studied decohesion, formation of wear debris and its recirculation with the help of triboscopic image using polyvinyl chloride deposited on Cu-Be alloy (with 4.0 µm coating of Ni and 2.5 µm coating of Au). Various other studies are also done using triboscopic method to study the evolution of third bodies combined with electrical contact resistance on polymeric coating [30][53], diamond like carbon coatings [29], antiseizure polymeric coating on grooved metallic substrate [31], duplex coatings [54], Ni-Si wafer [55] and solid lubricants [32].

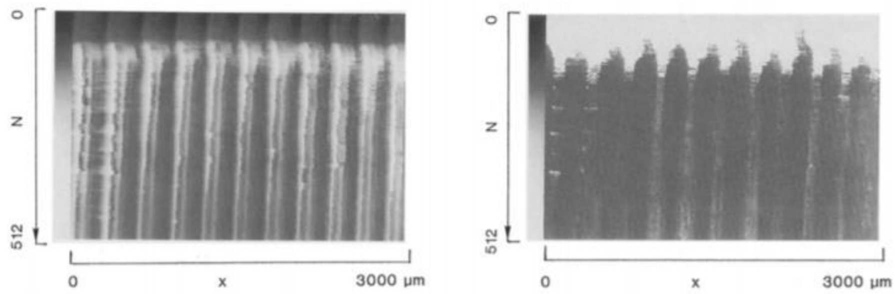

Figure 2.8 Left - Triboscopic image generated from the tangential force data with darker position as low coefficient of friction, Right - simultaneous study of electrical contact resistance with darker areas having low contact resistance [30]

Loubet et al. [56] studied the effect of topography on the tribological behavior of Cobalt coating deposited on fused silica with a commercial Si_3N_4 nano tip using triboscopy method. The peaks and valleys (denoted as H(x,N) indicating topography of the wear track with increasing track position and cycle no.) shown in Figure 2.9 with corresponding triboscopic image (denoted as T(x,N) indicating lateral force with increasing track position and cycle no.) indicates a higher tangential force at the peak positions marked as point A in the topography profile and corresponding position in the tangential force triboscopic image. These peak positions are removed with decrease in tangential force at the end of the test. The effect of ambient atmosphere is also studied using triboscopy method by Sánchez-López et al. [57], they observed the friction change of CN_x coating with transfer film formation in dry nitrogen atmosphere using triboscopy method. Fontaine et al. [58] also studied the effect of hydrogen for formation of transfer film and decrease in friction coefficient for DLC coating using triboscopy method.

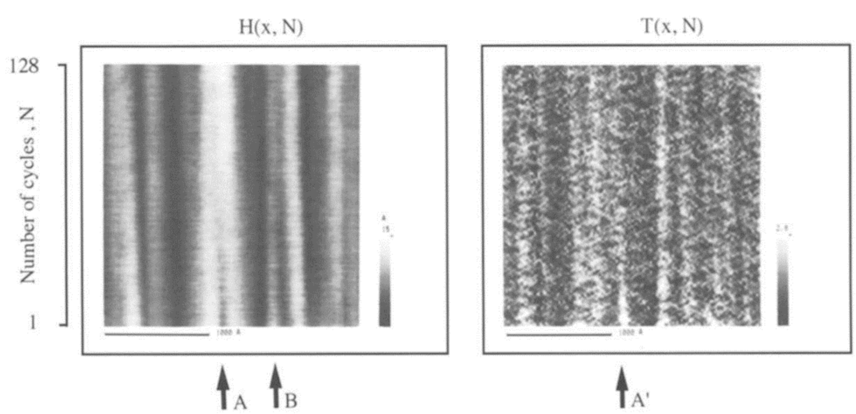

Figure 2.9 Surface topography H(x,N) and tangential force T(x,N) triboscopic image [56]

2.4 Effect of Cd and Al coating on tribological properties of steel

This section is divided into three parts; first section briefly describes the evolution of friction coefficient for steel on steel contact, followed by tribological behavior of the Cd coated steel substrate. The last section focuses on tribological behavior of bulk Al and coating.

2.4.1 Tribological Behavior of Steel

Before the coating is applied on steel substrate, the substrate material is pre-cleaned by grit blasting [59], [60]. The process of grit blasting used to increase adherence of coating modifies the surface roughness of material [61], [62]. The effect of surface roughness on the tribological behavior of mild steel-mild steel contact is studied by Elder et al. [63], shown in Figure 2.10. The stick slip phenomena arising from the surface profile of wear track leads to increase in coefficient of friction, identified from the corresponding friction plot.

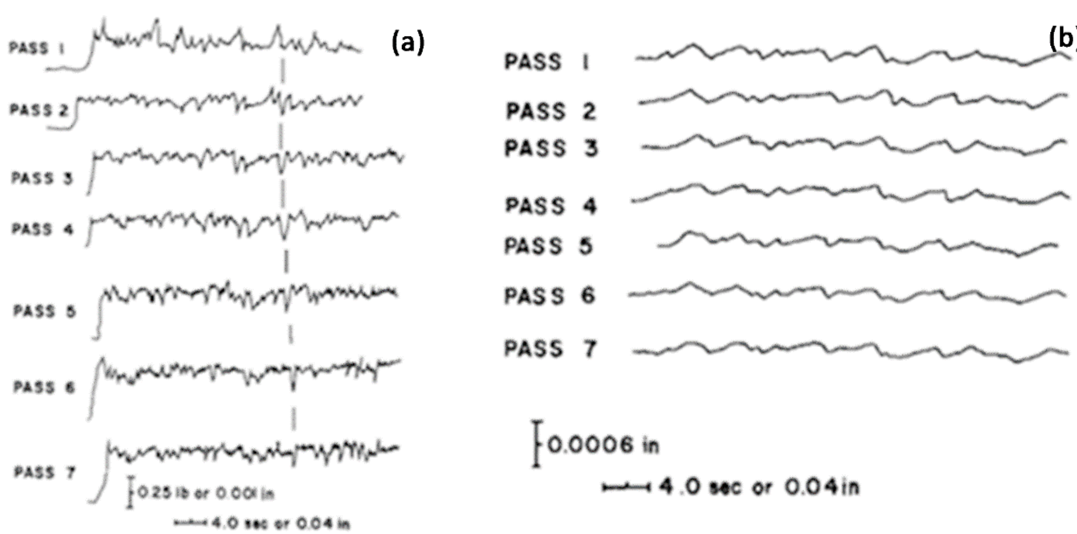

Figure 2.10 (a) Variation in friction with increase in number of passes and (b) corresponding surface profiles [63]

Detailed study of steel on steel contact by Suh et al. [64] observed different regions of evolution in average coefficient of friction with increasing sliding distance as shown in Figure 2.11.

Stage 1 and stage 2 is dependant on the plowing and adhesion of the surface asperities and each of these steps depend on the environmental factors.

The slope of stage 3 is dependent on the formation rate of wear debris and its entrapment at the surface asperities in addition to increase in adhesion due to asperity deformation. The higher the amount of wear debris present, higher will be the slope and increase in surface asperities area leading to increase in adhesion.

Stage 4 is identified by presence of constant amount of wear debris at the interface, the amount of wear debris created is equivalent to the amount of wear debris ejected out from the wear track with constant adhesive force due to asperity deformation.

The drop in average coefficient of friction shown as stage 5 in Figure 2.11 is due to sliding of a harder counterbody on a soft steel. If the counterbody has same hardness as that of the steel sample, the decrease in friction will not be present. Coefficient of friction in stage 5 is typical for cases where a hard counterbody is sliding on a relatively soft sample. In this stage the asperities of the hard counterbody is polished by the soft sample. The decrease in coefficient of friction is due to decrease in plowing and asperity deformation because of the less anchoring of the wear debris particle due to polished surface.

Stage 6 is associated with polishing of counterbody and substrate with some amount of wear debris present at pockets of wear track, this leads to steady state friction coefficient.

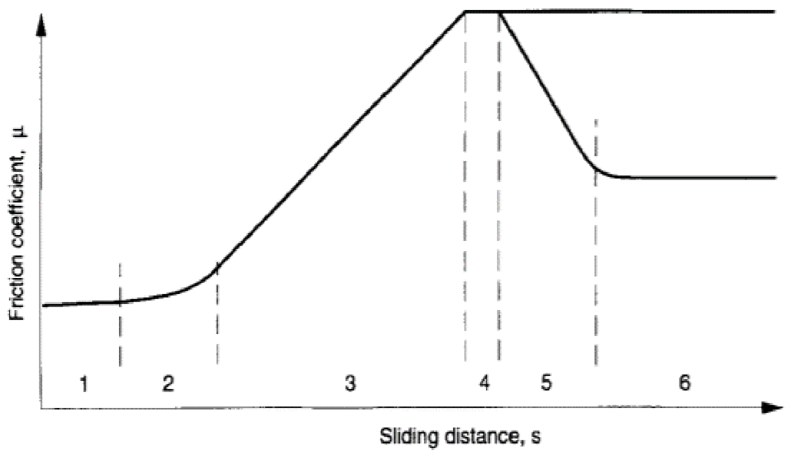

Figure 2.11 Stages of friction coefficient occurring in sliding steel contacts during sliding [64]

Suh et al. [64] also studied the effect of wear debris particle on the evolution of friction coefficient with Armco iron, the removal of wear debris at the contact region leads to a sudden decrease in the average coefficient of friction as shown in Figure 2.12. With generation of new wear debris at the contact interface, the coefficient of friction again increases to steady state value.

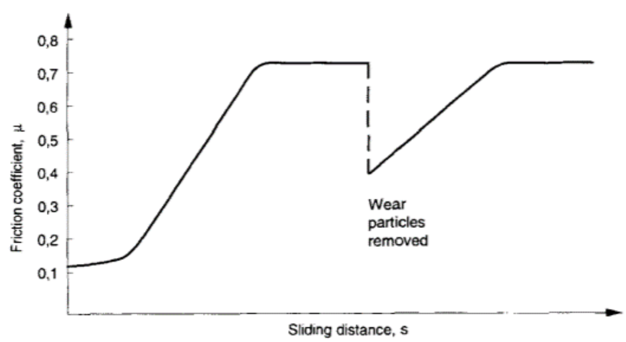

Figure 2.12 Effect of wear debris with steel on steel contact [64]

The wear mechanism that occurs during dry sliding between two bodies can change with change in tribological parameters. The wear coefficient as proposed by Archard [36] for adhesive wear can lead to severe or mild wear depending on the tribological parameters. Childs [65] used the wear coefficient to quantify the wear rate of steel on steel contact as shown in Figure 2.13. Along with adhesive wear, there are various other additional wear mechanism that can take place to change the wear rate of steel. Different mechanism of wear can lead to severe, delamination or lubricated wear for steel on steel contacts.. Klaffke [66], Mercer et al. [67] and Chowdhury at al.

[68] also observed the decrease in friction and wear with increase in relative humidity due to change in wear mechanism.

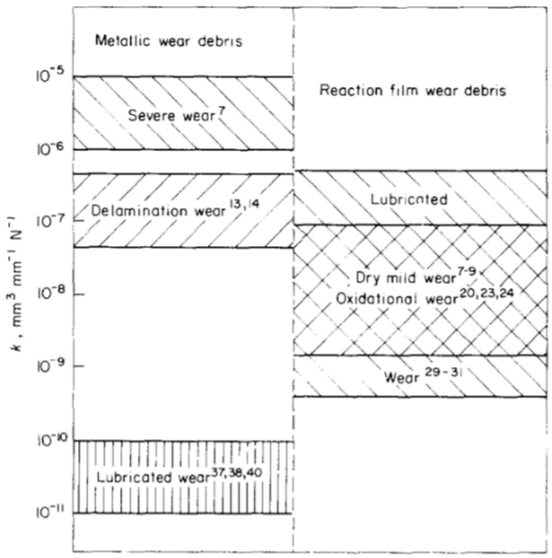

Figure 2.13 Wear Coefficient of steel on steel contact for dry and lubricated contacts [65]

2.4.2 Tribological Behavior of Cd Coating

Cd coating is applied on steel for its sacrificial corrosion protection properties. Since Cd is mostly studied for sacrificial protection, the tribological properties of the coating has limited available literature. Holmberg et al. [39] observed that the application of soft coating on hard substrate can modify the tribological properties of the substrate. Especially for Cd coating, Jahanmir et al. [69] observed a significant effect of Cd coating on the sliding wear behavior of steel substrate. The presence of 0.1 µm Cd coating on the surface modifies the friction coefficient of the coating in oxidizing and non-oxidizing environment as shown in Figure 2.14. This difference in tribological behavior of Cd coating in different atmosphere is attributed to oxidation of Cd coating in air as compared to Ar atmosphere. The wear track morphology shown in Figure 2.14 is observed to be rough for uncoated steel substrate as compared to relatively smooth surface for Cd coated steel substrate with groove marks in the sliding direction in Ar atmosphere, preventing plastic deformation and delamination wear of the steel substrate [18]. Ruggeri et al. [70] studied that the presence of soft Cd metal on the surface acts as solid lubricant, the Cd coating (with Ni and Cu coating applied underneath) at the contact interface becomes semi fluid enhancing the lubrication and decreasing the wear till the end of the testwith change in normal load and sliding speed. Thus the lubricous nature of the Cd [71] makes the coating further advantageous to be studied for its tribological behavior by third body formation. Sriraman et al. [72] studied the tribological behavior of low hydrogen embrittling (LHE) Cd coatings, which are relatively porous and soft coatings applied on high strength steel for aerospace application. *In situ* studies by Sriraman et al. [72] on electroplated Cd coatings showed extensive transfer film formation at the initial cycles, this transfer film formed at the contact region was subsequently removed and replenished with progress of test. Further increase in sliding distance led to removal of transfer film at the contact area with change of contact interface to sapphire on steel and transfer film adhering at the edges. Studies done by steel countersphere [72] with LHE Cd coating showed smoothening of wear track by extensive plastic deformation followed by delamination of the coating.

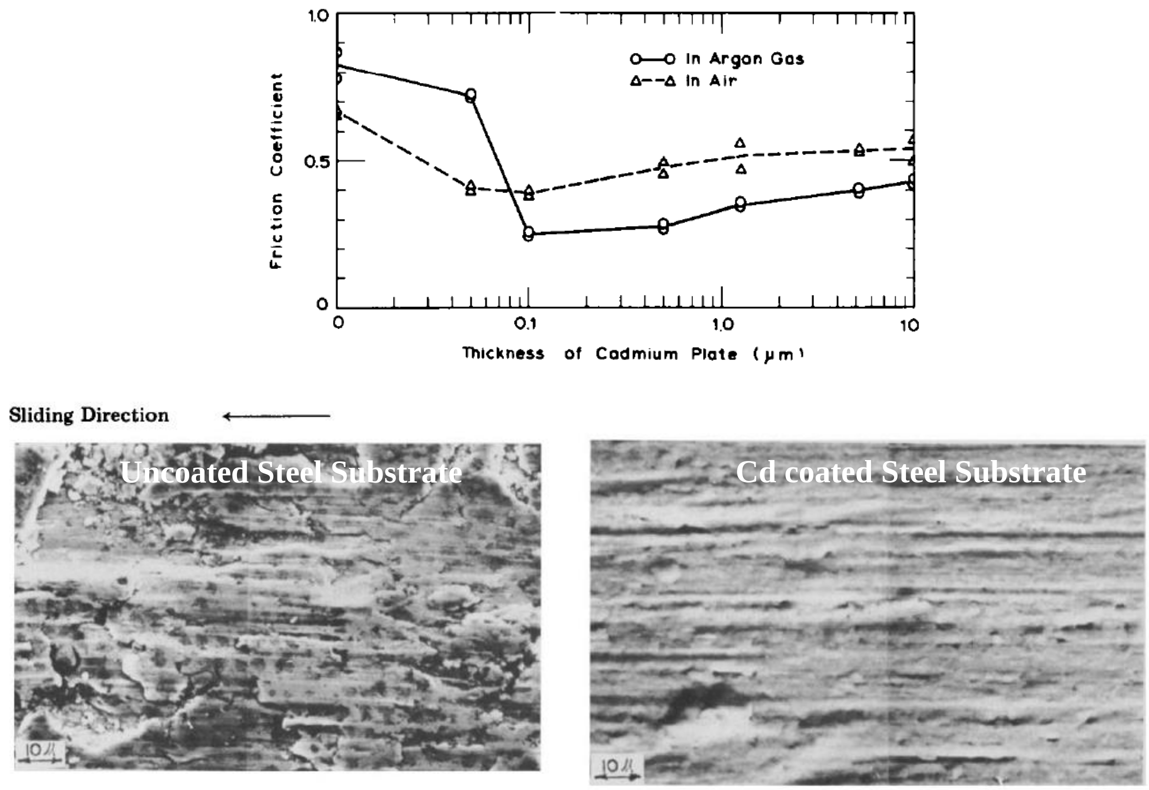

Figure 2.14 Coefficient of friction for different thickness of Cd Coating in Air and Argon atmosphere with wear track morphology of uncoated and Cd coated steel substrate after sliding test [69]

Wear rate measurements done by Jahanmir et al. [69] observed lubricous effect of Cd coating on steel substrate in different atmosphere as shown in Figure 2.15. The higher wear rate in air is due to oxidation of Cd coating as compared in Ar atmosphere. 0.1 µm Cd present on steel substrate leads to decrease in wear rate in inert atmosphere. Coatings thinner than 0.1 µm leads to wear rate comparable to that of steel substrate, where as coating with thickness higher than 0.1 µm also leads to increase in wear rate.

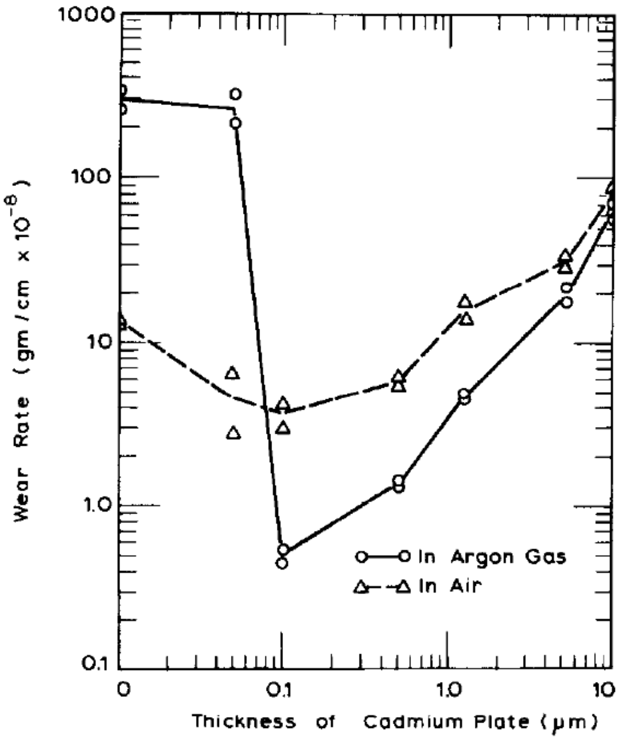

Figure 2.15 Wear rate dependence on the Cd coating thickness and atmosphere [69]

Jahanmir et al. [69] also observed oxidation of Cd coating when tested in air. The semi fluid nature and oxidation of Cd coating during sliding test can lead to change in shear strength during tribological test. With change in relative humidity, the Cd coating can also form $Cd(OH)_2$ (considering similar formation to that of Al [73]) in different percentage along with CdO leading to further change in shear strength. This change in shear strength with change in relative humidity during sliding can lead to change in third body morphology. Elder et al. [63] studied that the presence of the oxide layer (if lower shear strength) can lead to lower coefficient of friction. Also, the subsequent exposure of metallic surface (if relatively higher shear strength) at the contact interface increases the coefficient of friction according to Equation 2.10

$$\mu = \frac{s}{H} \tag{2.10}$$

Where s is the shear strength of the metal and H is the hardness of the material (considering similar hardness of oxide and subsequent metal after the oxide film is broken)

2.4.3 Tribological Behavior of Replacement Coatings (Zn-Ni and Al)

Cd, Al and Zn-Ni coating can be used as sacrificial coatings on steel substrates due to its low electronegative potential difference [3], [74]–[78] between steel substrate. The effect of morphology and Ni content on the tribological behavior of Zn-Ni coating was studied by Feng et al [19], [79] and Ghaziof et al. [80]. They observed that the bright Zn-Ni (in presence of additives) has lower coefficient of friction and wear as compared to dull Zn-Ni coating due to variation in Ni content. Studies done by Tafreshi et al. [81] at varying Ni content observed best tribological properties at 14 wt%. With change in countersphere material, Panagopoulos et al [82] observed a difference in wear wear rate due to change in wear mechanism. In situ tribological studies done on Zn-Ni coatings by Sriraman et al. [72] observed formation of transfer film at initial cycles which is frequently removed and replenished. Though Cd was selected due to its sacrificial corrosion protection properties, the improvement in tribological properties due to the lubricous nature of transfer film formation [72] added the benefits. Since Zn-Ni coating is comparatively harder than the steel substrate with limited transfer film formation [72] and requires additional baking process (to reduce hydrogen embrittlement of substrate) due to aqueous plating procedure [7], [83], Al coating is investigated for its viability as a potential replacement coating [27] due to transfer film formation [27] and non-aqueous plating process.

Aluminium is a potential coating for suitably replacing Cd coating due to its low electronegative potential difference between steel substrate as compared to Zn-Ni coating [74], [75]. Traditional deposition method with Aluminum coating in aqueous electrolyte is difficult due to excessive dissociation of water molecules forming hydrogen and oxygen before the Al can be deposited onto the substrate. One of the way to deposit Al is by melting the pure metal in vacuum [84] or electrodeposition in organic or ionic liquids [85], which minimises the effect of water vapor present in the ambient atmosphere. This different deposition method leads to difference in coating morphology [86], modifying the tribological properties. Although the processing conditions will affect the tribological properties, this section is only intended to get an overview of third body rheology affecting the friction coefficient.

Increase in roughness of wear track and grove formation with increase in normal load due to increase in adhesive wear and plastic deformation was observed by Kumar et al. [87] for pure Al. Similar studies done by Edalati et al. [88] on high pressure torsion (HPT) fine grain and coarse grain pure Al metal also observed plastic deformation and adhesion of material on the steel counterbody. The coarse grain Al microstructure has higher wear volume as compared to fine grain microstructure of Al confirming the dependency of morphology on the wear rate. The amount of adhesion on the steel counterbody was also observed to be more for coarse grain material as compared to HPT Al. Studies done by Shockley et al. [28] on cold sprayed Al coating with a pin on disk tribometer measured a change in coefficient of friction from 0.55 – 1.4 in dry atmosphere with frequent increase in coefficient of friction at intermittent intervals till the end of the test. The sudden change in the friction is attributed to stochastic nature of the transfer film formed during the tribological test. Antler et al. [89] observed prow formation with work hardening of the surface layer for Al-Al contact leading to wear of the counterbody. Other tribological studies done on pure Al metal [90] processed by severe plastic deformation method [91]–[93] observed a difference in wear rate due to morphological difference in microstructure.

In addition to the microstructural difference of bulk Al metal, the effect of tribochemical factor on the formation of oxide film influences the friction coefficient and wear during tribological studies. Lepper at al. [94] observed that tribological studies performed in vacuum and air has considerable effect on the wear track morphology. The wear track formed in vacuum were more smooth and shallow as compared to rough wear track formation in air, with higher volume loss in air as compared in vacuum. By studying the wear debris morphology, Kim et al. [73], [95] observed that the average coefficient of friction is significantly modified with change in relative humidity during sliding test. At higher relative humidity, formation of hydroxylated wear debris (studied by EDS, XPS and *ab initio* simulation methods) with finer morphology modifies the friction coefficient. Fretting wear studies done on Al alloy at varying relative humidity [96] also observed a difference in tribological studies. Endo et al. [97] observed a steady state after initial increase in tangential force due to breaking of oxide film, this steady state is attributed to absorption of water vapour by the oxidised wear particle making it softer. The wear rate of the Al alloy studied by the same author also indicates a variation in wear rate with change in humidity during the fretting test as shown in Figure 2.16.

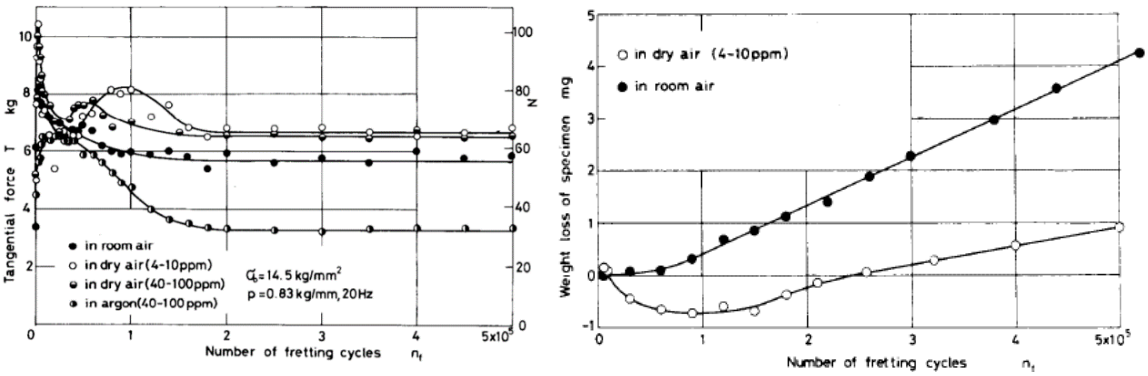

Figure 2.16 Tangential Force and Wear of Al alloy in different environment studied by fretting wear with absolute humidity written in the parenthesis [97]

2.5 Summary

Third bodies formed during the tribological test can be studied by different tribometry techniques available. By interlinking different tribometry techniques, the evolution of third bodies and its effect on the coefficient of friction can be better understood. Studies done on steel on steel contacts shows that the friction behavior and wear of the coating can vary with change in tribological parameters. The initial asperity deformation, surface profile of the wear track, formation of wear debris at the interface, counterbody hardness and relative humidity at the contact interface are few factors which can modify the friction and wear coefficient. Studies done on Cd and Al coatings showed formation of transfer film, modifying the contact interface. Although significant studies are done on coatings, direct comparison of friction coefficient and third body evolution is not fully explored and understood. The application of coatings for sacrificial protection in aerospace industries are done with 15-20 µm thickness [84], which will be removed within few sliding cycles depending on the normal load. Since the normal load, sliding distance and velocity for the test is similar, the effect of strain hardening, contact interface temperature was assumed to be similar.

The current work focuses on evaluation of aerospace coatings and its effect on the tribological behavior of steel substrate at varying relative humidity. The scope of this thesis work is to correlate the third bodies formed at varying relative humidity with friction coefficient and wear rate of the steel substrate. The three tribometry techniques briefly studied is used to interlink the evolution of friction coefficient and third bodies formed at the interface.

Chapter 3

3. Experimental Techniques

This manuscript basis thesis outline contains experimental methodology specific to the chapters, some of which are published and others are intended for publication. This chapter is intended to offer more detailed description of the techniques used apart from journal publications.

3.1 Materials

The materials studied for this thesis are commercial coatings obtained from sponsors. All the coatings are made for commercial purposes and are currently under use with limited knowledge of its viability to suitably replace LHE Cd coating. LHE Cd coating is obtained from commercial plating tanks used for landing gear components manufactured by Hèroux-Devtek. Al coatings are obtained from AAA Plating and Inspection, Inc. and Ipsen. Electrodeposited Al coatings are obtained from AlumiPlate.

3.1.1 Steel Substrate

The as-received steel (commercial steel plates from McMaster-Carr) are low carbon steel with a medium hardness (Rockwell B70) and yield strength of 373 MPa. The sheets are 1mm thick plates with oil coating on the surface to prevent corrosion during storage and transportation. The tribological test on the as-received steel was done by shearing the plates to coupons of 50 mm X 50 mm, followed by removal of oil by cleaning the surface with denatured ethyl alcohol and acetone before the start of test.

Before the plating process, the steel substrate is grit blast for mechanical cleaning and to improve adhesion of coating. The grit-blasting [59] of steel substrate was done in an industrial facility with 80-320# aluminium oxide particles prior to coating. To study the tribology of uncoated grit blast steel, the electrodeposited Al coating was removed by immersing 50 mm × 50 mm coupons in 5% KOH solution for 15 minutes. After the Al coating was completely dissolved, the uncoated grit-blasted steel substrate coupons were cleaned with denatured ethyl alcohol and acetone.

3.1.2 Low Hydrogen Embrittling (LHE) Cd Coating

The 1mm thick steel plates were hand sheared to 150 mm × 150 mm coupons followed by cleaning with abrasive grit blasting [59]. The Cd coating was done in alkaline cyanide bath solution with CdO – 20-30 g/l, NaCN – 90-135 g/l, Na_2CO_3 – 0-60 g/l and NaOH – 11-30 g/l at an industrial facility [60]. The current density for plating was 118-120 mA/cm^2 to generate an average coating thickness of 15 µm. After coating, a chromate conversion coating [98] was done to passivate the surface of coating. Tribological test was performed on sheared coupons of 50 mm × 50 mm.

3.1.3 Ion Vapor Deposited (IVD) Al Coating

The 1mm thick steel plates were hand sheared to 150 mm × 150 mm coupons followed by cleaning with abrasive grit blasting [59]. IVD Al coating [99] was done in a vacuum deposition chamber with nitrogen gas purging. The steel substrate was kept at a negative bias, Al wires were melted by resistor heating at 800-840 ℃ and evaporated to get a coating thickness of 20-25 µm on substrate. After the coating process, the coated panel was glass bead peened to close the open pores present on the surface. Finally, a chemical conversion coating [100] was done to passivate the coating. Tribological test was performed on sheared coupons of 50 mm × 50 mm.

3.1.4 Electrodeposited Al Coating

The 1mm thick steel plates are hand sheared to 150 mm × 150 mm coupons followed by cleaning with abrasive grit blasting [59]. The electrodeposition of Al coating is done in an aprotic (water free) organic plating solution using a patented process used by AlumiPlate Inc. [101]–[103]. After coating, a chemical conversion coating [100] was done to generate a passivation layer. The tribological test was performed on sheared coupons of 50 mm × 50 mm.

3.2 Load Calculation

The selection of normal load for pin-on-disk test is based on imitation to match initial maximum Hertzian contact stress to the contact stress calculated for a standard M12 × 1.75 mm fastener (Major Diameter – 12 mm and Pitch – 1.75 mm). Yakushev [104] and Birger [105] determined the fraction of load distribution on each thread of the bolt when load "P" is applied on the bolt axis (see Figure 3.1). Considering a standard high strength steel fastener of 1990 MPa tensile strength which are usually tightened upto 75% of the tensile strength, the corresponding load on the axis of bolt was determined to be 125.8 kN. Using M12 × 1.75 fastener dimension, the stress calculated on each thread is shown in Table 3-1.

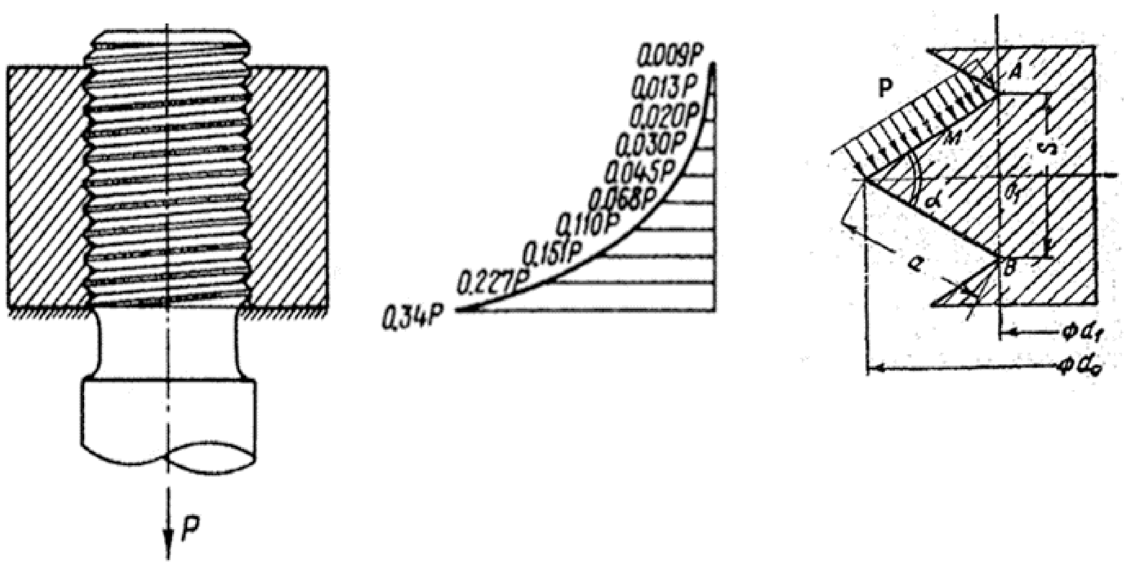

Figure 3.1 Bolt and nut assembly with load distribution on each thread [104], [105]

Table 3-1 Stress Calculation for M12X1.75 high strength steel fastener

Thread Number (from head of bolt)	**1**	**2**	**3**	**4**	**5**
Fraction of Load P	0.34	0.227	0.151	0.110	0.068
Contact Stress (MPa)	1127	752	500	364	225

3.3 Sliding Test

Sliding wear test was performed using a custom built linearly reciprocating pin-on flat disk tribometer as shown in Figure 3.2. Load was applied by using dead weights on the loading arm. The specimen stage and lens of the microscope (only required for *in situ* studies) is enclosed in a high-density polyethylene (HDPE) bag to control the relative humidity. Relative humidity (RH) was measured using Digi-sense thermohygrometer, which measures both relative humidity and temperature. Dry air was supplied into the HDPE bag by passing building air supply through a filter and desiccated column. Moist air was passed using commercially available dry air cylinder passing through a humidifier column. All the test were done within ±5% standard deviation of relative humidity at constant room temperature of 23 ˚C.

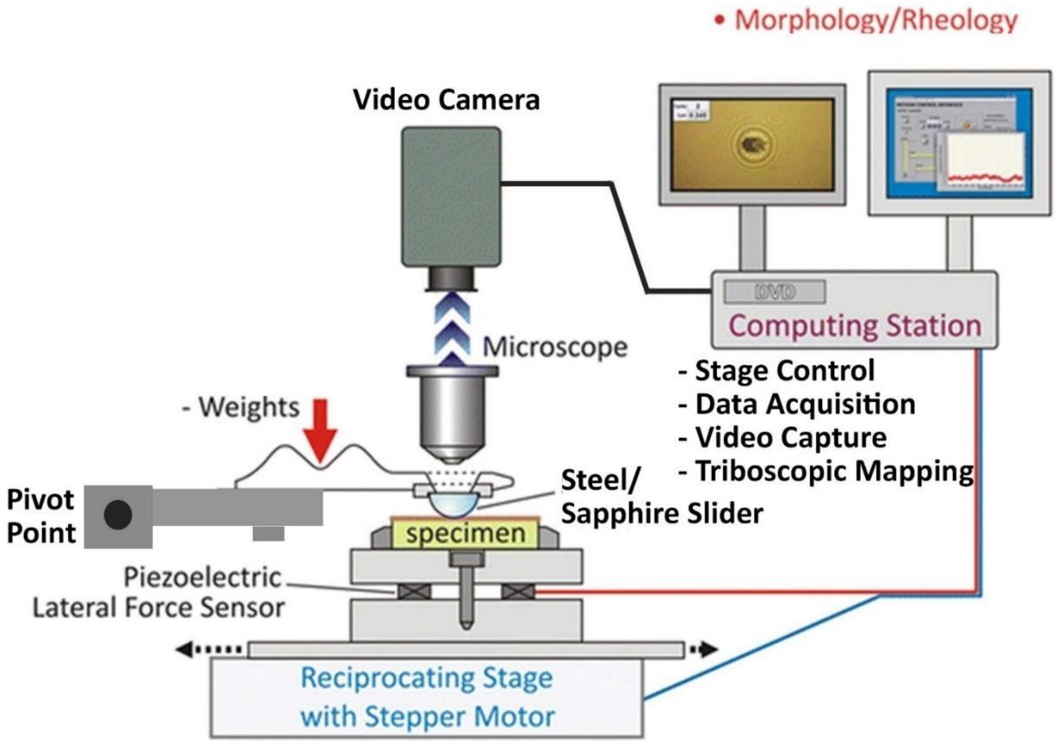

Figure 3.2 Schematic of custom built tribometer used for the study [24]

Hemispherical sapphire countersphere of 6.35 mm diameter is used for *in situ* tribometry. A video camera with a pixel resolution of 853 × 480 at 29.97 frames per second was attached to an optical microscope with 10x optical zoom. The video was recorded through the sapphire hemispherical countersphere with video camera attached on top of optical microscope. The obtained video of the test is paused at desired cycle number and track position using commercial video player to capture a snapshot. For blind test, a 6.35 mm diameter countersphere of 440C steel is used for tribological test.

The triboscopic image was generated by sampling the instantaneous coefficient of friction at 800 Hz (shown as sample rate in Figure 3.3). The sample spacing calculated for the measurement of instantaneous friction coefficient is 17.5 µm (calculated from the Sampling Rate and Sliding Velocity). During the generation of triboscopic image from software, the spatial spacing between each point of instantaneous friction coefficient is kept at 20 µm for both blind test and *in situ* test to avoid variation in plotting.

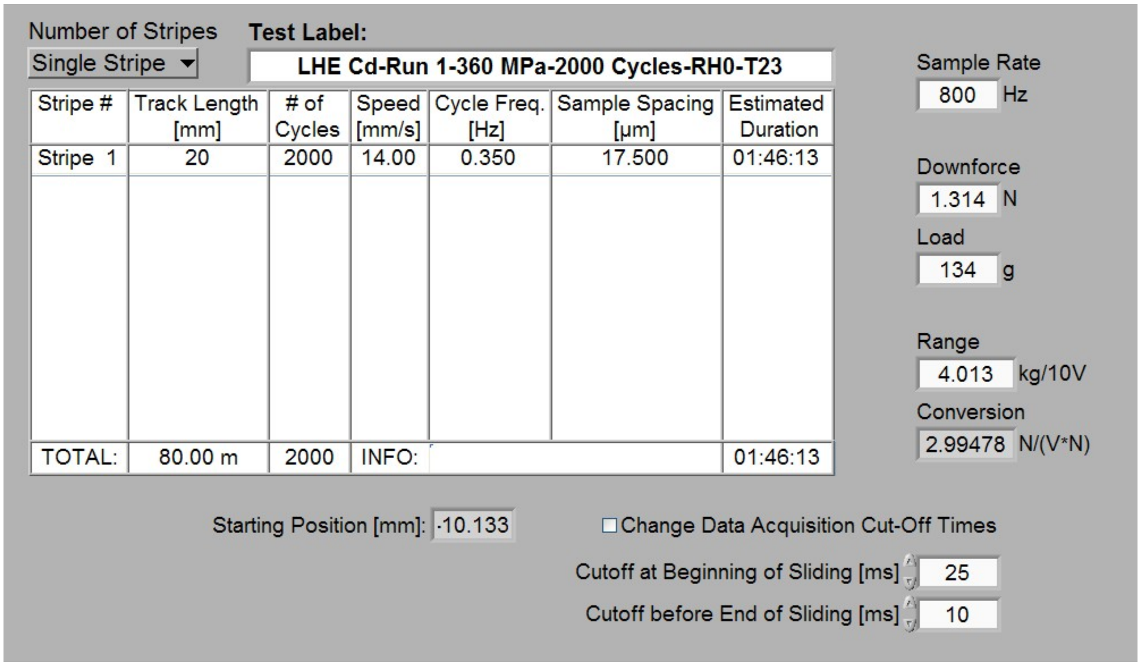

Figure 3.3 Data entry panel before the start of the tribological test

The tangential force was measured with a piezoelectric sensor at a sampling rate of 800 Hz. The coefficient of friction value was plotted as color coded map with track position and cycle number to generate what is often termed a “triboscopic image,” [30] representing the spatial and temporal evolution of the friction coefficient. The friction loop generated by measuring instantaneous tangential force in forward and backward direction is shown in Figure 3.4. The instantaneous coefficient of friction reported for current thesis work is done by removing 150 µm from either ends of the track length. The average coefficient of friction was determined by averaging the 90% of instantaneous coefficient of friction data (both forward and backward direction) from the center of the wear track measured over one sliding cycle. The change in third body morphology limited to few mm in sliding distance is measured using instantaneous coefficient of friction to observe and correlate the dynamic behavior.

The run-in and steady state average friction coefficient transition cycle no. is determined by mathematical calculation and plotting of derivative curve vs. increasing cycle number. The cycle at which the derivative value change to zero is determined as the transition cycle from run-in to steady state coefficient of friction.

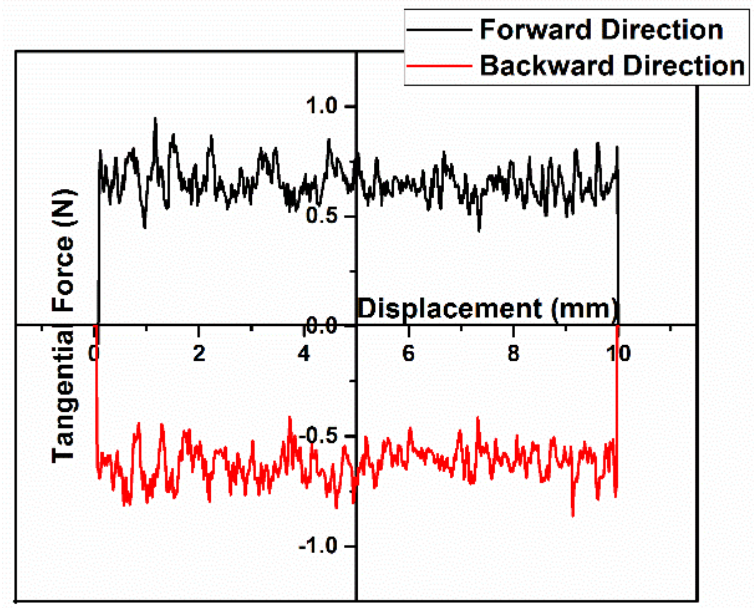

Figure 3.4 Friction Loop generated for one cycle

Contact stress of 364 MPa was calculated on fourth thread of bolt, this contact stress is used for calculation of normal load for metallic Cd coating. The material parameters used to calculate the initial maximum Hertzian Stress for current tribological studies are shown in Table 3-2. The normal load calculated from the initial maximum Hertzian stress was determined to be 1.3 N for Cd coating on the 4th thread of M12 × 1.75 fastener (determined from Table 3-1)

Table 3-2 Material Data Sheet used for this thesis study [106], [107]

Material	Modulus (GPa)	Poisson's Ratio (ν)
440C Steel	200	0.283
Sapphire	166	0.285
Low Carbon Steel	200	0.29
Cadmium	55.2	0.33
Aluminum	68	0.36

The total number of tests done for thesis work is shown in Table 3-3. The blind test is done with a 440C steel countersphere where as for *in situ* studies a sapphire hemisphere is used. For generating triboscopic image, 2000 sliding cycle was used for blind test. Total track length of 20 mm and sliding velocity of 14 mm/s was used for blind test. For measurement of wear rate of coating and the substrate, stripe test is performed. Two set of stripe test with a decrease in track length by 2 mm at 1, 5, 10, 20, 50, 100, 200, 300 cycles and 300, 500, 850, 1000, 1250, 1500, 1750, 2000 cycles are done. For each sample, three tests are done for repeatability. *In situ* test are correlated with the specific features observed from triboscopic image, requiring one test for each type. Total track length of 10 mm and sliding velocity of 3 mm/s up to 1600 cycles was used for *in situ* test.

Table 3-3 Number of test done for this thesis work

Coating / Relative Humidity	**Blind Test**			
	Cd **No. of Cycles (No. of Test)**	**IVD Al** **No. of Cycles (No. of Test)**	**Electrodeposited Al** **No. of Cycles (No. of Test)**	**As-Received/Grit-Blast Steel Substrate** **No. of Cycles (No. of Test)**
RH 60	2000 Cycles(3) Stripe Test (3)	2000 Cycles (3) Stripe Test (3)	2000 Cycles (3) Stripe Test (3)	2000 Cycles (3) Stripe Test (3)
RH 30	2000 Cycles(3) Stripe Test (3)	2000 cycles (3) Stripe Test (3)	2000 Cycles (3) Stripe Test (3)	2000 Cycles (3) Stripe Test (3)
RH 0	2000 Cycles(3) Stripe Test (3)	2000 Cycles (3) Stripe Test (3)	2000 Cycles (3) Stripe Test (3)	2000 Cycles (3) Stripe Test (3)
***In situ* Test**				
RH0	1600 cycles (1)	1600 cycles (1)	1600 cycles (1)	-

For *In situ* test, similar normal load of 88 gm was selected for both Cd and Al coating. For blind test, all the coatings and steel substrate are evaluated at 1.3 N (calculated from M12 × 1.75 fastener shown in Figure 3.1 for 4th thread using Cd coating parameters). The corresponding initial maximum Hertzian stress for both types of test is shown in Table 3-4.

Table 3-4 Calculation of Initial Maximum Hertzian Stress and Contact Radius

In situ		
Sample	Initial Maximum Hertzian Contact Stress (MPa)	Contact Radius (μm)
Cd	340	35.2
Al	380	33.0
Blind Test – Constant Load of 1.3 N		
Low Carbon Steel	670	30.1
Cd	390	40.3
Al	440	38.2

3.3.1 Spectral Analysis

For statistical analysis of the instantaneous co-efficient of friction (spectral analysis) identified from triboscopic image, discrete temporal features from each steady state regime was identified, the instantaneous coefficient measured for those cycles are used for frequency counts. Relative frequency count of instantaneous friction coefficient values associated with discrete temporal features are calculated with a bin center of 0.05.

3.4 Characterization

3.4.1 X-Ray Diffraction

X-ray diffraction of coating was done with a Bruker discover D8 diffractometer with 2D HISTAR area detector, source of Co Kα radiation (17.9 nm) at 35 kV and 45 mA and indexed from ICDD JCPDS Standards. The sheared samples are mounted on carbon tape,slit diameter of 0.8 mm for the X-ray source is used to obtain the diffraction pattern in three segments of 34.5 2θ angle. The three segments are stitched with background and smoothening corrections using EVA software available with the Bruker equipment.

3.4.2 Microscopy

The sample preparation for the cross-section assembly of the coating was done by cold mounting the sample with Technovit 4000 Copper filler. Grinding of the mount sample was done by 600, 800, 1200 and 2400 SiC grit grinding paper followed by cloth polishing with 0.9 µm and 0.3 µm alumina powder suspension in amyl alcohol. The final polishing step was done with 0.25 µm diamond paste with an extender. The coating thickness was measured using "ImageJ Analysis" software at 500x, 1000x and 2500x images obtained from Scanning electron microscope (SEM) (FEI Inspect F-50) equipped with Energy Dispersive Spectrometer (EDS). The surface morphology, wear track and transfer film after the test was also studied using SEM equipment with EDS whenever required.

3.4.3 Nanoindentation

The hardness and modulus of the coating was measured by nanoindentation method. To avoid the surface roughness and substrate effect, the polished cross-section of the coating was used to measure the hardness of coating. A Hysitron Triboindenter with three plate capacitive transducer was used to measure the force and displacement as shown in Figure 3.5. A high frequency oscillating voltage is applied on the two outer plates [108], the voltage amplitude between the center plate is referenced to determine the position between the two outer plates. The movement of the center plate towards the lower plate during indentation test changes the transducer output voltage, which is subsequently measured and converted to displacement values. Force measurement is done by application of large DC bias voltage to bottom plate, the magnitude of the voltage applied and attractive force between the bottom plate and centre plate is used to calculate the force.

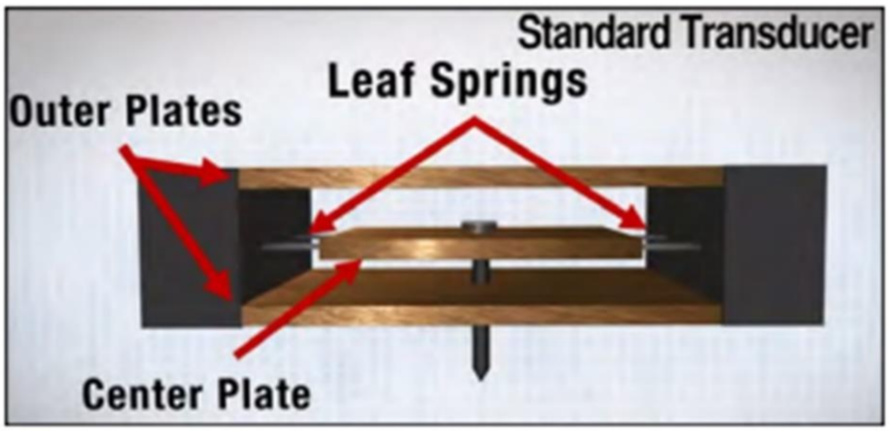

Figure 3.5 Standard transducer assembly [108]

The measurement of hardness and reduced modulus of the coating was done using a standard diamond Berkovich indenter [109] with a scheme of 5-2-5. The 5-2-5 scheme is 5 seconds loading, 2 seconds holding at peak load and 5 seconds of unloading time. The load displacement curve thus obtained was analysed by Oliver-Pharr method [110] to calculate the hardness and reduced modulus as shown in Figure 3.6.

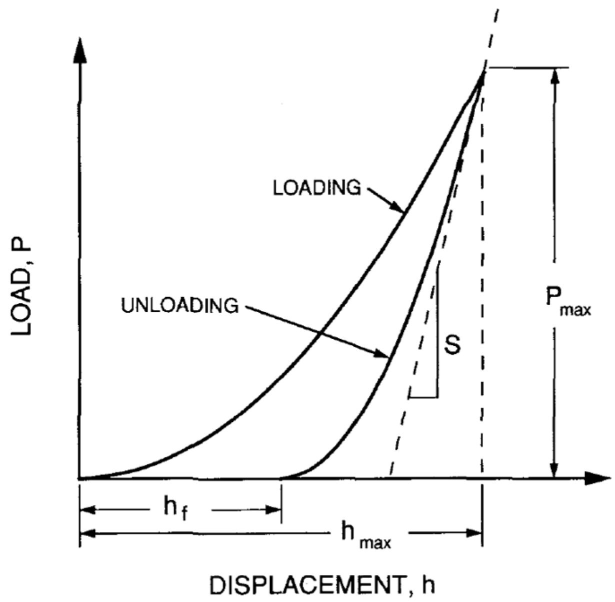

Figure 3.6 Typical load displacement curve obtained from nanoindentation method [110]

The reduced modulus was calculated from the tangent at the maximum slope of unloading curve, defined as stiffness (S) from equation 3.1

$$S = \frac{dP}{dh} = \frac{2}{\sqrt{\pi}} E_r \sqrt{A} \tag{3.1}$$

Where E_r is the reduced modulus (see Equation 2.6)

A is the projected area of elastic contact dependent on the contact depth h_c measured for Berkovich indenter [111]

$$A(h_c) = 24.5 h_c^2 + C_1 h_c^1 + C_2 h_c^{\frac{1}{2}} + C_3 h_c^{\frac{1}{4}} + \cdots \tag{3.2}$$

The contact depth h_c is calculated from the formula

$$h_c = h_{max} - 0.75 \frac{P_{max}}{S} \tag{3.3}$$

Where h_{max} is the maximum indentation depth and P_{max} is the maximum load applied

The hardness of the coating is measured by Equation 3.4

$$H = \frac{P_{max}}{A} \tag{3.4}$$

A maximum load of 5 mN was used to measure the hardness of the coating and averaged over 6 or more results.

3.4.4 Spectroscopy

The FTIR spectroscopy of LHE Cd wear track was done with Bruker Tensor 27 IR spectrometer using grazing angle ATR to characterize CdO and $Cd(OH)_2$ peaks. Raman spectroscopy was also used to characterize the change in chemical composition of steel substrate at varying relative humidity. A Renishaw Raman microscope with 524.5 nm Ar^+ laser as excitation source is used. A laser source of 2.5 mW with 50% saturation is used to avoid burning of the sample. Acquisition time of 60 seconds is used to obtain a good signal. The data thus obtained is analyzed using WiRE program to obtain peak position which was subsequently matched with data available from literature.

3.4.5 Wear Track Analysis

Two different optical profilometer were used to measure the surface profile of the wear track. Wear rate of the coating and the substrate was determined using optical surface profiler (Zygo NewView 8000). Surface features measured for chapter 6 was done using Wyko NT8000 optical interferometer.

The average surface roughness (S_a), root mean square roughness (S_q) and maximum valley depth surface roughness (S_z) was measured using ISO 25718 standard [112] available with Zygo optical profilometer.

Wear volume of coating or substrate material was determined from stripe test obtained after the tribological test. Volumetric analysis of the coating or the substrate material was measured keeping unworn coating surface as the reference plane. Using analysis software integrated with the Zygo equipment, the reference plane was raised by the coating thickness. For measurement of volume below the wear scar (shown in Figure 3.7), Mask 1 is assigned as reference plane and Mask 2 as the working plane. The net volume below the Mask 2 is calculated and normalized with length of Mask 2.

For the measurement of steel substrate wear rate, the reference plane (Mask 1) shown in Figure 3.7 is kept at same elevation as the working plane (Mask 2). The volume of wear scar was measured below Mask 2 and normalized with the length of scan.

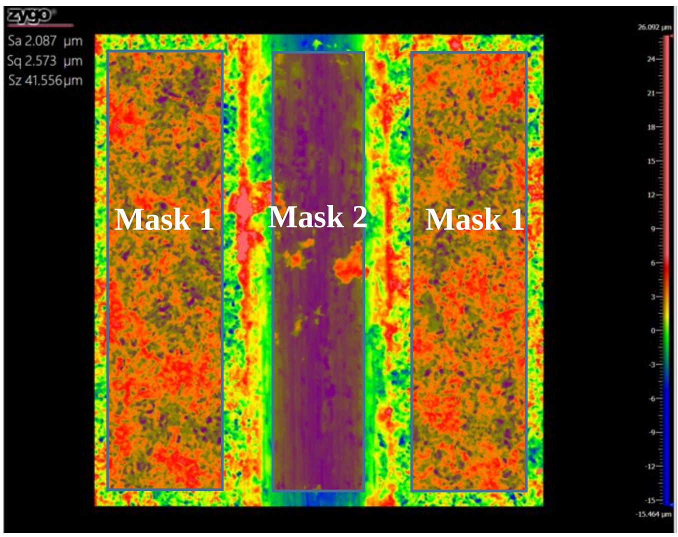

Figure 3.7 Example of masking for wear measurement

The surface features for chapter 6 was determined using Wyko NT8000 optical interferometer and open source Gwyddion v2.33 analysis software. The height profile data were exported to Gwyddion software followed by cropping of data to match similar features observed from SEM image.

Chapter 4

4. Tribological behaviour of 1018 low carbon steel at varying relative humidity

This section is a baseline study for the steel substrate on which Cd or Al coating are applied, this chapter is not intended for publication and is only studied as a reference material. Two different surface roughness of steel substrate at varying relative humidity is studied to compare the friction coefficient. Since, the surface of steel substrate is modified by grit blasting [61], [113], [114], [62] prior to coating process for better adherence of the coating and mechanical cleaning, this surface modification leads to change in surface roughness [61] which can alter the tribological properties [115], [116]. This work focuses on comparing the tribological behavior of as-received steel (without grit blasting) and grit-blasted steel at varying relative humidity.

Coupons of 50 mm × 50 mm were hand sheared from AISI 1018 steel sheets, commercially available with a thickness of 0.8 cm plates (named as "As-Received Steel" for current study). Substrate sample with grit blasting were not commercially available. To evaluate samples similar to grit blasting before the plating process, samples were prepared by dissolving the coating form post-coated test coupons. Grit blast samples were prepared by dissolving commercially available Electrodeposited Al coatings deposited on AISI 1018 steel coupons. The coated panel was sheared to 5 cm × 5 cm coupons followed by dissolution of Al coating in 5% KOH solution. The AISI 1018 steel panels thus obtained were used for tribological test as "grit-blast" sample.

Tribological test on both type of steel coupons were carried out by a linearly reciprocating 440C 1/4” diameter spherical countersphere sliding on the AISI 1018 steel coupons. Dead weight was applied on the arm to provide a constant normal load of 1.3 N, corresponding to initial maximum Hertzian stress of 670 MPa. The track length was 20 mm with sliding velocity of 14 mm/s for 2000 cycles corresponding to a total sliding distance of 80 metres. The relative humidity during the experiment was controlled by enclosing the setup in a HDPE bag with provisions to pass dry or humidified air, maintaining humidity at 0, 30 and 60% with a standard deviation of 5% at 23 °C. The wear track morphology was studied using Philips FEI Inspect F-50 instrument.

4.1 Average Coefficient of Friction

The average friction coefficient vs cycle no. for as-received steel sample and grit-blast sample at varying relative humidity for 3 runs each (averaged) is shown in Figure 4.1. The initial run-in and steady state average friction coefficient is demarcated by arrow marks for each relative humidity shown in Figure 4.1 Increase in relative humidity from RH0 to RH60 decreases the average coefficient of friction for both type of steel substrates. At RH0, the average coefficient of friction increased to 0.9 followed by a steady state CoF of 0.8 till 2000 cycles. With increase in relative humidity to RH30 and RH 60, the average CoF shows similar trend as that of RH0 but with lower steady state CoF. The steady state average CoF is 0.55 for RH30. With increase in relative humidity to 60%, the average steady state CoF is 0.45.

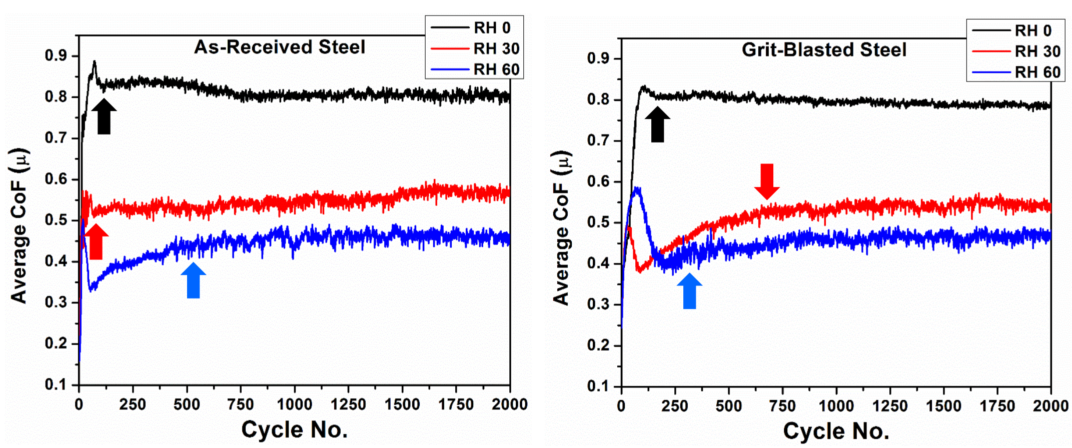

Figure 4.1 Average CoF vs Cycle no. of (a) As-received AISI 1018 steel sample (b) Grit - blasted steel indicating a decrease in coefficient of friction with increase in relative humidity

Table 4-1 shows the no. of cycles required to reach steady state for as-received and grit-blast steel substrate. At RH0, the cycles required to steady state is lower for both types of steel substrate in comparison to RH30 and RH60. For grit blast sample, the steady state is attained at later number of cycles as compared to as-received steel substrate. Suh et al. [64] observed that the transition from run in period to steady state average friction was due to constant adhesion due to asperity deformation and continuous removal and formation of abrasive particles at the sliding interface. Higher S_z of grit blast sample indicates presence of sharper peaks for grit blast sample, requiring higher cycles to attain asperity deformation at similar normal load, sliding velocity and relative humidity. The effect of grit blasting on the steel substrate is only evident for initial run-in period, the steady state average coefficient of friction is eventually similar irrespective of the surface roughness.

Table 4-1 Cycles to steady state for as-received and grit-blasted steel substrate

Relative Humidity	Cycles to Steady State	
	As-Received Steel	Grit-Blast Steel
60	286, 353, 495	288, 267, 309
30	237, 128, 104	666, 301, 198
0	87, 88, 85	116, 155, 145

4.2 Wear Track Morphology

The surface of as-received steel and grit-blast steel is shown in Figure 4.2. The features observed from as-received steel substrate are more uniform and smooth as compared to grit-blast steel. The average surface roughness (S_a) calculated from optical profilometry (shown in Table 4-2) is similar but root mean square surface roughness (S_q) measurements indicates a higher roughness for grit-blast steel. Comparison of surface roughness by measurement of maxima and minima of crest and trough (S_z) shows more surface roughness for grit-blast steel. The higher S_z measurement of grit-blast steel as compared to as-received steel indicates more probability of asperity deformation for grit-blast sample as compared to as-received sample.

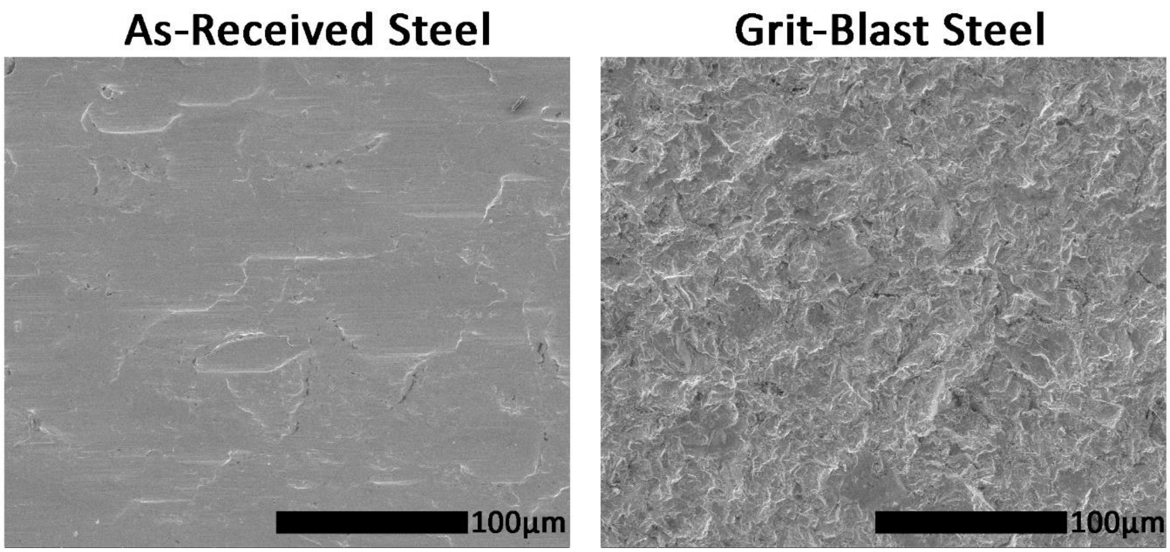

Figure 4.2 Surface Morphology of steel substrate

Table 4-2 Surface Roughness parameters for as-received steel and grit-blast steel

Sample	S_a (µm)	S_q (µm)	S_z (µm)
As-Received Steel	1.568	1.872	14.991
Grit-Blast Steel	1.919	2.429	33.627

The wear track morphology of as-received and grit-blast steel at RH0 is shown in Figure 4.3. After the first sliding cycle, initiation of asperity deformation is observed. The deformed asperity surface area observed after first cycle for as-received steel is higher as compared to grit-blast steel (deformed asperities scattered through out the surface). After 100 cycles, wear debris particles are scattered in pockets of as-received steel. Grit-blast steel at 100 cycles has less or very fine wear debris formed (as compared to as-received steel) on the wear track, along with some predominant features of asperity deformation. At 1000 cycles, extensive wear debris formation was observed for both type of steels. The difference in S_z of as-received and grit blast steel indicates a higher run-in period required for grit blast steel to attain stable asperity deformed area similar to morphology reported by Suh et al. [64].

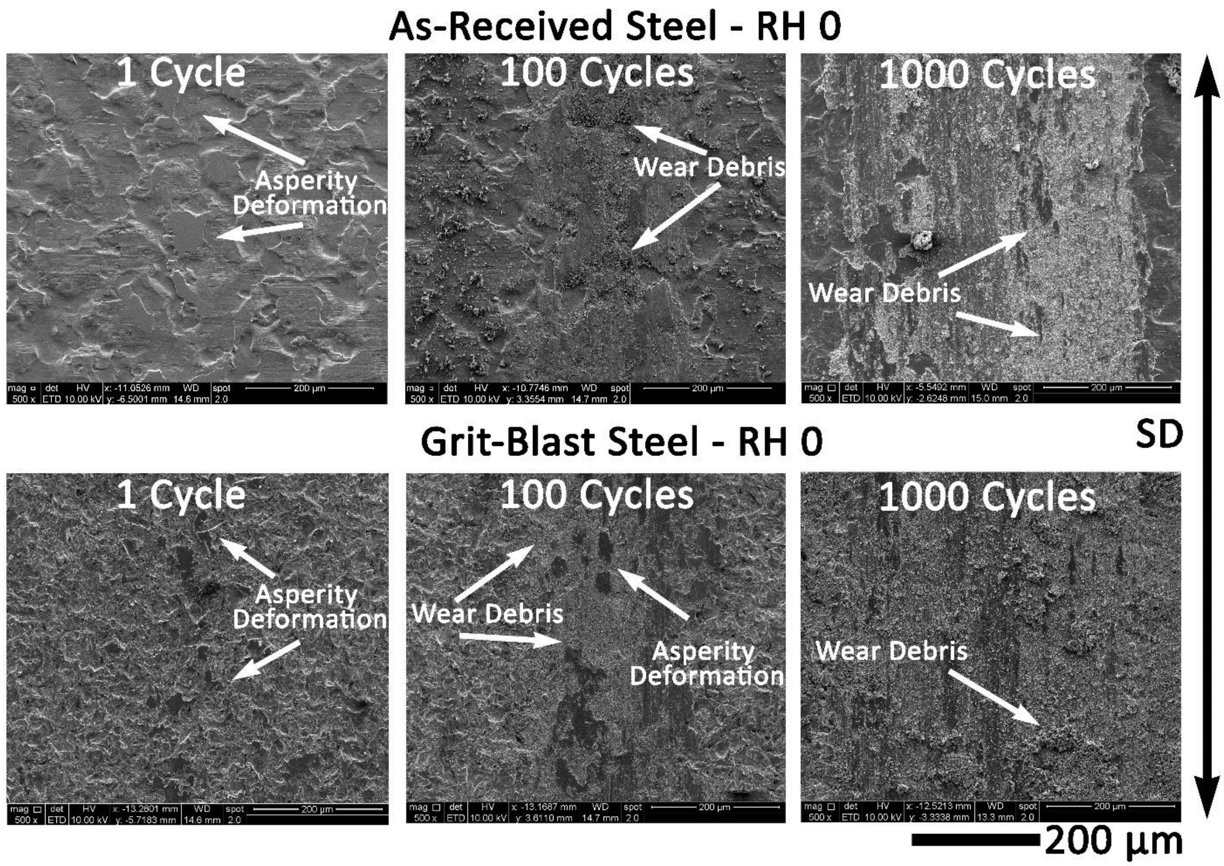

Figure 4.3 Wear track morphology of as-received and grit-blast steel at RH0

The wear track morphology after first sliding cycle for both type of steel (shown in Figure 4.4) at RH30 has asperity deformation (shown in Figure 4.3), similar to RH0. The wear track morphology observed at100 cycles for RH30 is different form RH0, the amount of wear debris observed for as-received steel at RH30 is less than at RH0. Also for grit-blast steel, the surface area of asperity deformation was observed to be more as compared at RH30. At 1000 cycles, the wear debris formed was mostly scattered on the sides of the wear track with predominant asperity deformation. The wear track is more irregular as compared at RH0 with few unworn regions present on sides of the wear track.

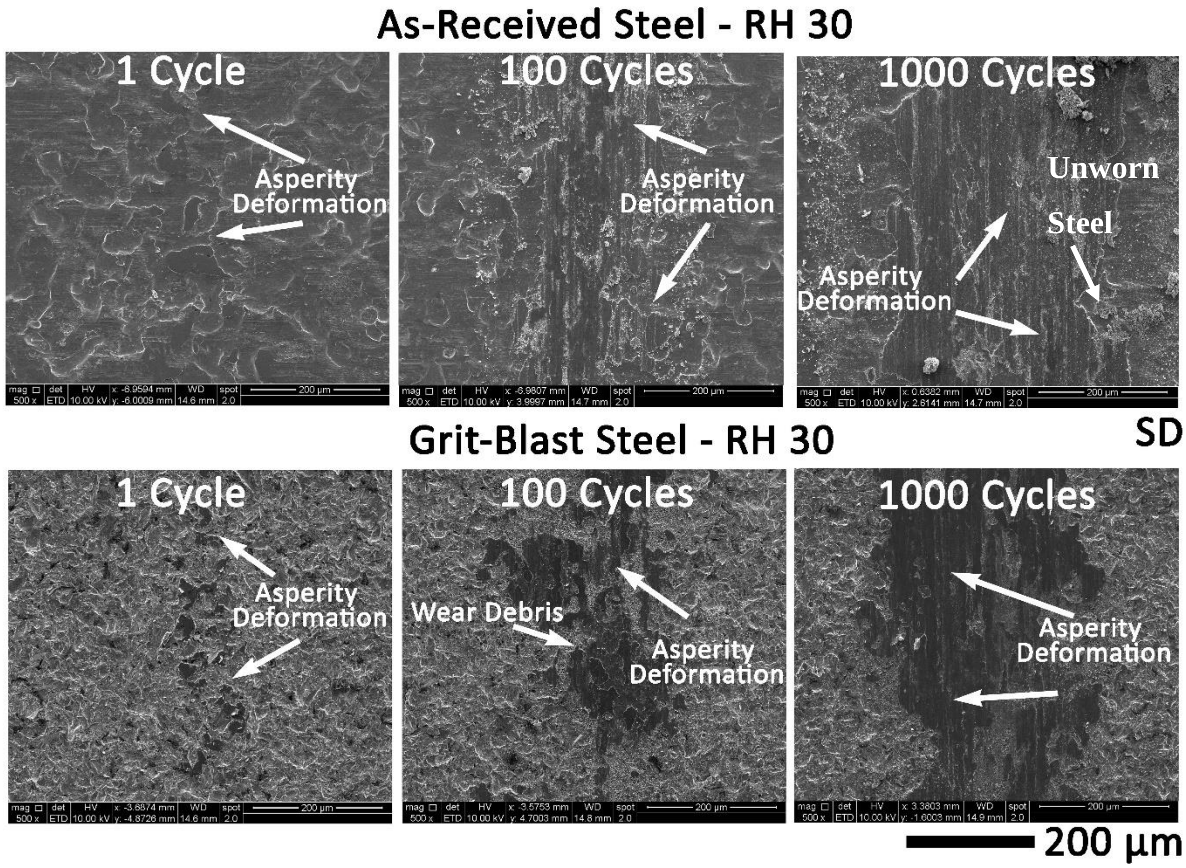

Figure 4.4 Wear track morphology of as-received and grit-blast steel at RH 30

With increase in relative humidity to RH60, the wear track morphology at first cycle is similar to RH30 and RH0 as shown in Figure 4.5. With increase in sliding cycles to 100, the wear track morphology has predominant asperity deformation with further reduction in wear debris. At 1000 cycles, scattered wear debris at the sides of wear track is observed for both type of steel, the wear track formed follows an interlinking of asperity deformation with irregular shape.

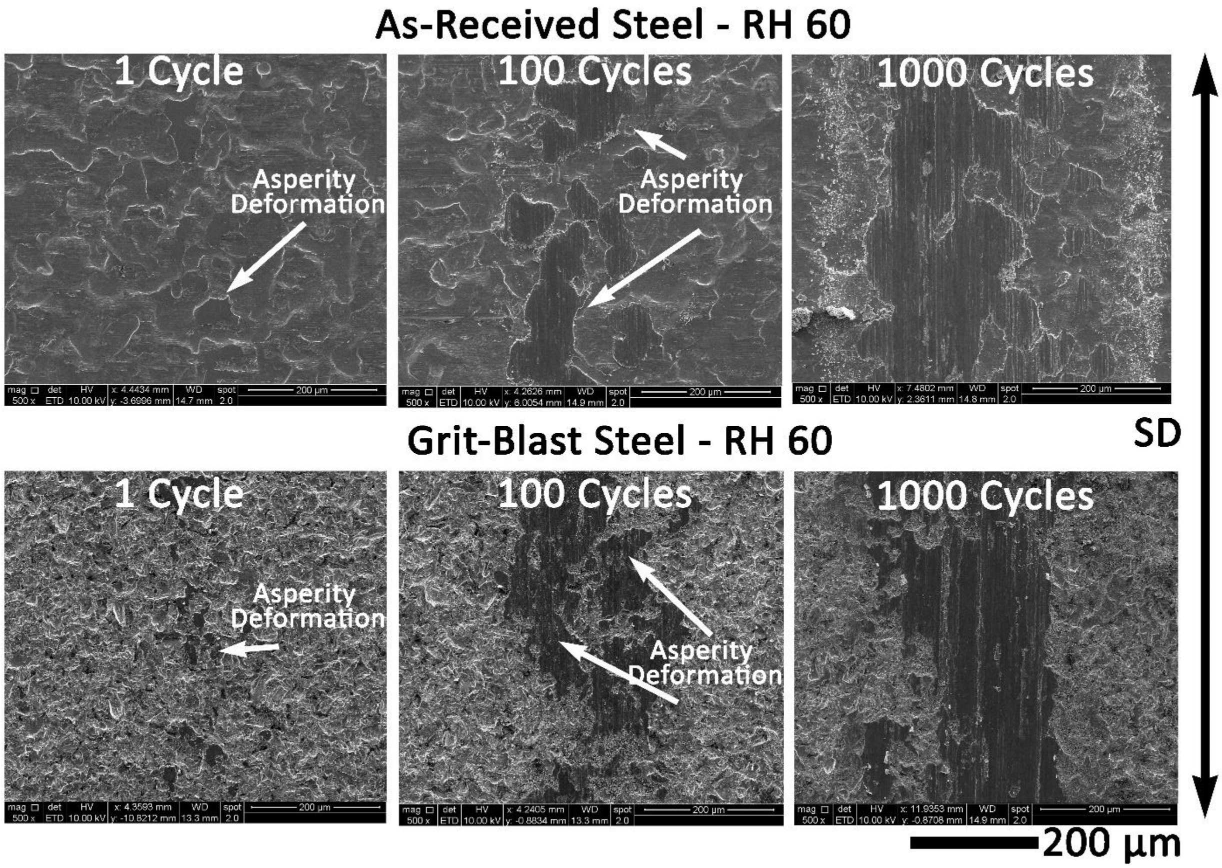

Figure 4.5 Wear track morphology of as-received and grit-blast steel at RH 60

As the relative humidity increases, the average coefficient of friction decreases. The steady state average coefficient of friction is similar for as-received and grit-blast steel. Asperity deformation and formation of wear debris due to plastic deformation at RH0 is dependant on the initial surface roughness of the substrate (initial run-in), the grit-blast sample with higher S_z requires higher number of cycles to attain steady state. With increase in relative humidity, the third body morphology at the interface changes (formation of wear debris) leading to decrease in average coefficient of friction. Initial asperity deformation as investigated from SEM image is associated with increase in average coefficient of friction. With progress of the test, there is formation of wear debris at the interface due to plastic deformation and fracture of the asperities. The formation of wear debris at the sliding interface changes the interfacial contact mechanism leading to steady state average coefficient of friction regime. Similar studies done by Suh et al. [64] for steel on steel contact also observed initial adhesion of the surface asperities followed by formation of wear debris near the surface asperities as well as increase in adhesion due to asperity deformation. The amount of wear debris formation at the contact interface and asperity deformation area changes with change in relative humidity. This change in third body formation mechanism at the contact interface with change in relative humidity modifies the friction coefficient. In addition to asperity deformation, the presence of wear debris at the contact interface (acting as abrasive particles) increases the friction coefficient at lower humidity.

The current study helped in understanding the friction coefficient evolution due to change in relative humidity for different surface roughness of steel. The initial run-in period associated with asperity deformation and formation of wear debris occurs at later cycle for higher surface roughness grit blast sample as compared to steel substrate. The steady state average coefficient of friction is same for both grit-blast and as-received steel at same relative humidity. With increase in relative humidity, the average coefficient of friction decreases due to change in third body morphology.

Chapter 5

5. Combining in situ tribometry and triboscopy to understand third body behavior of a Cd coating

P. Behera, K. R. Sriraman, R. R. Chromik & S. Yue

This chapter is in manuscript style and published in IOPscience, *Surf. Topogr. Metrol. Prop.*, vol. 5, no. 1, p. 014001, 2017. This chapter focuses on identifying the instantaneous coefficient of friction change with change in third body morphology for Cd coating. The change in instantaneous coefficient of friction with change in third body morphology is studied by performing *in situ* tribometry to observe transfer film morphology and its correlation with features identified from triboscopic image. The features identified from the in situ studied are further correlated with blind test.

Department of Mining & Materials Engineering

McGill University, Montreal, QC, Canada H3A 0C5

5.1 Introduction

Metallic surfaces in sliding contact occur often in industrial applications. More often than not, the contact is lubricated, but dry sliding is possible. Soft metallic coatings may act as solid lubricants and find applications requiring moderate reduction in friction and mitigation of ‘running-in’ wear [39]. Using the ‘third body concept’ proposed by Berthier [22], metallic coatings (first bodies) placed in sliding contact will lead to the formation of third bodies [22], which will influence the friction coefficient. Metallic coatings [117] may be used to reduce the friction and wear by modifying the velocity accommodation mechanism between the two first bodies [23]. Blau [118] postulated that the transfer of metal from one surface to the other changes the sliding characteristics and leads to changes in contact area, morphology of the materials and re-deposition of heterogeneous material from either of the first bodies.

Due to the nature of the buried interface for standard tribology testing, the dynamic nature of third body generation and its recirculation at the contact is difficult to understand and correlate with friction coefficient changes. Real-time studies that can capture the physical and mechanical changes occurring at the interface, simultaneously recording and linking the friction coefficient to third body flows, requires *in situ* methods [24]. In situ and other real-time or “on-line” methods have been developed over the years. Monitoring of the electrical contact resistance and friction force with spatial sensors, often called ‘triboscopy’, allows one to correlate friction and third body activity to specific locations on the worn surface or to specific third body flows in the contact region [29]–[31]. An “on-line” tribometer, developed in the group of Dienwiebel [119] probes the worn surface (outside the contact) with a holographic microscope, allowing one to observe surface morphology changes that may correlate with the friction. *In situ* tribometry, using a transparent counterface, allows direct observation of the sliding interface and has been used to study third body formation and evolution for solid lubricants [48], [50], composite coatings [27], [52] and wear resistant coatings [24], [26]. All of these techniques observe third bodies in different ways and are most effective when coupled with *ex situ* observations of worn surfaces by standard visual, morphological, chemical and mechanical characterization techniques [24]. Less frequently, these in situ methods are coupled with one another. Recently, Stoyanov et al. reported on a lubricated sliding contact for aluminum using both in situ and on-line tribometry [27].

While the in situ methods have been most often applied to solid lubricant [25], [27], [50], [120], there have been many recent studies on metals [20], [26], [27], [72], [119]–[125]. In the work of Sriraman et al. [72] they studied Low Hydrogen Embrittling (LHE) Cd coatings, which are relatively soft coatings applied on high strength steel for fasteners and landing gear components which withstand sliding motion during their application. The lubricous nature of the Cd [71] makes the coating further advantageous to be studied for its tribological behavior by third body formation. *In situ* studies by Sriraman et al. [72] on electroplated Cd coatings showed transfer film formation followed by recirculation of third bodies and finally removal of the transfer film. Jahanmir et al. [18] and Birkett et al. [126], using standard tribology testing, showed that the presence of 0.1 μm Cd coating on hard substrate reduces the wear rate in comparison to uncoated substrate materials.

In situ methods have helped understand third bodies at the sliding interface and their effect on the tribological properties in a way that is unobtainable by other methods. However, a common criticism is that the counterbody used in these studies (i.e. typically sapphire) are different from engineering applications and could affect somewhat the tribological behavior [127] and evolution of third bodies. As mentioned above, the buried interface may also be probed, in a somewhat different manner, utilizing triboscopic maps generated with a metallic countersphere. Belin et al. [31], [29], [30] used triboscopic maps to study the degradation of thin films by coupling cyclic tests with friction coefficient imaging showing increase in coefficient of friction as well as seizure of the coating. These studies showed a method to investigate the instantaneous variation in friction with respect to time and position and combine the average coefficient of friction with microscopic peculiarities at each point within the wear track. Though triboscopic maps are used to study coating degradation, it is most often combined with electrical contact resistance methods where a high electrical contact resistance is measured when the polymeric coating deposited on metallic substrate is intact and subsequent decrease in electrical contact resistance as the insulating polymeric coating is degraded with increase in sliding cycles, limiting the study only to non-metallic coating.

The current work focuses on studying the third body evolution by *in situ* tribometry and triboscopy, correlating the observations of dynamic nature of third bodies to the detailed analysis of time and spatially resolved friction maps from triboscopy. Friction maps generated for tests on coatings with steel countersphere were studied for third body evolution by an analysis of spectral features that could be tied to behavior observed by in situ tribometry. The tribological tests were carried out in a linearly reciprocating ball on flat surface with a sapphire countersphere to correlate the *in situ* studies with the triboscopic images and extend it to metallic countersphere by spectral analysis.

5.2 Experimental Methodology

5.2.1 Plating conditions and coating characterization

The Cd coating was plated in an industrial facility in an alkaline cyanide bath solution with CdO – 20-30 g/l, NaCN – 90-135 g/l, Na_2CO_3 – 0-60 g/l and NaOH – 11-30 g/l. The current density for plating was 118-120 mA/cm^2 to generate an average coating thickness of 15 µm. After coating, a trivalent chromate conversion coating was done to generate a passivation layer in nm range. The plating was done on 6” X 6” inch low carbon 1010 steel and baked at 200 ^{0}C for 24 hrs, the plates were then sheared into 1” X 1” inch coupons for tribological test.

SEM analysis of the surface and cross-section of the LHE Cd coating was done by Philips FEI Inspect F-50 instrument equipped with a field emission gun, operated at 20 kV for surface morphology and 10 kV for cross-section analysis at 2500X magnification.

The hardness of the coating and substrate was measured by nanoindentation technique using Hysitron triboindenter. The loading and unloading is done for 5 secs with a maximum force of 5000 µN and holding time of 2 secs at the maximum load using a calibrated Berkovich diamond indenter. The hardness of the coating and substrate was determined by using Oliver and Pharr analysis [110].

5.2.2 Tribological Test Parameters

The tribological tests were carried out with a linearly reciprocating ball on a flat tribometer [52]. For in situ tests, the counterface was a sapphire hemisphere (3.175 mm radius), while for standard tribology tests (blind test) a 440C steel countersphere (3.175 mm radius) was used. The average surface roughness of sapphire countersphere was 0.068 µm and average surface roughness of steel countersphere was 0.135 µm. The normal load applied to the contact was set with dead weights applied on the arm. For in situ test, 0.863 N was applied, while for standard testing 1.275 N was used. This led to an initial maximum Hertzian contact stress of 390 MPa for both type of tests. The friction force was measured with a piezoelectric sensor at a sampling rate of 800 Hz and a low-pass filter cutoff frequency 200Hz is used to attenuate noise form the measurement. The lateral resolution of the friction measurements was on the order of 20 µm, which was smaller than theoretical contact radius calculated according to Hertzian [44] two body contact theory (sapphire countersphere – 34.3 µm and steel countersphere – 33.1 µm). The coefficient of friction value was plotted as a color coded map as a function of track position and cycle number to generate what is often termed a "triboscopic image," [30] representing the spatial and temporal evolution of the friction coefficient. Friction versus position along the wear track for individual cycles was also plotted either as the average friction calculated by averaging the instantaneous coefficient of friction from forward and backward directions or as 'instantaneous' friction coefficient, which is for either sliding direction (forward and backward direction) and unaveraged.

For in situ tests, a video camera with a pixel resolution of 853 X 480 at 29.97 frames per second, attached to an optical microscope with 10x optical zoom was used to record video of the contact through the sapphire hemispherical counterfaces and to study the third body evolution during the test. The video of the test is paused at the desired cycle number and track position and a snapshot was captured as an *in situ* micrograph.

The relative humidity during both the *in situ* test and blind test was maintained by passing dry air to the instrument enclosed within a plastic bag. The relative humidity for both of the test was kept at 0% RH which was assigned a designation of RH0. The track length for both of the test was 10 mm with a sliding velocity of 3 mm/s. The total number of cycles for *in situ* test was 1600 cycles leading to total sliding distance of 32 meters whereas for blind test the total number of cycles was 2000 cycles leading to a total sliding distance of 40 meters. Sampling rate and spatial resolution was the same for both *in situ* and blind test.

5.3 Results

5.3.1 Coating Characterization

The surface morphology of as-received LHE Cd coating (Figure 5.1(a)) consists of spherical platelets. The porous structure of this coating is necessary to allow hydrogen to escape during bake-out procedures required for high strength steel fasteners. The coating cross-section has non-uniform thickness (shown in Figure 5.1(b)), with a top surface roughness due to the platelet morphology. The coating/substrate interface shows pockets of Cd filling the inherent roughness of the steel substrate. The coating has an average thickness of 11 ± 2 µm. The hardness of the coating measured on the cross-section of Cd coating is 0.42 ± 0.09 GPa, while the hardness of the steel substrate measured on un-coated steel substrate surface is 1.91 ± 0.06 GPa.

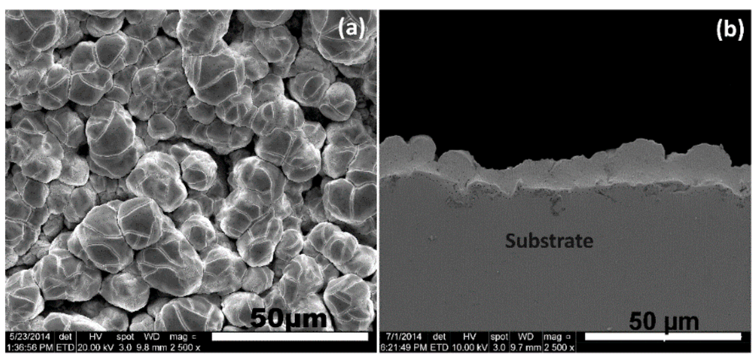

Figure 5.1 SEM Characterization of LHE Cd Coating (a) Surface Morphology, (b) Cross-section

5.3.2 In situ and Triboscopic Studies

As shown in Figure 5.2, Berthier [22] divided the flow of third bodies into five different types, encompassing the "tribological circuit". The detachment of materials from the first bodies to form third body is called as source flow (Q_s). The movement of third bodies across the interface is called as internal flow (Q_i). Third bodies ejected out from the contact region are called ejection flow (Q_e). The ejection flow can be reintroduced into the contact region leading to recirculation flow (Q_r) or can be permanently removed from the tribological circuit and become wear flow (Q_w).

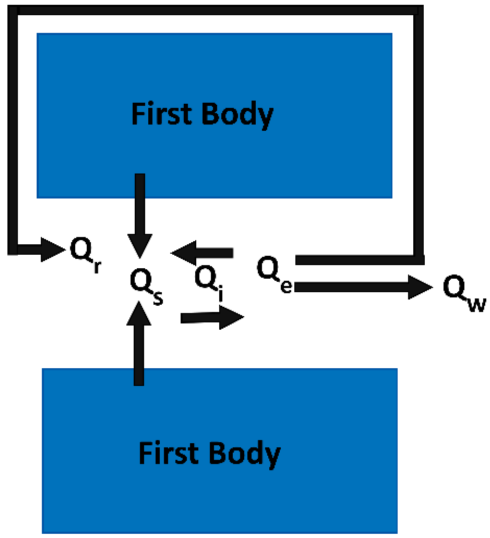

Figure 5.2 Tribological circuit by Berthier [1]

From the start of the tribological test, Cd coating acts as source flow (Q_s) for formation of third bodies. *In situ* micrographs showed formation of transfer film in the first cycle (see Figure 5.3) by plastic flow [48] and adhesion of the coating due to its ductile characteristics. During early cycles as the test progresses, Q_s continues with increase in transfer film size at 10 cycles (see Figure 5.3) as compared to the first cycle. The transfer film area at 1 cycle is ~0.019 mm^2, which increases to ~0.041 mm^2 at 10 cycles (measured from Figure 5.3). At cycle 1(run-in), the instantaneous coefficient of friction vs track position is predominantly higher than at 10 cycles. This is due to the adhesive transfer of the coating to the counterface and formation of the wear track, which is likely accompanied by ploughing of the rough coating by the sapphire countersphere. This process of shearing and adhesion of the metal is known as prow formation [89], [128], [129]. Eventually, as the transfer film grows and becomes more stable in size, the source flow, $Q_{s,}$ subsides to some extent and the friction is reduced slightly due to decrease in prow formation.

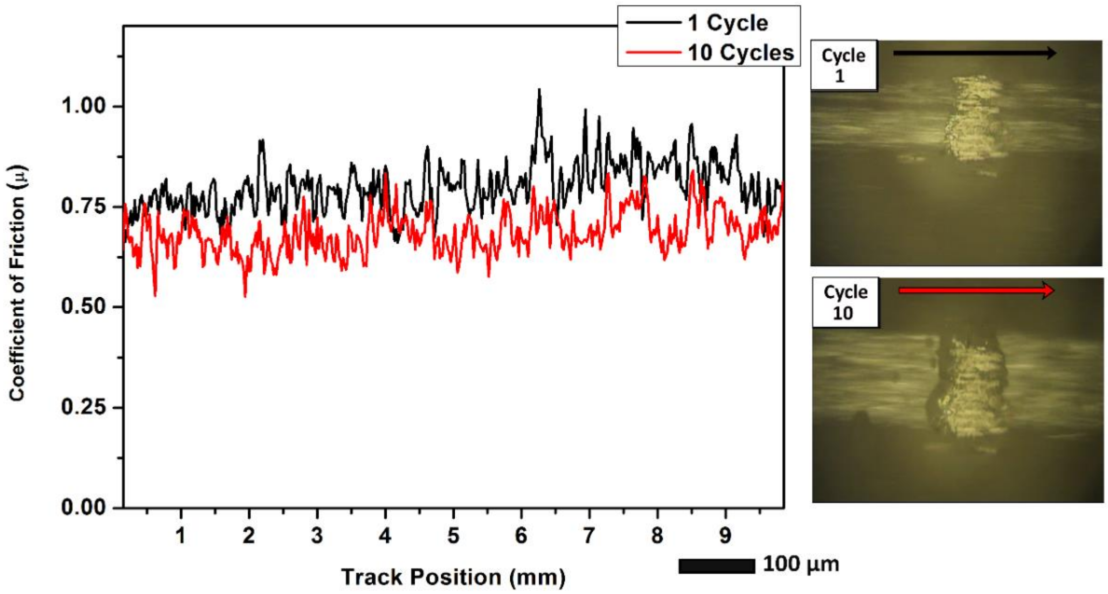

Figure 5.3 Coefficient of friction (averaged from forward and backward portion of given cycles) vs track position with *in situ* image at 1 and 10 cycles indicating higher coefficient of friction due to prow formation at 1 cycle which is subsequently lowered at 10 cycles due to decrease in prow formation

The instantaneous coefficient of friction in forward and backward direction vs track position is shown in Figure 5.4 at cycle 11. The appearance of the transfer film at point 1 (transfer film area ~0.039 mm^2) at 11 cycle in forward direction is comparable to the transfer film area at cycle 10 (see Figure 5.3), indicating transfer film stability. However, during the backward sliding of the countersphere the transfer film becomes unstable resulting in ejection and subsequent replenishment, which is a mix of Q_e and Q_s. At point 2 (see Figure 5.4) removal of transfer film (Q_e) leads to a sudden decrease in instantaneous coefficient of friction. After the removal of transfer film, re-initiation of source flow (Q_s) in backward direction increases the instantaneous coefficient of friction due to prow formation, marked as point 3 with corresponding micrograph.

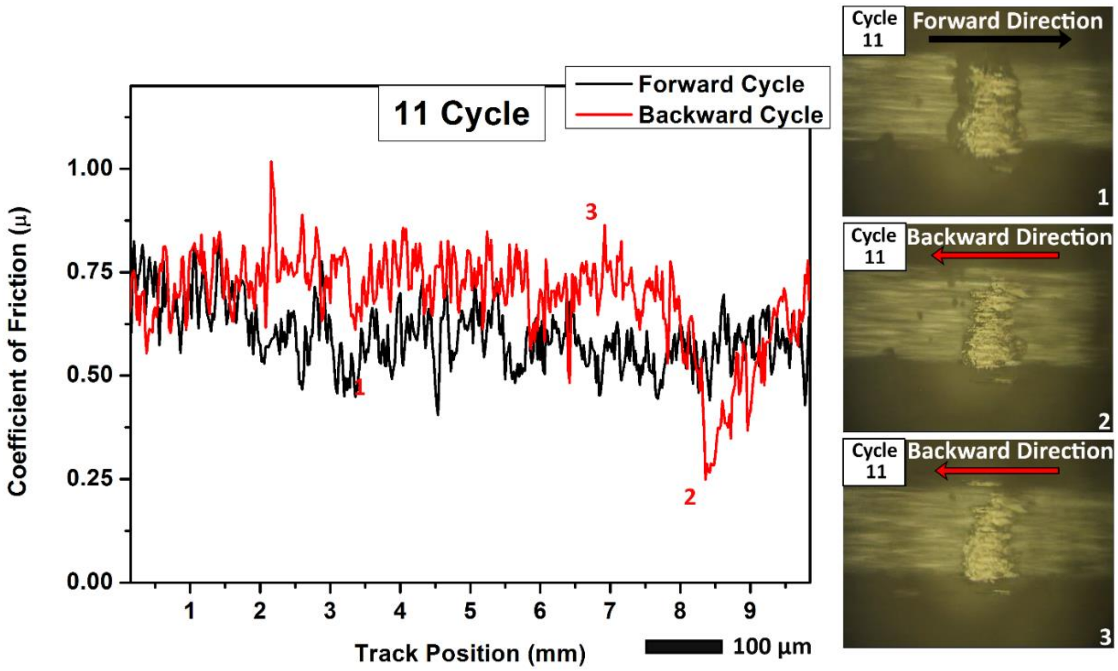

Figure 5.4 Instantaneous coefficient of friction vs track position with *in situ* image at 11 cycle, indicating presence of transfer film at the contact interface in position 1, removal of transfer film at position 2 and formation of new transfer film at position 3

As the test progresses, the transfer film becomes stable (transfer film area of 0.046 mm^2 - measured from Figure 5.5) indicating a reduction in source flow (Q_s) similar to 10 cycle and 11 cycle (forward direction). At the end of the forward direction of the countersphere at 35 cycle shown in Figure 5.5, attachment of small wear debris (2806 μm^2 in area) at the right edge of the contact region increases the instantaneous coefficient of friction. The small chunk is eventually ejected (Q_w) at the end of the forward direction shown as spike in the coefficient of friction. This phenomenon of ejection of wear debris particle at the end of the wear track occurs many times during the test but most of the features are buried within the interface and are difficult to observe from the *in situ* video. At cycle 35, this phenomenon is clearly observed and reported.

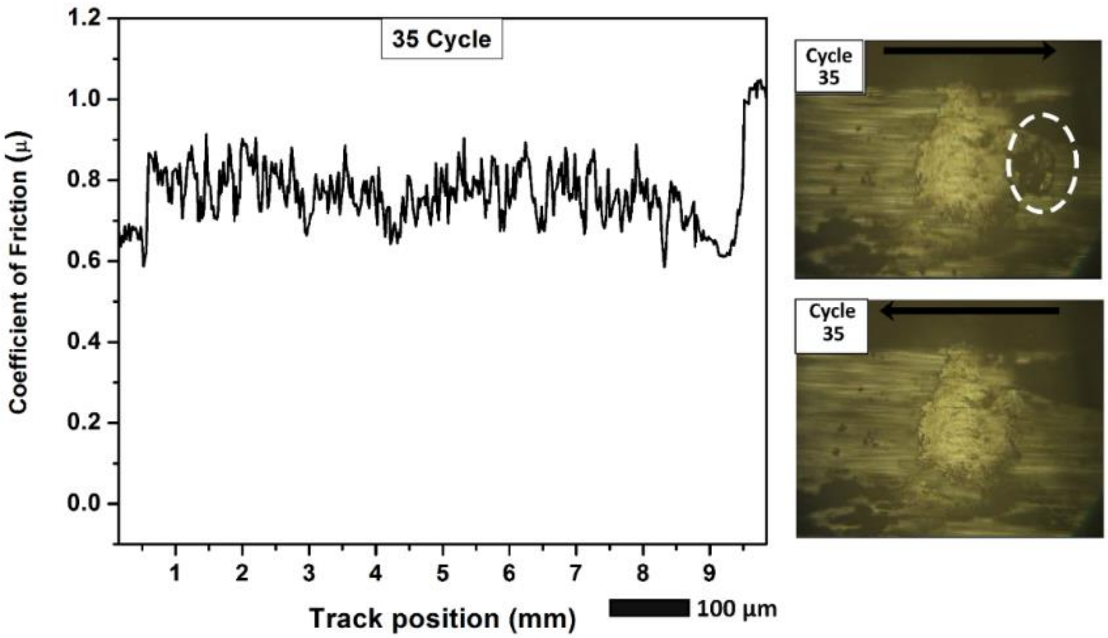

Figure 5.5 Coefficient of friction (averaged from forward and backward portion of given cycles) vs track position with *in situ* image at 35 cycle indicating recirculation of wear debris and subsequent ejection of wear debris observed at the end of wear track

At 46 and 49 cycle, adherence of wear debris at the end of the wear track is observed (See Figure 5.6); this adherence increases the coefficient of friction at around 3.5mm till the end of the wear track due to increase in contact area. The coefficient of friction at point 2 is relatively higher than at point 1, the adherence of wear debris at point 2 leads to increase in coefficient of friction as compared to point 1. Though point 1 has coefficient of friction relatively lower than point 2, point 1 has higher instantaneous coefficient of friction than at 3.5 mm, this might be due to adherence of wear debris that is not revealed in the *in situ* micrograph.

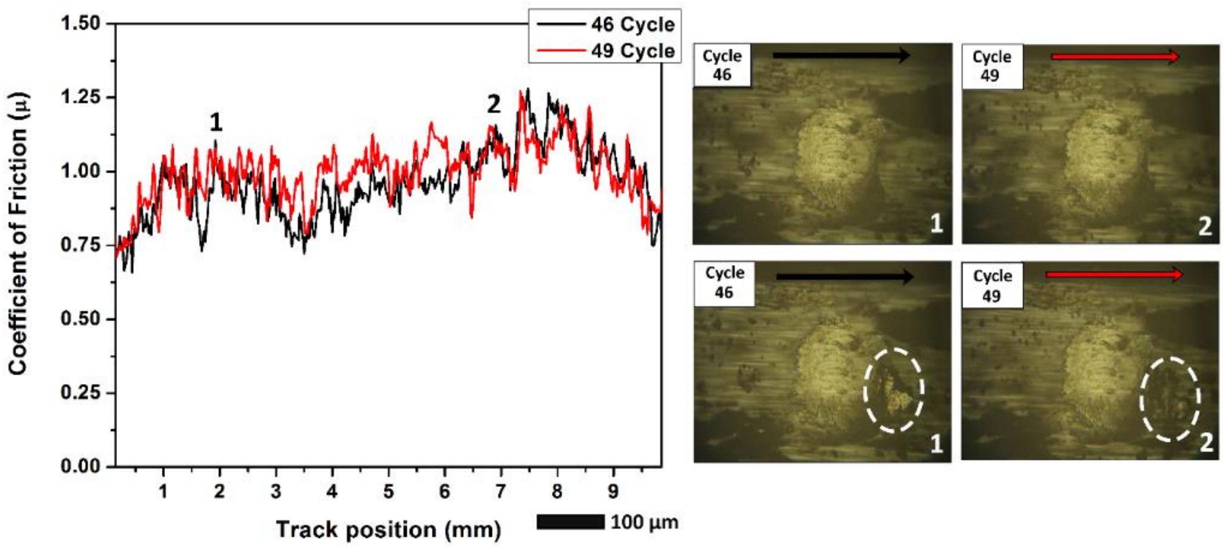

Figure 5.6 Coefficient of friction (averaged from forward and backward portion of given cycles) vs track position with *in situ* image at 46 cycle and 49 cycle indicating adherence of the wear debris, increasing the coefficient of friction at position 2 as compared at position 1 with additional attachment of wear debris.

Localized increase in coefficient of friction leads to increase in average coefficient of friction at 271 cycle, shown in Figure 5.7. The contact region increases at 271 cycle due to attachment of third body to the countersphere at the top part of the *in situ* micrograph (see Figure 5.7, 271 Cycle). This third body has particulate morphology indicating extruded third body reintroduced into the contact region and hence was attributed to recirculation flow, Q_r. At 283 cycle, the removal of this extruded third body decreases the average coefficient of friction as shown in the *in situ* micrograph.

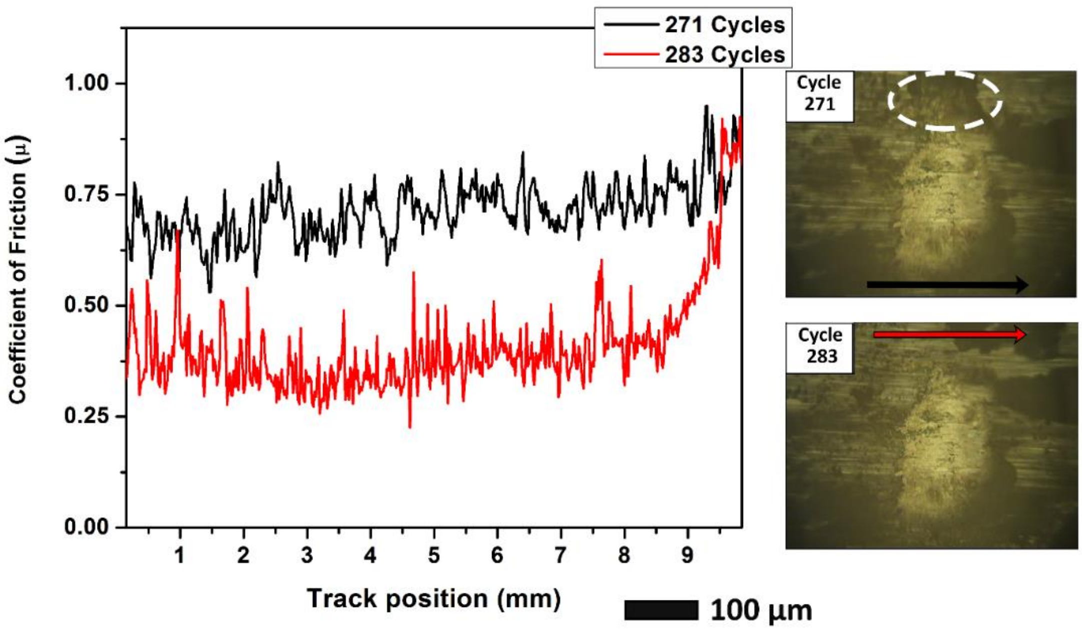

Figure 5.7 Coefficient of friction (averaged from forward and backward portion of given cycles) vs track position with *in situ* image at 271 and 283 cycles indicating the increase in coefficient of friction with adherence of additional transfer film at 271 cycle and subsequent decrease in coefficient of friction as the transfer film is removed at 283 cycles.

To summarize the instantaneous coefficient of friction associated with third bodies up to 300 cycles at RH0, triboscopic image is plotted in Figure 5.8. At initial cycles, the high coefficient of friction due to prow formation by source flow (Q_s) at 1 cycle can be identified from the triboscopic image, which subsequently stabilizes to a relatively lower coefficient of friction at 10 cycles. With further progress of the test, the transfer film is removed and a new transfer film is formed by Q_s at 11 cycles. This removal of the wear debris by Q_w also leads to a friction coefficient change identified by the triboscopic image. The wear debris attached at the contact region (at 46 cycles) increases the instantaneous coefficient of friction as seen in triboscopic image, the continuation of similar features for next 20 cycles at the same track position indicates recirculation flow (Q_r). The average coefficient of friction as shown in Figure 5.7 at 271 cycles is higher as compared at 283 cycles, this is due to modified contact condition by attachment of extruded third body at the contact region. This vertical features thus formed during the test (see Figure 5.8 at 271 cycle) is due to intermittent attachment of third body at the interfacial contact region (it is difficult to identify all the vertical features due to limitation in resolution of optical microscope and transfer films obscuring the visibility of third body for every vertical features in the test).

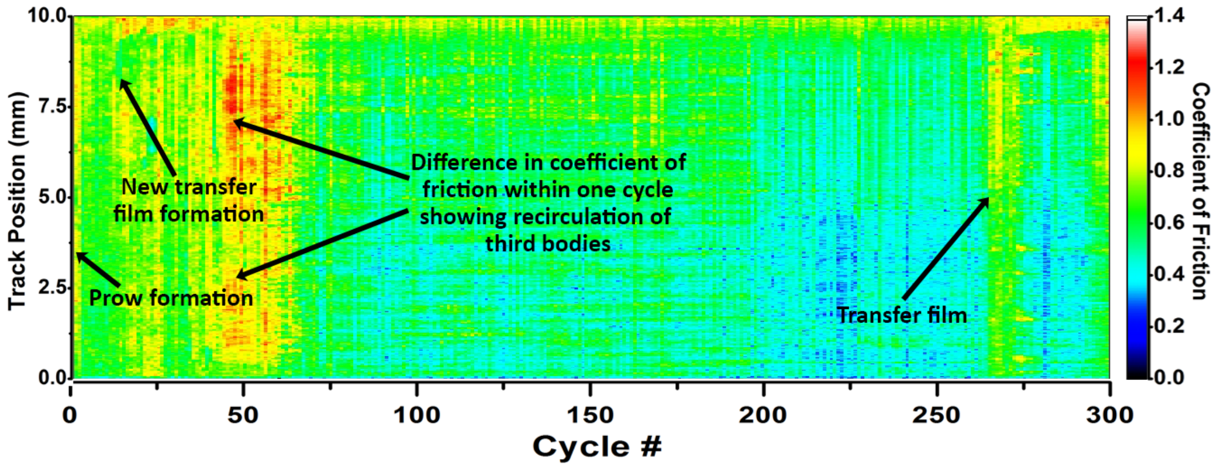

Figure 5.8 Triboscopic image summarizing the change in friction coefficient with morphological changes at the contact region observed by *in situ* tribometry. Prow formation as observed in Figure 5.3, new transfer film formation as observed in Figure 5.4, recirculation flow observed in Figure 5.5 and transfer film formed by extruded product as observed in Figure 5.7.

The triboscopic image up to 1600 cycles overlapped with a plot of the average coefficient of friction is presented in Figure 5.9 (a). Information later in the test is often more difficult to observe due to a thick and stable transfer film. However, at cycle 1100 (see Figure 5.9 (b)) holes and scoring marks on the transfer film are seen. The hole is replenished after few cycles indicating source flow (Q_s) with additional attachment of transfer film at the bottom (shown as recirculation flow in Figure 5.9 (c)). Though the bulk layer of Cd coating might have been removed, the presence of Cd coating at the islets of the steel substrate acts as reservoir for the replenishment of the third body. The scoring of the transfer film (categorized as horizontal scratched regions on the transfer film) increases as shown in Figure 5.9 (b) and Figure 5.9 (c); the transfer film is completely removed at the end of the test (1599 cycle) leading to decreased occurrence of vertical features as seen from the triboscopic image and *in situ* micrograph at the end of test. The average instantaneous coefficient of friction plotted at 1520 and 1599 cycles is shown in Figure 5.9 (d). The *in situ* micrograph indicates that even though there is transfer film present, the instantaneous coefficient of friction vs track position at 1520 and 1599 cycles have peaks at relatively same track position indicating predominant wear track morphology effect as compared to morphological changes associated with transfer film.

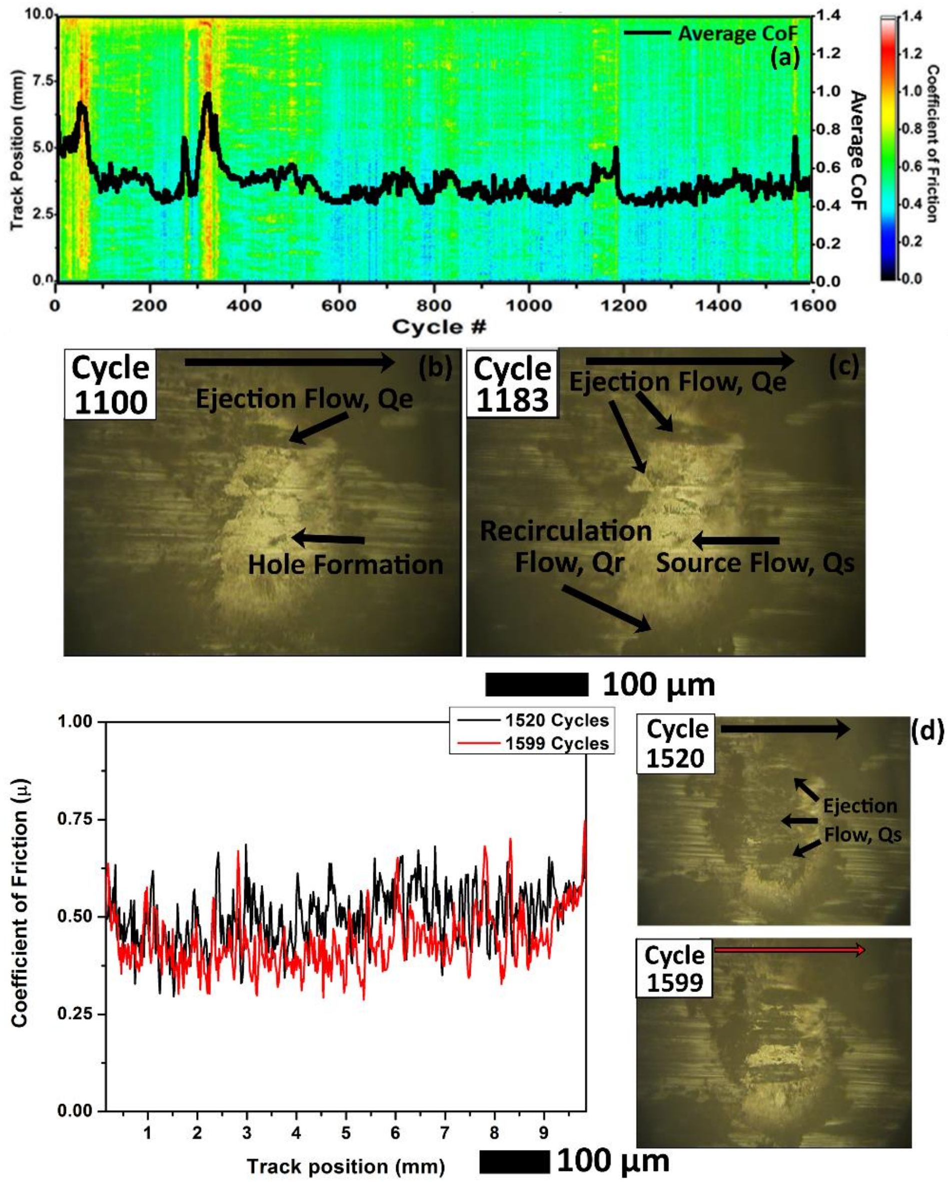

Figure 5.9 (a) Average coefficient of friction superimposed on triboscopic image of the full test, in situ micrograph at (b) 1100 cycles indicating scoring marks and hole formation on the transfer film, (c) 1183 cycles indicating replenishment of some previously formed holes, increasing in scoring and additional transfer film attachment at the contact interface, (d) Coefficient of friction (averaged from forward and backward portion of given cycles) vs track position at 1520 and 1599 cycles showing removal of transfer film and predominant effect of wear track morphology

5.3.3 Triboscopy with steel counterbody (Blind test)

For comparisons to *in situ* tribology, a more 'traditional' countersphere of AISI 440C steel was used for tribological testing of the Cd coating at RH0. The results from *in situ* micrograpahs correlated with the triboscopic images in the previous section were used as a basis to understand the triboscopy for the blind tests. Similar behavior as seen in case of *in situ* triboscopic studies are also seen in blind test (from triboscopic images). The initial overall high instantaneous coefficient of friction at 5 cycles (shown in Figure 5.10) as compared to 8 cycles is due to prow formation. With further progress of test, the high coefficient of friction at 27 cycles than 8 cycles is due to change in contact conditions by formation of transfer film by source flow (Q_s). The change in instantaneous coefficient of friction before and after 5 mm of track length at 52 cycles is similar to the features seen at 45 cycles form *in situ* studies (see Figure 5.6) indicating attachment of wear debris (recirculation flow, Q_r) at the contact region.

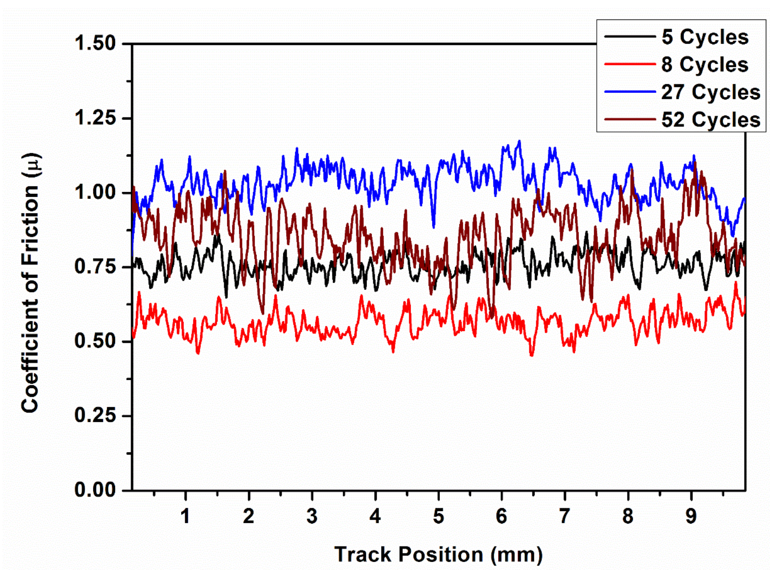

Figure 5.10 Coefficient of friction (averaged from forward and backward portion of given cycles) vs track position at cycle 5, 8, 27 and 52 indicating change in coefficient of friction with progress of test.

Triboscopic image with steel countersphere is plotted up to 300 cycles as shown in Figure 5.11. Features that were similar to Figure 5.8 are identified and demarcated. Feature 1 similar to prow formation in Figure 5.8 is shown in Figure 5.11, this feature was observed at higher number of cycles as compared to sapphire countersphere. Feature 2 is similar to new transfer film formation by source flow (Q_s). Wear debris attachment seen in Figure 5.9 is also observed with steel countersphere in feature 3. New transfer film formation by extruded third bodies from the contact region observed at 271 cycles for *in situ* test can be demarcated as Feature 4 from Figure 5.11.

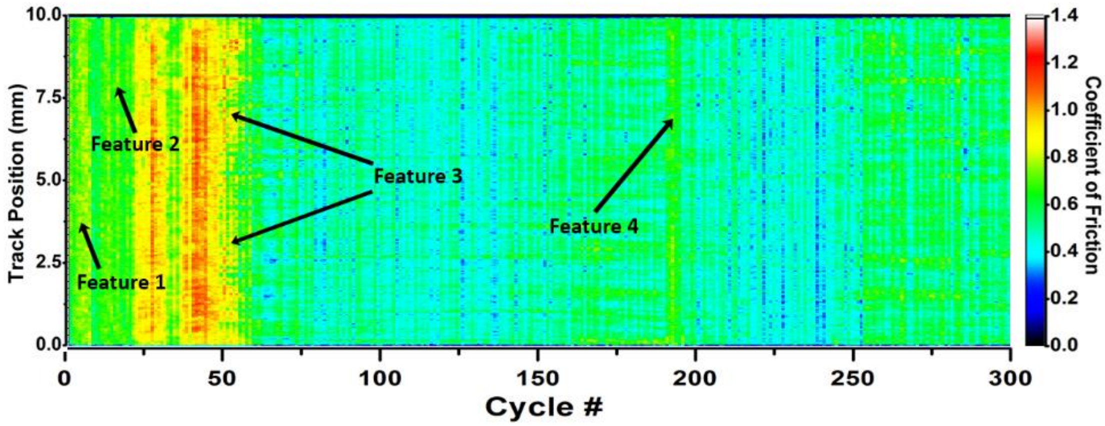

Figure 5.11 Triboscopic image of blind test up to 300 cycles to observe features similar to *in situ* test

The average coefficient of friction overlapped with triboscopic image up to 2000 cycles for blind test is shown in Figure 5.12. Average coefficient of friction overlapped with the triboscopic image shows an initial spike in friction coefficient to 1.0 which is similar for both *in situ* test and blind test. Stable regime of coefficient of friction at approx. 0.5 approx. is similar for both *in situ* test and blind test. Dsicrete vertical features seen at 70 cycles for *in situ* triboscopic image is similar to features seen at 50 cycles for blind test. Morphological changes like initial run-in period, transfer film formation, attachment of wear debris and attachment of additional extruded transfer film occurring at the contact region leading to change in spatial and temporal changes in the friction coefficient for *in situ* test can also be correlated with the blind-test by comparing the triboscopic image.

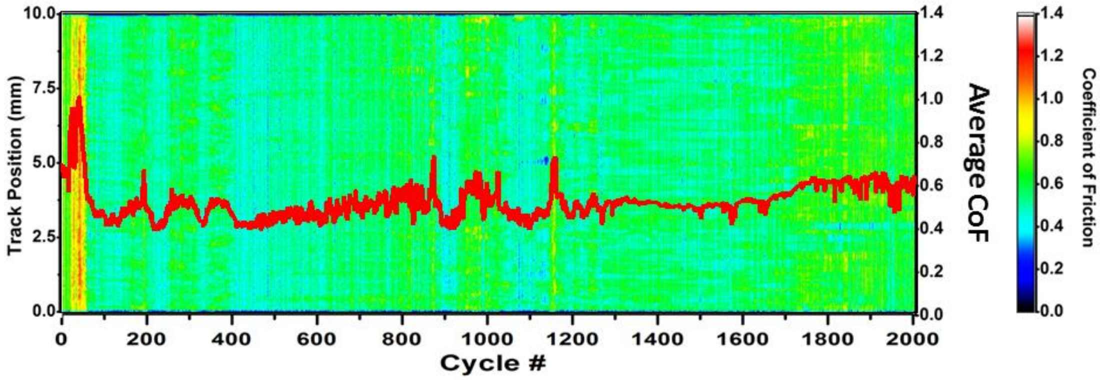

Figure 5.12 Triboscopic image overlapped with average coefficient of friction showing sudden increase in average coefficient of friction due to formation of third bodies at the contact region with steel countersphere at RH0

5.3.4 Spectral analysis of in situ and blind test

Specific correlations between triboscopic images are difficult by simple inspection, thus a 'spectral' analysis was carried out where the distribution of measure friction coefficients over a certain range of cycles is plotted. Comparison of the spectral analysis of the instantaneous friction data for sapphire (*in situ*) and steel (blind test) countersphere helps to ascertain the extent to which similarities exist in friction trends. Regions studied for spectral analysis were typically features that were stable over a given range. These could be regions of relatively constant friction across the wear track or regions where there are intermittent changes across the track. The analysis was carried out over a range until some abrupt increase and decrease of average coefficient of friction occurred, signaling some change in the contact and/or wear track conditions. A relative frequency distribution of the instantaneous coefficient of friction was done with a binning of 0.05 and a bar chart was plotted to comprehend different vertical features.

Discrete vertical features associated with wear debris attachment at the contact region for short no. of cycles is identified from *in situ* and blind test (see Figure 5.13). The features from the triboscopic image are analyzed for similarity in relative frequency distribution of instantaneous coefficient of friction. At cycle 37-69 for *in situ* test (see Figure 5.6) and 18-63 for blind test has instantaneous frequency distribution between 0.4 and 1.1 and maxima at 0.9 due to Q_s and Q_r of the bulk layer of the coating. The distribution of relative frequency at cycle 263-282, 517-560, 674-772 for *in situ* test is due to formation of transfer film from the extruded Cd coating ejected from the contact region during the tribological test (see Figure 5.7), this relative frequency distribution is similar for blind test at 188-196 and 859-875 cycles. The initiation of scoring mark and holes with depletion of transfer film by ejection flow (Q_e) observed around 1100 cycles for *in situ* test with subsequent replenishment of the holes and scoring marks leads to increase in average coefficient of friction. For *in situ* test at 1123-1193 and 1552-1572 cycles the replenishment of the holes and attachment of additional transfer film (see Figure 5.9(c)) shows an instantaneous frequency coefficient of 0.55-0.6 maxima which is comparable to relative frequency distribution at 1144-1160 cycles for blind test.

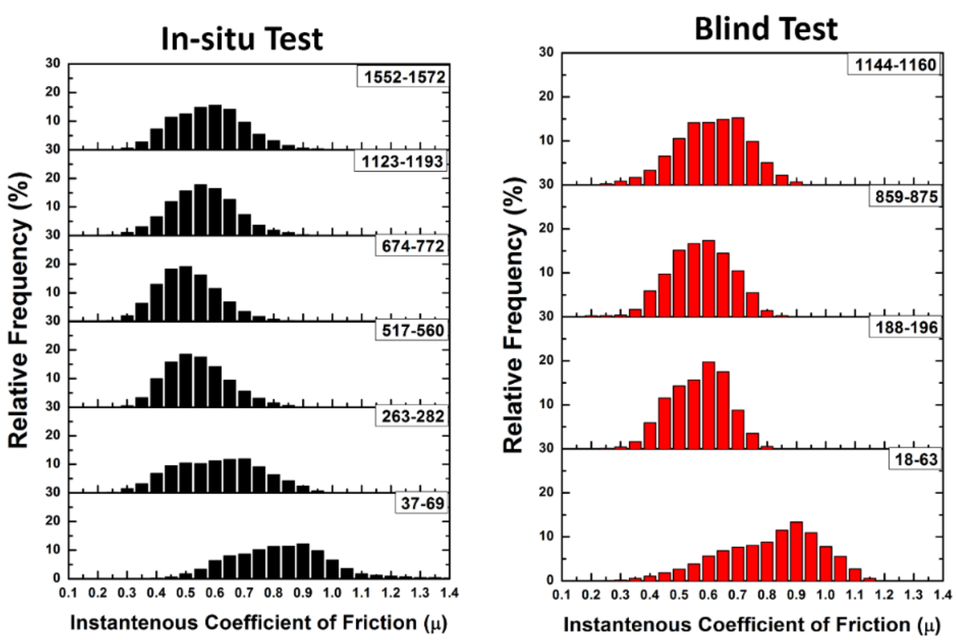

Figure 5.13 Relative frequency distribution of vertical features identified from the triboscopic image of *in situ* and blind test with selected range of cycle number indicated at top right corner of each plot

Regions with mix of vertical and horizontal features identified from the triboscopic image (see Figure 5.14) are analyzed for similarity in relative frequency distribution between *in situ* test and blind test. Relative frequency distribution at cycle 490-503 shows a more uniform distribution of instantaneous coefficient of friction as compared at 254-313 for blind test, but the maxima for both of the relative frequency distribution is at 0.55-0.6 indicating similarity in the third body morphology. Features analyzed for relative frequency distribution for *in situ* test at 768-794 and 851-908 cycles compared to blind-test at cycle 891-940 and 1045-1138 is similar indicating similar behavior of third bodies at the contact region during sliding. Similar relative frequency distribution is also observed at cycle at 798-848 for *in situ* test compared to relative frequency distribution for blind test at cycle 941-988 cycle. Relative frequency distribution at cycle 934-986 for *in situ* test is also similar to features analyzed at cycle 1306-1384 for blind test. The overall similarity between the *in situ* test and blind test for relative frequency distribution of instantaneous coefficient of friction for similar features identified from the triboscopic image indicates similar behavior of the third bodies. Thus the morphological changes in the third bodies identified from the combination of *in situ* image with the triboscopy can be extended to the blind test to identify the evolution of third bodies.

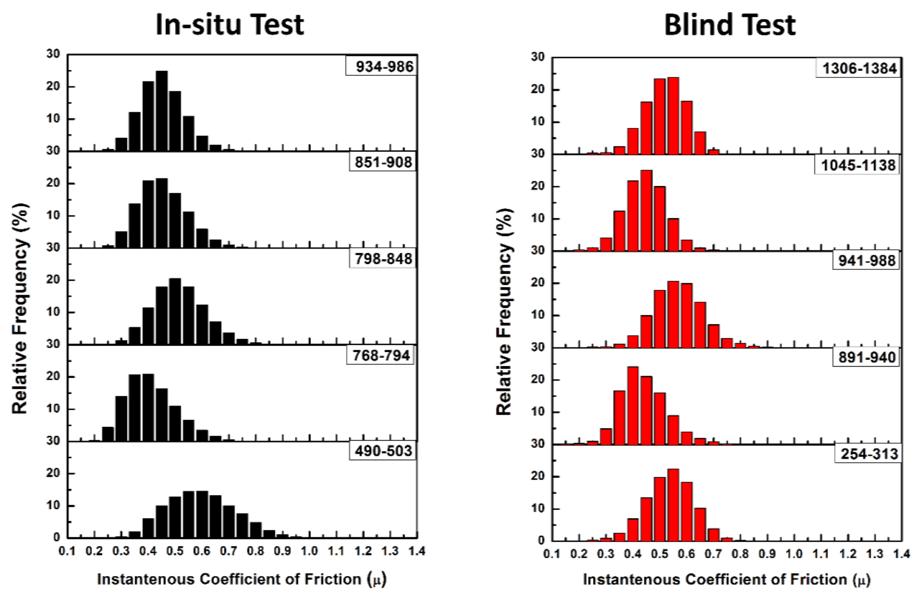

Figure 5.14 Relative friction coefficient frequency distribution of similar features identified from *in situ* and blind test with selected range of cycle number indicated at top right corner of each plot.

5.4 Discussion

Dry sliding of a Cd coating was studied by *in situ* tribometry. Metal transfer films form in early cycles and persist for most of the test. While the opaqueness of these films prevent observation directly at the sliding interface, the size and morphology of the transferred material can be monitored to determine some information about third body flows. The transfer film formed at 1 cycle of the test increases in size as the test progresses, the transfer film thus formed by source flow is removed stochastically with formation of new transfer film immediately with new source flow. Attachment of wear debris and recirculation of wear debris at the contact region, formation of hole and scoring mark on the transfer film is also observed by *in situ* tribometry. Similar behavior of third body flow at the contact region like transfer film formation, its instability and subsequent removal was also observed by Sriraman et al. [72]. Increase in average coefficient of friction with formation of transfer film due to plastic flow, instability of transfer film and its healing for soft Al coating similar to current study is also observed by Shockley et al. [27]. Phenomenon of prow formation by activation of source flow and recirculation of the third bodies, intermittent occurrence of internal flow and ejection flow was also observed by Shockley at al. [28] for cold sprayed Al coating.

While many of the third body flows for metals were observed previously, this study was the first to make direct correlations between these *in situ* observations and measurements of the spatial friction by triboscopy. Third body formation and changes to third body morphology at the contact region can significantly alter the instantaneous coefficient of friction leading to a subsequent change in average coefficient of friction. The formation of third bodies, its morphological change and circulation in the tribological circuit can be correlated with change in instantaneous coefficient of friction values leading to distinctive features in triboscopic image. The formation of transfer film associated with plastic flow and adhesion was associated with high coefficient of friction (see Figure 5.3). Removal of the transfer film was often associated with a drop in coefficient of friction at the particular track position followed by increase in coefficient of friction due to prow formation (see Figure 5.4). The attachment of wear debris at the contact region is associated with a mix of high and low coefficient of friction occurring for a few cycle as vertical feature with discontinuous color coding (see Figure 5.7). These triboscopic features are also observed by Belin et al. [31] during initial run-in and ploughing of polymeric varnish coating of graphite powder coating on AS12UN coating showing continuous horizontal features (reversed axis - X-axis corresponds to number of cycles and Y-axis as position in this study) indicating high average coefficient of friction, further confirmed with electrical contact resistance method. Constant replenishment of the third bodies can be correlated to Cd acting as reservoir of solid lubricant [130] as shown by Belin et al. [30] with degradation of thin films with localized pockets acting as reservoirs to avoid decohesion and seizure of the coating.

Relative frequency distribution of similar features identified from *in situ* test and blind test shows similar trends indicating some similarity in third body flow at the contact region. Though the dynamic nature of the tribologial test leads to different features formed at different cycle no. for each type of test, the similarity in relative frequency distribution might be attributed to similar behavior of Cd coating at same relative humidity and contact stress with less dependency on counterspheres used. Thus relative frequency distribution or spectral analysis is a useful method to correlate the third body flow for tests performed with different tribological parameters. While this was the case for sapphire and steel versus a Cd coating, future work on other material systems would be sure to reveal instances where the counterface materials strongly influence the tribological behavior.

In situ tribometry coupled with triboscopic image used in this study provided unique way to understand the dynamic behavior of third body flow at the contact interface. The *in situ* micrographs correlated with the signature instantaneous coefficient of friction can be extended to different counterspheres and different tribological parameter combined with spectral analysis. However, the formation of extensive transfer film can also obscure the interface leading to omission of some of the third body flow occurring at the buried interface. This is why in this study, specific correlations were presented but other interesting features on the triboscopic images were not fully explored. That is, often a friction change may occur but there is no direct correlation to something observable by *in situ* tribometry. The 'buried' interface problem remains for metals tribology as even with powerful *in situ* methods processes and third body flows directly at the interface are often unobservable. Despite these difficulties in interlinking all the third body morphological changes with frictional changes at the interface, this study was useful in demonstrating the usefulness and effectiveness of a combined *in situ* and triboscopy study.

5.5 Conclusions

The current study helps in better understanding the dynamic nature of third bodies formed at the sliding interface and its subsequent effect on change in coefficient of friction. Combining *in situ* with triboscopic image helped in identifying the signature change in coefficient of friction with change in third body morphology at the interface. Spectral analysis of the specific features identified from the triboscopic image also revealed a correlation between tribological test performed with different counterspheres.

Tribological test performed on LHE Cd coating using *in situ* method revealed higher coefficient of friction during initial run-in period, removal of stable transfer film leads to sudden drop in coefficient of friction followed by increase in coefficient due to initiation of new source flow. Attachment of wear debris at intermittent positions on the wear track by recirculation flow increases the instantaneous coefficient of friction, specific to the track position. The effect of third body morphology at the sliding interface is also revealed from the triboscopic image; the change in coefficient of friction associated with change in third body morphology present at the interface can be identified from distinct features formed on the triboscopic image. Triboscopic image generated with steel counterspheres revealed similar features as identified from *in situ* triboscopic image indicating similarity in third body flow at the interface. Spectral analysis of the distinct features identified from the triboscopic image indicates change in third morphology with progress of test. Spectral analysis also helped in understanding the similarity in third body morphology with change in countersphere from sapphire to steel.

Combing *in situ* method with triboscopic image helped in linking the third body flow at the interface with distinctive features formed on the triboscopic image. The evolution of coefficient of friction also depends on other factors like change in chemical morphology and roughness of the third bodies which can be identified by combining other characterization technique like raman spectroscopy, FTIR spectroscopy and interferometry (on-line tribometry) coupling with *in situ* tribometry. The obscuring of the interface by formation of transfer film also limits the identification of features formed on the triboscopic image coupled with *in situ* tribometry which can be identified with better resolution of the interface.

Acknowledgments

The authors are thankful to Lisa Lee and Salim Brahimi for their support and inputs for this work. We would also like to thank Natural Science and Engineering Research Council Canada (NSERC), Boeing Research and Technology, Pratt & Whitney Canada, Héroux Devtek, Canadian Fastener Institute and Messier-Bugatti-Dowty for their financial support and for providing samples.

Chapter 6

6. Effect of relative humidity on third body evolution of LHE Cd coating

P. Behera, L. Lee, K. R. Sriraman, R. R. Chromik & S. Yue

This chapter is intended to be published. In the previous chapter, effect of transfer film on the evolution of friction coefficient with a sapphire and steel countersphere is correlated. This chapter focuses on effect of varying relative humidity and its subsequent effect on the third body morphology; detailed study on the wear track morphology is done to correlate the change in instantaneous coefficient of friction when transfer film is not present.

Department of Mining & Materials Engineering

McGill University, Montreal, QC, Canada H3A 0C5

6.1 Introduction

Metallic coatings alter the wear and friction coefficient of the substrate material by modifying third body formation and its recirculation [22]. Furthermore, application of some soft metallic coating acts as solid lubricant [71], modifying the friction coefficient. The velocity accommodation due to third body formation for soft coating studied by Berthier et al [23] observed to be irreversible shear due to plastic deformation. Third bodies formed during sliding of metallic coatings [28], [124], [131], [132] are dependent on the mechanical properties of the coating. Sacrificial Cd coating applied on aerospace materials is soft and acts as a lubricant [133] forming third bodies [72] at the contact region making it beneficial for its specific use.

Though there have been recent work on metallic sliding [27], [28], [122], [124], [125], [131], [132], [134], the dynamic nature of the third bodies formed at the interface is difficult to understand and correlate with the change in coefficient of friction occurring within one cycle of the test. *In situ* tribometry method [24] used to study the evolution of third body morphology is limited to transfer film morphology, is not frequently used to correlate the change in coefficient of friction when transfer film is not present. Korres et al [119] devised 'on-line' tribometry to observe the surface morphology changes contributing to friction changes which is used by Stoyanov et al. [120] to study the friction coefficient with *in situ* method and on-line tribometry method. Though this method can be utilized to study the effect of wear track morphology on the friction coefficient, it is only limited to correlation with average friction coefficient and difficult to correlate with spatial change in coefficient of friction observed within one cycle. Belin et al. [29]–[31] introduced the method of measuring spatial coefficient of friction within one cycle by 'triboscopy' method but it is mostly coupled with electrical contact resistance method to correlate with the coating detrition.

Change in relative humidity affecting the friction and wear behavior can be one of the key components as a tribochemical phenomena. Studies done by Mercer et al [67] and Klaffke [135] on steel showed a decrease in friction coefficient and wear rate with increase in humidity. In contrast to this, Larsen-Basse [136], [137] observed a reverse trend where steel has higher wear rate with increase in relative humidity. Modification of the surface properties with change in environmental conditions studied by Rehbinder [116], Bowden et al. [138], Lancaster [139] and Elder et al. [63] observed a change in friction and wear properties. In addition to steel substrate, studies done by Cuong et al [140] with coating observed the variation in tribological behavior of boron carbide sliding against steel countersphere due to change in structure of the carbide and formation of lubricant layer indicating the contribution of humidity to the coating wear. Though much work at varying relative humidity is done for steel and coatings, the effect of ambient atmosphere on the tribological properties of Cd coated steel is limited to Ar atmosphere and air [18].

In situ studies done by Sriraman et al [72] on Cd coated steel observed transfer film formation with frequent recirculation of Cd at the contact region. Studies done in Chapter 5 combing *in situ* and triboscopy method for Cd coating observed temporal features occurring due to transfer film formation and subsequent change in coefficient of friction with change in transfer film morphology. Spectral analysis performed on similar features identified from the triboscopic image indicated change in third body morphology with progress of the test with some similarities between sapphire and steel countersphere. Jahanmir et al. [69] studied that with change in atmospheric condition from air to argon atmosphere, the wear rate of the coating decreased by three orders for 0.1 µm Cd coated steel.

In situ method helps in understanding the third body behavior, especially transfer film morphology and its correlation with friction coefficient. On-line tribometry also helps in understanding the morphology of the wear track but is limited to average coefficient of friction data. Triboscopy method introduced by Belin et al. [29], [31], [54] measures the coefficient of friction at high sampling rate and can be correlated with the spatial friction coefficient changes occurring within one cycle. Pervious work done with triboscopy method [29]–[31] is limited to temporal and spatial change of friction coefficient for non-metallic coating, coupled with electrical contact resistance method to evaluate the coating failure. Combing triboscopy method with third body morphology can help in understanding the dynamic contact interface.

The current work focuses on studying the triboscopic maps generated for metallic coatings and correlating them with third bodies. The tribological test was done in a linearly reciprocating ball on flat surface tribometer with steel countersphere to correlate the instantaneous coefficient of friction changes with wear track features. SEM and surface profilometry is done to investigate the spatial distribution of instantaneous coefficient of friction due to wear track morphology change and correlating this change with triboscopic image.

6.2 Experimental Methodology

6.2.1 Plating conditions

The Cd plating on steel substrate is done in an industrial facility by immersing the steel plates in an alkaline cyanide based bath solution with CdO – 20-30 g/l, NaCN – 90-135 g/l, Na_2CO_3 – 0-60 g/l and NaOH – 11-30 g/l. The substrate is git-blast and acid pickled before immersion, current density applied for plating is 118-120 mA/cm^2 to generate a coating thickness of 15 µm in 5 minutes. After plating, the Cd coating is immersed in trivalent chromate conversion solution to generate a passivation layer. After the plating process, the 1018 Cd coated steel panel was baked at 200 ^{0}C for 24 h followed by hand shearing of plates to 50 X 50 mm inch coupons.

6.2.2 Characterization

Investigation of the wear track and transfer film is done by scanning electron microscope (SEM) (FEI Inspect F-50) equipped with field emission gun and energy dispersive spectrometer (EDS).

X-ray diffraction of LHE Cd coating is done by Bruker discover D8 diffractometer with 2D HISTAR area detector, source of Co Kα radiation (1.79 Å) at 35 kV and 45 mA and indexed from ICDD JCPDS Standards.

FTIR (Bruker Tensor 27 IR spectrometer, United States) and Raman spectroscopy (Renishaw, UK) is used to study the chemical composition on wear track. Raman spectra analysis is done on bare 1018 steel substrate at varying relative humidity after completion of the test whereas for Cd coated steel the FTIR analysis is done on wear track after 50 cycles.

White light interferometer (Wyko NT 8000, USA) is used to determine the wear track morphology. The post processing of the data from white light interferometer is done using Gwyddion v2.33.

6.2.3 Tribological Test Parameters

A linearly reciprocating ball on flat tribometer [52] with a 440C steel countersphere of 3.175 mm radius was used. The average surface roughness of steel countersphere was 0.135 µm. Dead weights were applied on the loading arm to set constant normal force. Track length of 20 mm and sliding speed of 14 mm/s for 2000 cycles corresponding to total sliding distance of 80 meters is done for tribology test. This corresponds to initial maximum Hertzian contact stress of 390 MPa with a normal load of 1.314 N. Triboscopic images are generated by recording the friction coefficient at a sampling rate of 800 Hz using lateral piezo sensor setting. The spatial resolution of triboscopic images is 20 µm, which is smaller than the theoretical contact radius (33.1 µm) according to Hertzian [44] two body contact theory. Instantaneous coefficient of friction (color coded) is plotted with track position in Y-axis and cycle no. in X-axis to generate "Triboscopic image" [30]. The tribological test evaluation of the steel substrate is done with same tribometer and similar track length and sliding velocity. Initial maximum Hertzian contact stress was calculated to be 670 MPa, corresponding to load of 1.3 N. Wear track, transfer film and cross-section of LHE Cd coating is investigated with FEI 50 SEM field emission gun equipped with EDS detector.

6.3 Results

6.3.1 Coating Characterization

Surface morphology of the coating shown in Figure 6.1 (a) has porous Cd layer formed due to agglomeration of platelets. Cross-section of the coating shown in Figure 6.1 (b) has non-uniform continuous Cd coating with intermittent through thickness cracks and coating surface roughness inherent to the steel substrate. The average cross-section of the coating is 11±2 µm.

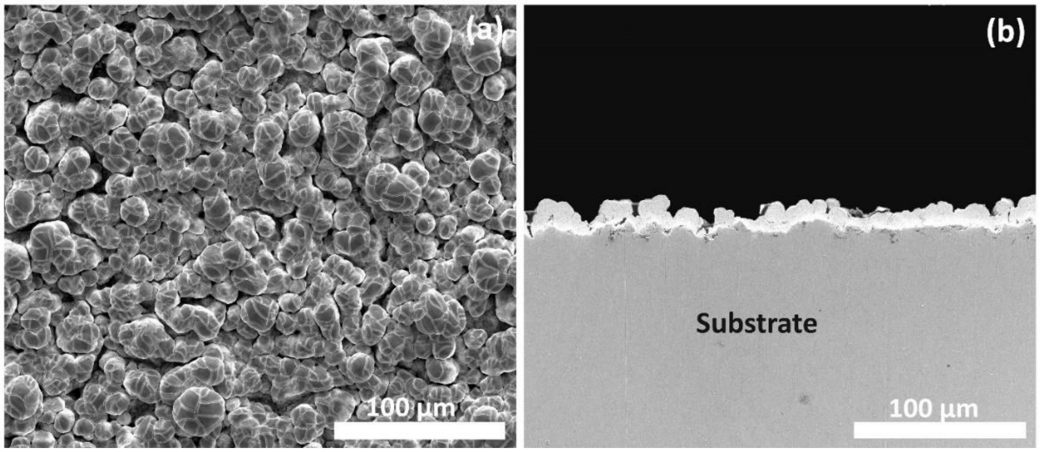

Figure 6.1 SEM Characterization of LHE Cd Coating (a) Surface Morphology, (b) Cross-section

XRD characterization of the coating is done to detect any impurity or second phases formed during the plating process. Peaks correspond to Cd HCP phases as shown in Figure 6.2.

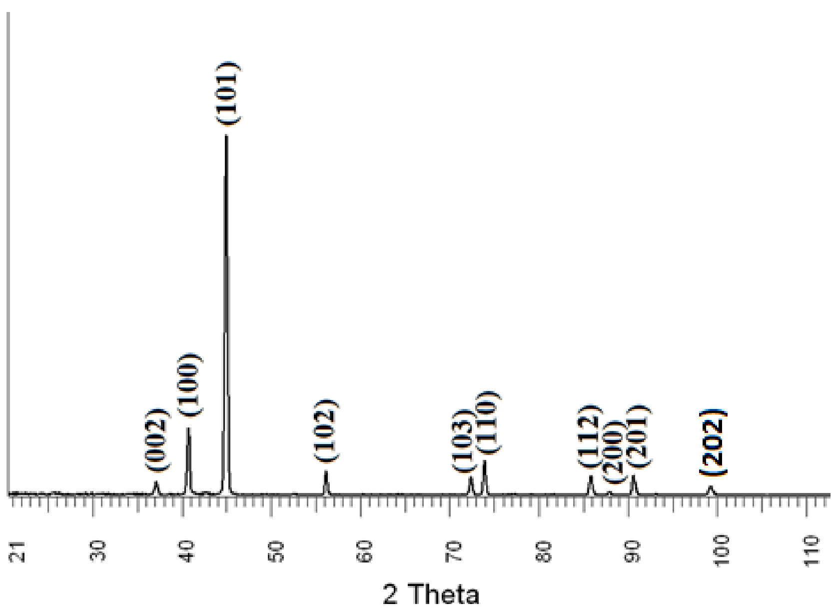

Figure 6.2 XRD Phase Characterization of LHE Cd Coating

6.3.2 Tribology test and Triboscopy

6.3.2.1 Average Friction Data at RH60

The evolution of friction coefficient with increase in sliding distance of LHE Cd coating is evaluated at relative humidity of 60% and Initial maximum Hertzian contact stress of 390 MPa (See Figure 6.3). The average coefficient of friction is divided into four regimes with increase in cycle number i.e., high coefficient of friction of 0.53±0.04 up to 250 cycles (Regime I), which changes to low coefficient of friction of 0.40±0.06 (Regime II) and subsequent increase in coefficient of friction to 0.79±0.03 up to 2000 cycles (Regime III). The transition from Regime I to Regime II is within 1-5 cycles whereas the change in coefficient of friction from Regime II to Regime III is more gradual, the evolution of third body at Regime II to Regime III is studied in a greater detail named as "Transition Regime". The wear track and transfer film is investigated by SEM and EDS to observe third bodies in four regimes.

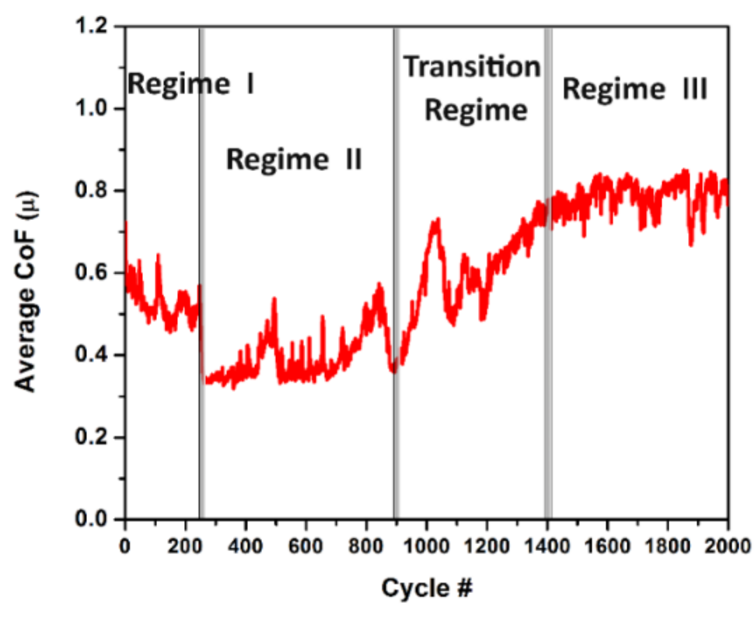

Figure 6.3 Average CoF vs Cycle # at 390 MPa Contact stress and RH 60 indicating four regimes in tribological test

Figure 6.4 shows the (a) wear track and (b) transfer film at 200 cycles within Regime I of the test. Wear track at 200 cycles has smeared layers of Cd coating due to adhesive wear. The soft and lubricating nature of Cd metal [141] leads to smearing of bulk Cd layer during the initial cycles of sliding test. Transfer film with smearing marks is observed on the countersphere. EDS analysis at two spots on the wear track confirms predominant Cd coating and a mixture of Cd and Fe peaks, identified as darker spot in the micrograph. The contrast in SE image on the wear track depicts Fe substrate as dark patches and Cd coating as lighter patches. The 3-D profiling at the same position on the wear track indicates elevated points as Cd, the Fe substrate peaks present at relatively lower height as compared to Cd coating.

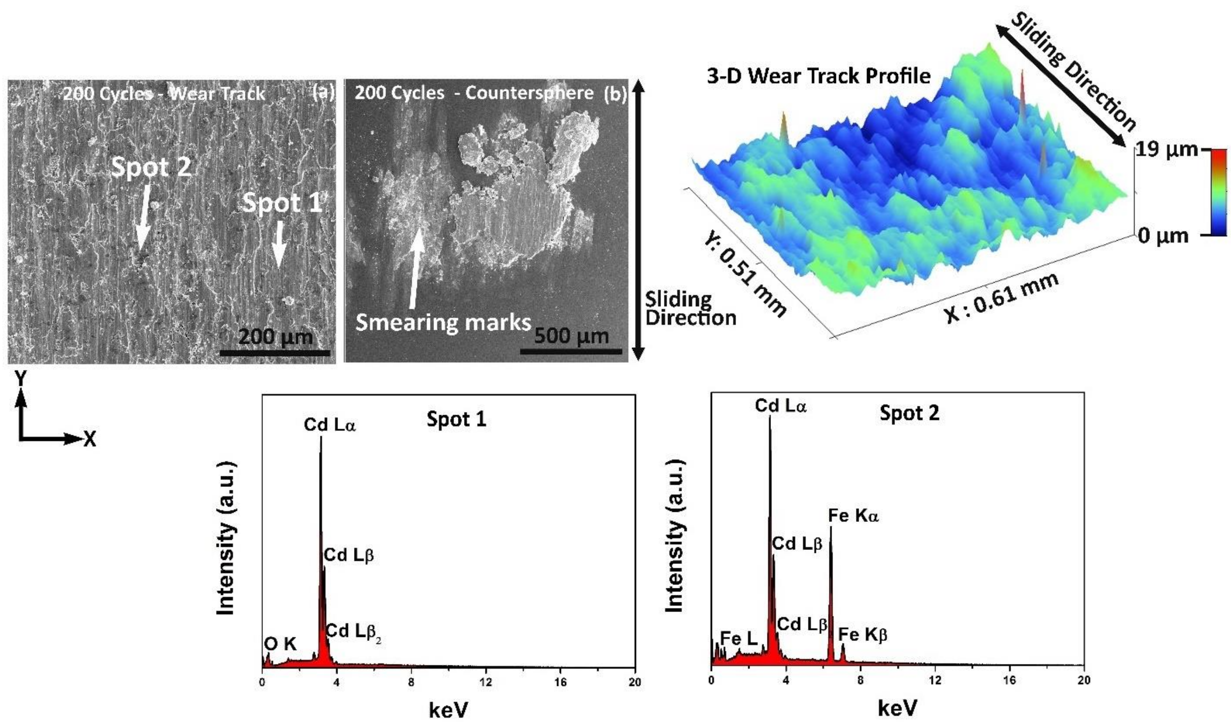

Figure 6.4 (a) Wear track morphology indicating smeared Cd layer, 3D profile and EDS analysis of wear track indicating Cd contact during sliding and (b) Adhesive wear features of countersphere SEM image at 200 cycles

At 500 cycles in Regime II, the morphology of wear track (see Figure 6.5(a)) has scattered particle type wear debris at the contact region. The wear track has a contrast of dark and bright patches with wear debris scattered around the dark patches. Morphology of the countersphere (see Figure 6.5 (b)) is different than 200 cycles (see Figure 6.4), the transfer film formed during the initial cycle has been removed from the contact region with few wear debris particles adhering to the sides of the contact region. EDS analysis of dark patches on the wear track has a mixture of Cd and Fe peak whereas bright patch is predominantly Cd phase. The wear debris are predominantly

Cd peak. The presence of Cd at the contact interface with protuberence of the steel substrate decreases the shear strength and contact area, leading to a decrease in friction coefficient [142].

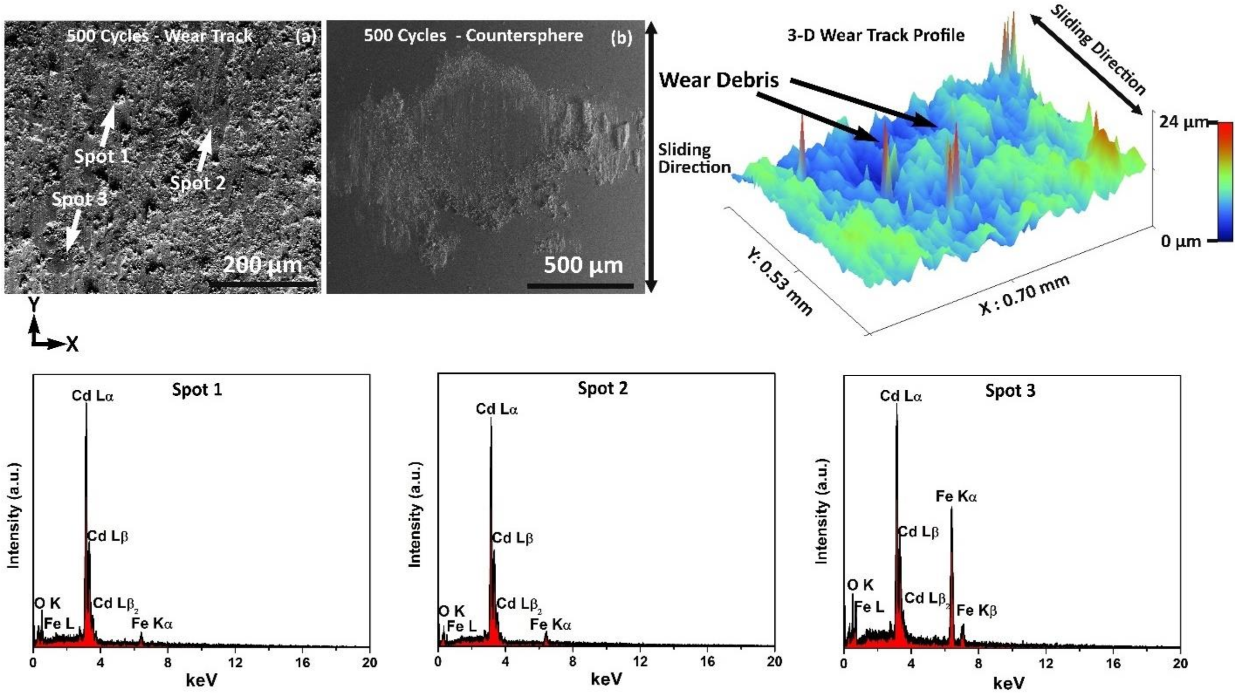

Figure 6.5 (a) Wear track morphology with wear debris scattered on the wear track, 3D profile and EDS analysis of wear track indicating higher relative elevation of wear debris particles, (b) countersphere SEM image indicating removal of transfer film and attachment of wear debris at 500 cycles

At 1000 cycles, the wear track and transfer film in “Transition Regime” is shown in Figure 6.6, the average coefficient of friction changes from 0.4 to 0.79 as shown in Figure 6.3. The wear debris is removed at transition regime. EDS analysis at relatively bright patches shows predominant Cd peaks where as darker features has predominant Fe peaks. Countersphere imaging at 1000 cycles (see Figure 6.6 (b)) has formation of fine compact transfer film with different morphology than 200 cycles. The transfer film is more compact with a scar mark at the middle of the countersphere indicating contact of transfer film with a more harder morhology (steel substrate) present on the wear track. 3-D profile of the wear track has less wear debris and contact of transfer film with steel substrate.

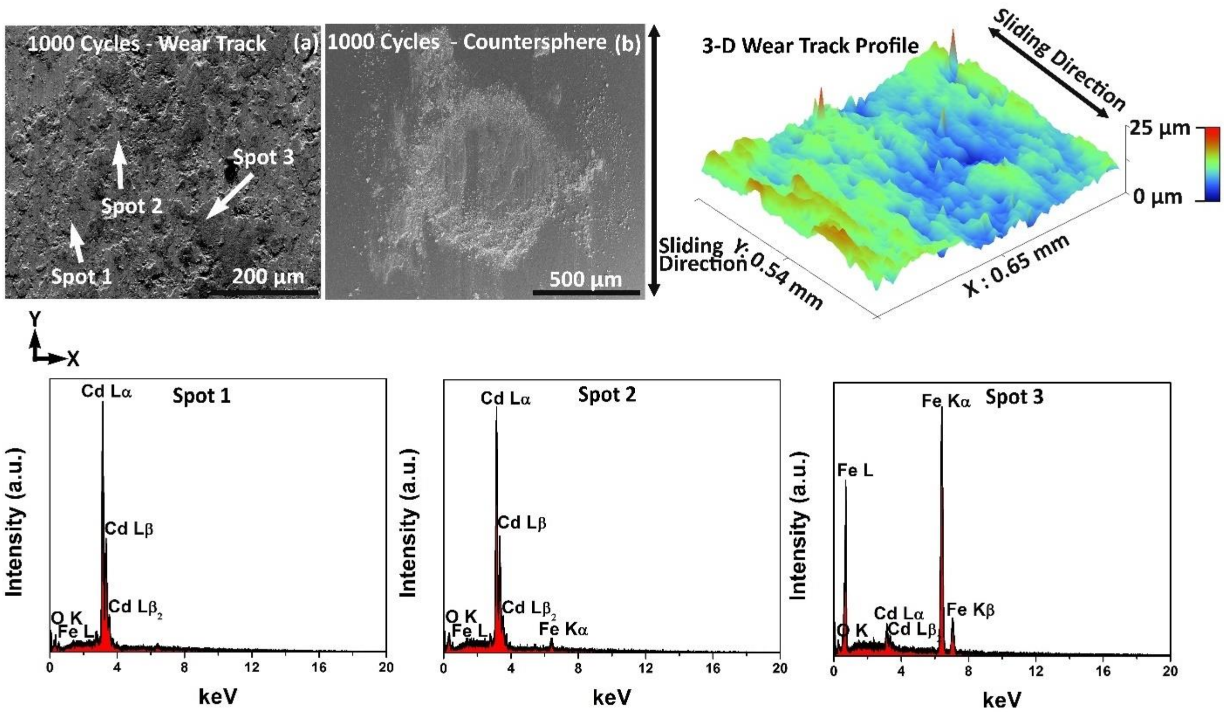

Figure 6.6 (a) Wear track morphology, 3D profile and EDS analysis of wear track showing protuberance of steel substrate at the contact region (b) countersphere SEM image at 1000 cycles indicating thin layer of transfer film formation

At 1500 cycles (Regime III), SEM micrograph of wear track has predominant dark patches with intermittent pockets of bright patches (see Figure 6.7 (a)). Fine wear debris seen at 500 cycles are mostly removed from the contact region. Countersphere shown in Figure 6.7 (b) has a circular wear scar at the centre of the steel ball (average wear scar diameter of 546 ± 38 µm was measured using the image shown in Figure 6.7 (b)), with wear debris sticking at the periphery. EDS analysis of bright pockets have a mixture of Cd and Fe whereas the dark features have dominant Fe peak. Increase in dark patches signifies that the contact has changed to steel on steel. Higher shear strength of steel substrate (due to depletion of Cd from the surface) with increased area of contact (circular scar on the steel countersphere), increases the coefficient of friction [143]. 3-D profile of the wear track indicates presence of steel susbtrate at relatively higher height (dark patches) with no wear debris present on the wear track.

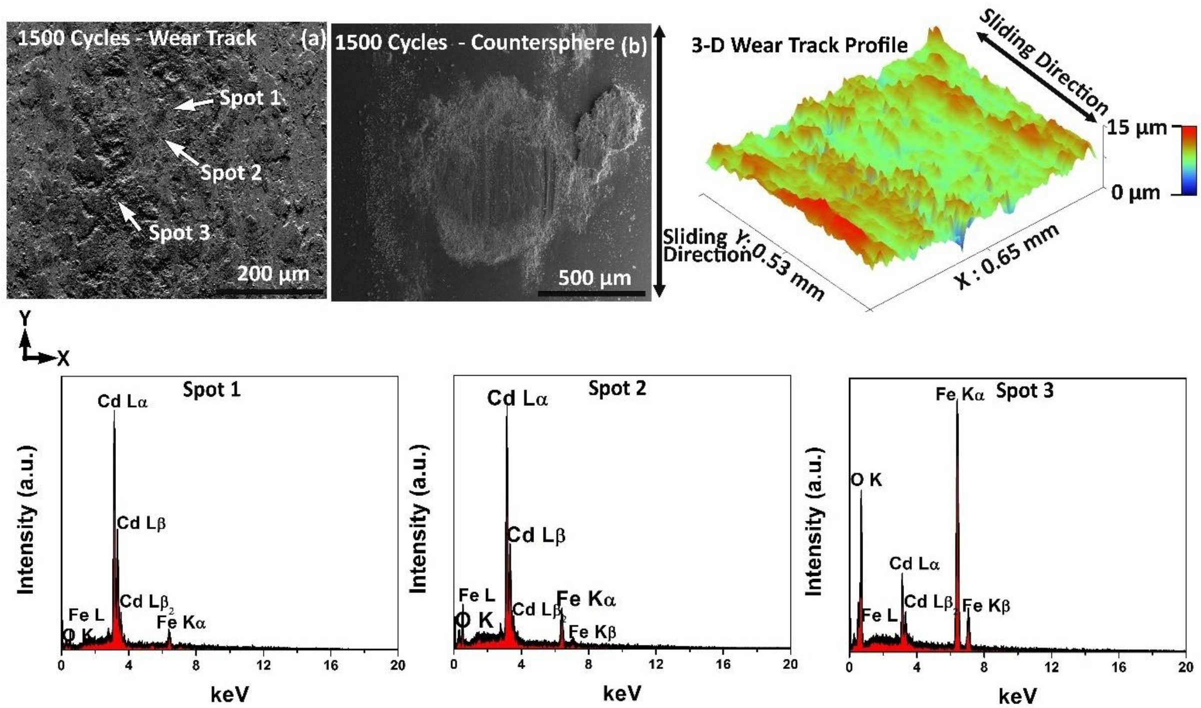

Figure 6.7 (a)Wear track morphology, 3D profile and EDS analysis of wear track indicating steel substrate (b) countersphere SEM image at 1500 cycles showing wear scar at the contact region

To study the spatial evolution of third bodies, triboscopy method is used to observe the change in instantaneous coefficient of friction with track position at varying relative humidity. Triboscopic image overlapped with average coefficient of friction at RH60 is shown in Figure 6.8. Regime I, II, III and Transition Regime (see Figure 6.3) is demarcated on the triboscopic image. The formation of transfer film in Regime I (see Figure 6.3) increases the average coefficient of friction, this transfer film formation in Regime I leads to formation of discrete temporal features in triboscopic image as observed in chapter 5. Low average coefficient of friction (Regime II) shows a mix of temporal and spatial features. The temporal features are formed due to transfer film formation by wear debris attachment at the contact interface for few number of cycles, similar to features observed in chapter 5. Regime II continues up to 900 cycle where Cd pockets and wear debris is depleted and the contact changes from Cd lubricating layer and steel at the wear track to steel countersphere with steel substrate. With progress of sliding cycle in Regime II, increase in steel substrate peaks at the contact region can be seen as increase in area fraction (not quantified) occurring at the same point as shown in Figure 6.8. The gradual removal of wear debris and depletion of Cd pockets leads to gradual increase in average of friction coefficient (Transition

Regime). Within transition regime, there is formation of transfer film at approx. 950-1050 cycles by attachment of fine wear debris particle, this leads to a drop in average coefficient of friction which subsequently increases after the transfer film is removed. The morphology of transfer film formed at Regime I (bulk Cd layer formed by adhesive wear shown in Figure 6.4 (b)) is different than Transition regime due to fine wear debris attachment (see Figure 6.6 (b)). After the Transition regime, the removal of wear debris at the contact region and depletion of transfer film leads to Regime III (steel substrate contact with steel counterpshere). After 1300 cycles, the wear debris activity is minimized with mostly steel on steel contact. Few wear debris attachment at the contact region thereafter leads to decrease in coefficient of friction as seen in Regime III.

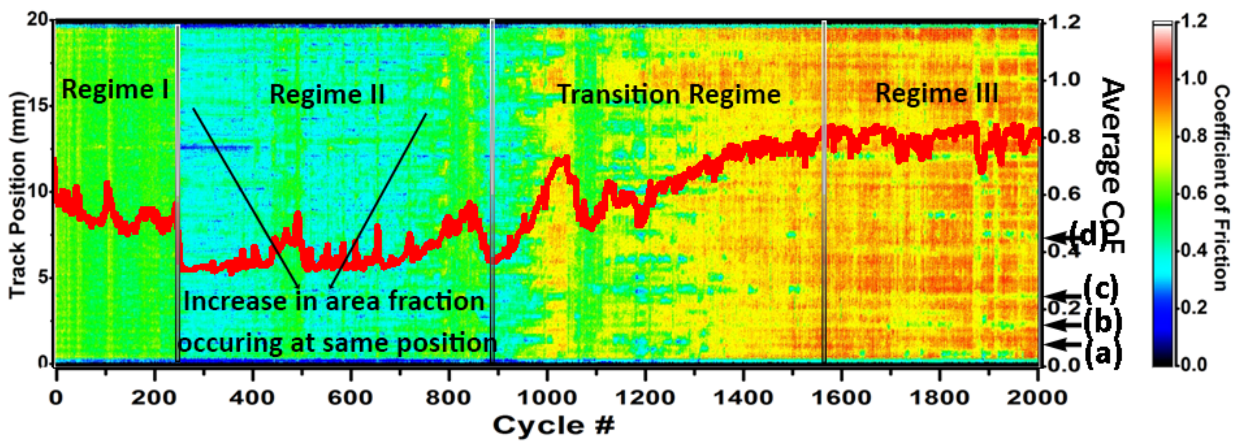

Figure 6.8 Triboscopic image superimposed with average coefficient of friction at RH60

At the end of test (2000 cycles), the change in instantaneous spatial friction identified from the triboscopic image is correlated with wear track morphology, investigated by SEM and profilometry at different positions. Four different regions (see Figure 6.8) are marked after end of test to investigate the difference in instantaneous coefficient of friction values. The different regions on the wear track are marked from (a) to (d), these features are identified from the triboscopic image and averaged (shown as horizontal line in Figure 6.9 (a)). Minimum length of features identified from triboscopic image was 750 µm, considering the wear scar observed from countersphere to be 546 µm (shown in Figure 6.7). Figure 6.9 (a) shows friction coefficient of 0.85. Combining SEM (showing dark features as Fe substrate and bright features as Cd Pockets) with optical profilometry, higher elevation of steel substrate with countersphere is observed. The Cd coating present is relatively lower level than steel substrate; which in turn increases the coefficient of friction (higher shear strength of steel substrate). As compared to Figure 6.9 (a), wear track morphology of Figure 6.9 (b) has less prominent steel substrate contact with countersphere (relatively same elevation as that of steel and Cd), increasing the contact with Cd pockets leading to a transition from high to low coefficient of friction of 0.7 coefficient of friction. Wear track morphology features in Figure 6.9 (c) has friction coefficient of approx. 0.5 due to predominant Cd contact with countersphere. In Figure 6.9 (d), presence of Cd and steel substrate further decreases the coefficient of friction. Similar area fraction of steel substrate calculated from the SEM image (Figure 6.9) shown in Table 6-1indicates that the protuberance of the steel substrate and presence of wear debris on the surface dominates the instantaneous friction coefficient than the area fraction of steel substrate present.

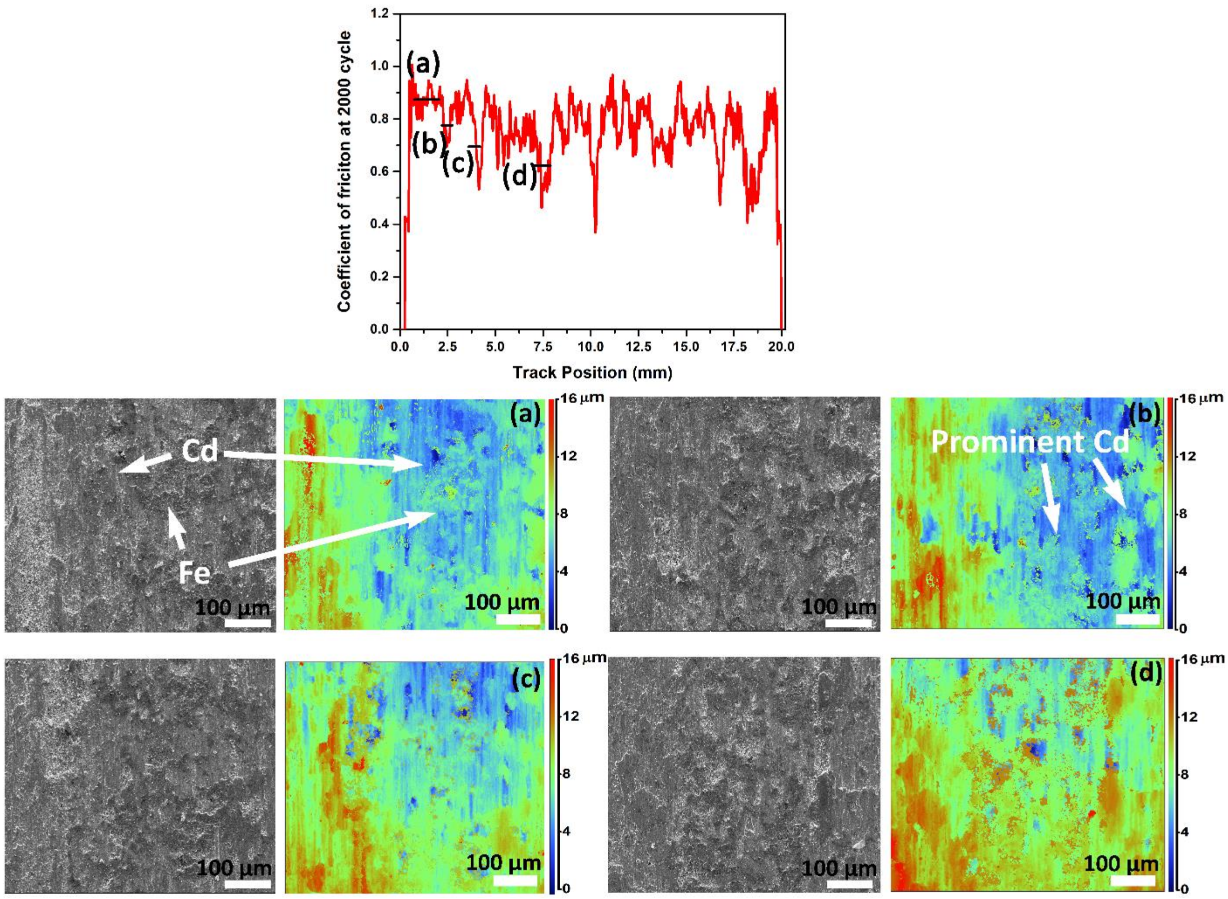

Figure 6.9 Coefficient of friction with track position at end of test (2000 cycle) showing (a) Elevated Fe substrate (b) scattered and less elevated Fe substrate (c) Cd pockets at an elevated region (d) Wear debris and Cd pockets

Table 6-1 Percentage area fraction of Steel Substrate on the wear track

Figure no.	% Area of Steel Substrate
(a)	15.7
(b)	17.2
(c)	20.0
(d)	15.0

6.3.2.2 Average Friction and Spatial Friction at RH 30

The details provided at RH30 is less than RH60 because of similarity in average coefficient of friction (ending at transition regime) observed at RH30. From the triboscopic image and average coefficient of friction, it is evident that the average coefficient of friction is within "Transition Regime" at the end of the test, as shown in Figure 6.10. Initial bulk layer of Cd is mostly removed by adhesive wear, observed as temporal features. At Regime II, decrease in relative humidity increases the occurrence of temporal features in the triboscopic image (frequent wear debris attachment as observed in chapter 5), indicating change in third body morphology with change in relative humidity. More frequent temporal features observed at RH30 leads to delay in onset of steel on steel contact.

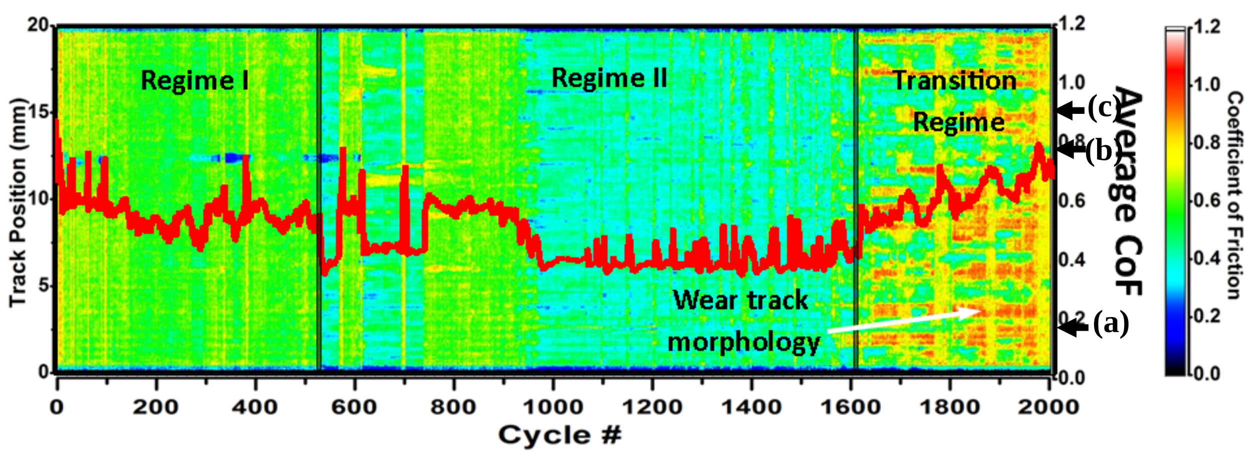

Figure 6.10 Triboscopic image overlapped with average coefficient of friction at RH30

Figure 6.11 shows the instantaneous coefficient of friction vs track position at 2000 cycles. The high instantaneous coefficient of friction region (see Figure 6.11 (a)) has scattered wear debris at the contact interface with prominent contact of steel substrate. The low instantaneous spatial coefficient of friction shown in Figure 6.11 (b) has Cd layer present at an elevated point leading to decrease in instantaneous coefficient of friction. The Cd present in Figure 6.11 (c) has dominant elevated point at the sides of the contact interface, leading to decrease in instantaneous coefficient of friction.

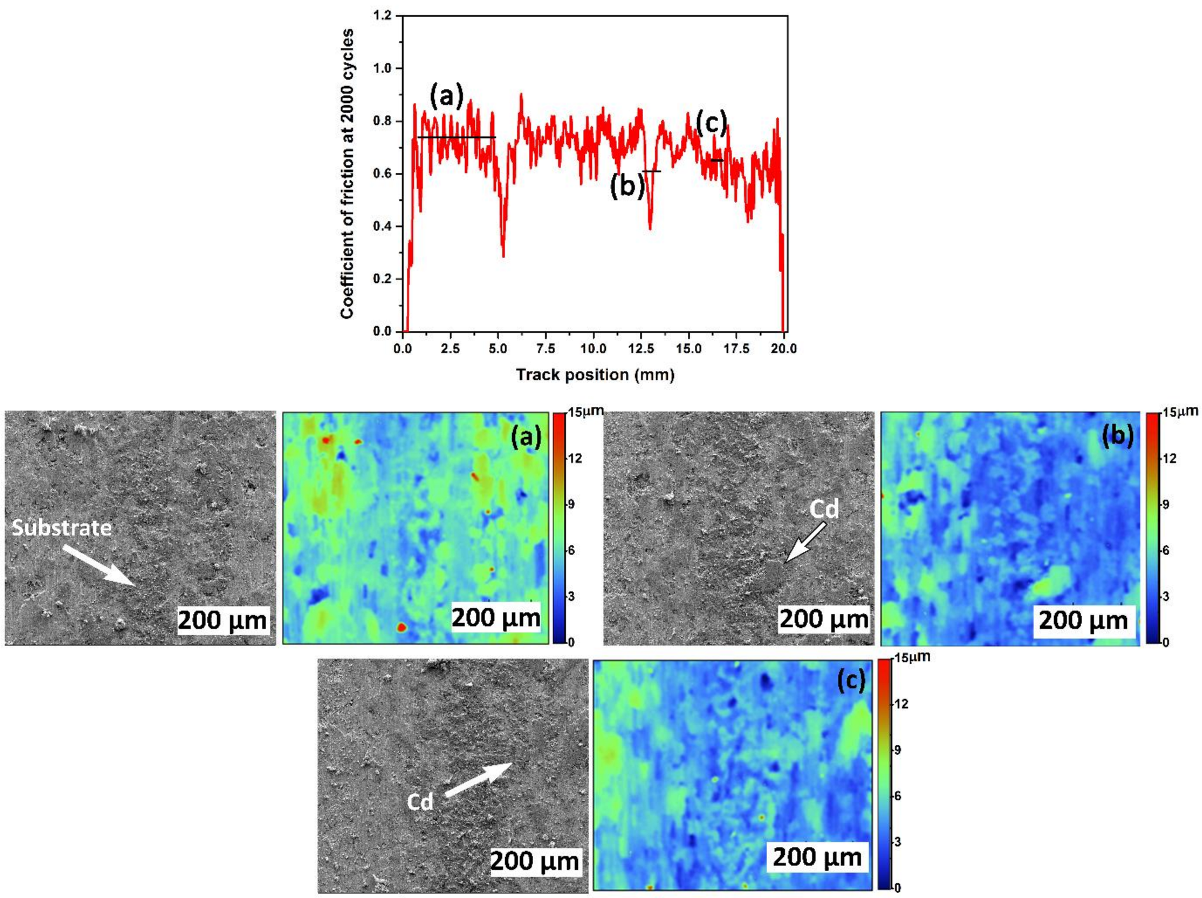

Figure 6.11 Coefficient of friction with track position at end of test (2000 cycle) showing (a) Elevated Fe substrate (b) Cd coating present at the contact interface (c) Cd present at an elevated region on the sides of the contact interface

6.3.2.3 Average Friction and Spatial Friction at RH 0

The decrease in relative humidity to 0% or dry air (RH0) at initial maximum Hertzian contact stress of 390 MPa (see Figure 6.12) leads to discrete and reoccurring temporal feature (transfer film) formation (Regime I) till 148 cycles. The occurrence of discrete temporal features is more frequent within Regime II as compared at RH60 and RH30, increasing the average coefficient of friction. Low average friction within Regime II persists till the end of the test. The cycles required for transition from Region I to Region II associated with temporal features cannot be correlated with varying relative humidity due to bulk surface layer removal occurring within few hundred cycles.

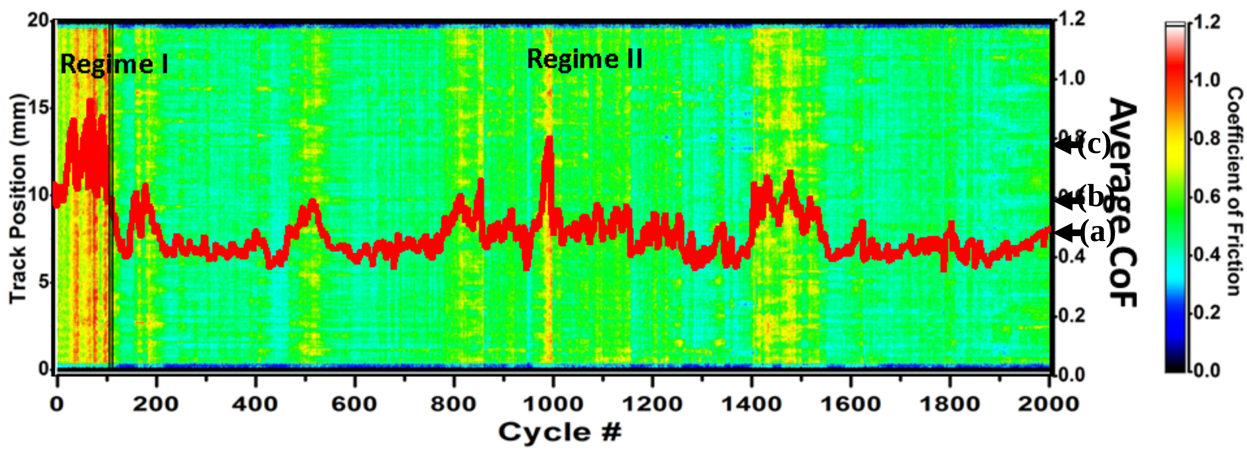

Figure 6.12 Triboscopic image overlapped with average coefficient of friction indicating frequent occurrence of transfer film as compared to RH60 and RH30.

The change in instantaneous coefficient of friction with respect to track position at the end of the test is investigated as shown in Figure 6.13. The fluctuation in instantaneous coefficient of friction within one cycle is less as compared at RH60 and RH30. Figure 6.13 (a), (b) and (c) shows the wear track morphology of the coating (with average coefficient of friction of 0.5) in Regime II. The wear track morphology observed by SEM indicates presence of steel substrate but the contact interface has scattered wear debris and patches of Cd. Wear debris scattered on the wear track till the end of test delays the onset of steel on steel contact.

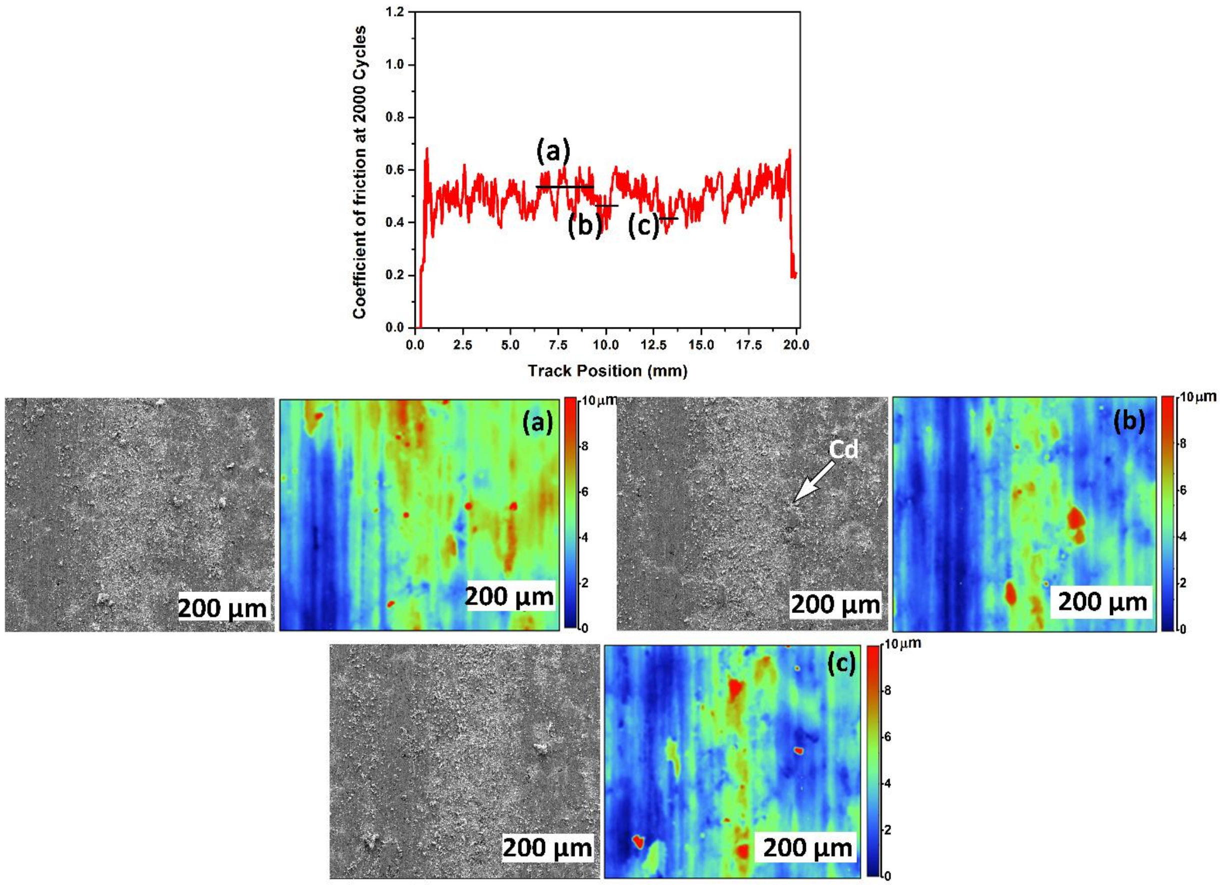

Figure 6.13 Coefficient of friction with track position at end of test (2000 cycle) showing (a), (b) and (c) wear debris scattered on the surface with steel and Cd

6.3.3 Spectral Analysis

Frequency count distribution of the instantaneous coefficient of friction identified as temporal features from the triboscopic image is done to observe the change in third body morphology with change in relative humidity. The change in transfer film morphology with change in relative humidity is identified by statistical analysis of the instantaneous friction coefficient of the temporal features (associated with transfer film morphology as studied in chapter 5).

The relative frequency distribution with instantaneous coefficient of friction in Regime I is shown in Figure 6.14. At RH60, the distinct temporal features in Regime I starts at 44 and 107 cycle, with instantaneous friction coefficient frequency distributed between 0.45 to 0.75 and maxima frequency at 0.6. At RH30, the discrete temporal features in Regime I has instantaneous friction coefficient frequency distribution between 0.50 and 0.85 with maxima frequency at 0.75 during initial cycles which later changes to 0.8. The maximum frequency distribution at RH30 is at 0.75 as compared to 0.8-0.9 at RH0, indicating the difference in third body morphology. The discrete temporal features in Regime I at RH0 has instantaneous frequency distribution between 0.60 and 1.0 with maxima frequency of 0.8 at initial cycles which later changes to 0.9. The difference in instantaneous coefficient of friction distribution with change in relative humidity signifies a change in third body morphology affected by the moisture content present in the ambient atmosphere.

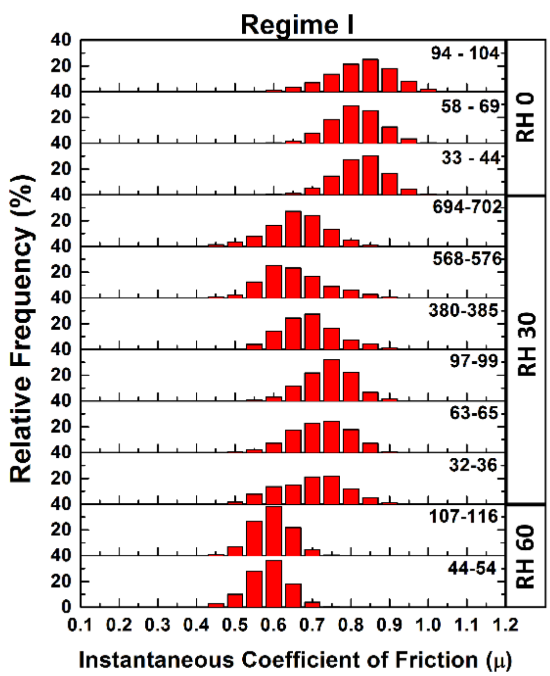

Figure 6.14 Spectral analysis of temporal features at varying relative humidity in Regime I indicating change in relative frequency counts with change in relative humidity.

At Regime II (see Figure 6.15); relative frequency distribution is more uniform as compared to Regime I (see Figure 6.14). At RH60, instantaneous coefficient of friction varies from 0.2 to 0.6 as compared to distribution of 0.45 to 0.75 during Regime I. In Regime II at RH30, the maxima of frequency distribution changes as compared at RH60. At RH0, the maxima of the instantaneous coefficient of friction and relative frequency is at higher value as compared to RH30 and RH60. This change in instantaneous coefficient of friction distribution in Regime II also indicates change in third body morphology with change in relative humidity.

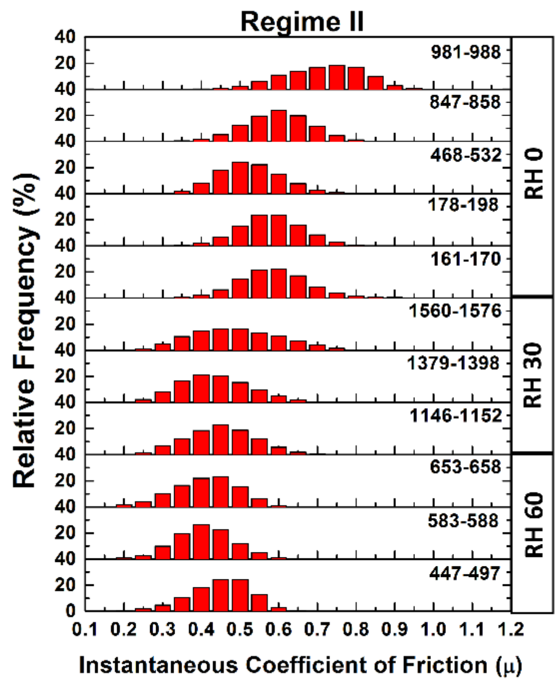

Figure 6.15 Spectral analysis of temporal features at varying relative humidity in Regime II indicating change in maximum relative frequency counts with change in relative humidity.

The frequency distribution at RH60 in Regime III (see Figure 6.16) varies from 0.5 to 0.85. Comparing the frequency distribution at RH60 in Regime I, Regime II and Regime III, relative frequency distribution at Regime I has maxima of 0.6 but this distribution becomes more uniform at Regime II and Regime III, indicating change in third body morphology (size and distribution) with progress of test. At transition region (RH30), the temporal features are more sporadic as seen from triboscopic image (Figure 6.11). From the spectral analysis, the frequency distribution changes from 0.4 to 0.9, indicating dominant effect of wear track along with the transfer film.

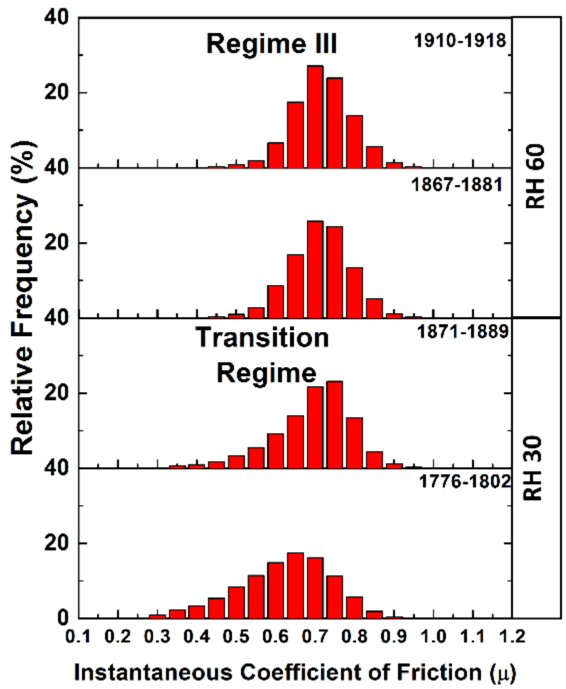

Figure 6.16 Spectral analysis of temporal features at varying relative humidity in Regime III at RH60 and Transition Regime at RH30.

6.3.4 Wear Track Analysis

Table 6-2 shows the effect of relative humidity on on-set of Regime II and Regime III. With decrease in relative humidity, the on-set to Regime II is quicker. At RH0, the on-set of steel on steel contact (Regime III) is absent till the end of test.

Table 6-2 Mixed mode, Steel vs Steel contact of LHE Cd coating at different relative humidity from three tribological test

% Relative Humidity	Cycles to Regime II	Cycles to Transition	Cycles to Regime III
0	148, 175, 264	1878, 1754, --	--
30	216, 229, 272	1554, 1436, 1283	--
60	267, 286, 221	896, 863, 901	1570, 1401, 1338

The FTIR spectra of wear track and ternary phase diagram of Cd with oxygen and water is shown in Figure 6.17. FTIR spectra peaks are characteristic peaks of oxide and hydroxide formed on the wear track. The ternary phase diagram of atmospheric oxygen with Cd and humidity confirms the formation of both cadmium hydroxide and oxide. The CdO characterized from FTIR spectra is at 496 cm^{-1} which is present at all three-relative humidity. The characterization peak for $Cd(OH)_2$ overlaps with the CdO characterization peak at 496 cm^{-1}, the other characteristic peak for $Cd(OH)_2$ is at 1628 cm^{-1} (overlaps with Fe_3O_4) and at 3416 cm^{-1} (overlaps with Fe_3O_4). With increase in relative humidity in the atmosphere, the relative percentage of cadmium hydroxide and iron oxide formed on the wear track will increase. The peaks at 1011 cm^{-1} and 2929 cm^{-1} are identified as peaks corresponding to iron oxide [144].

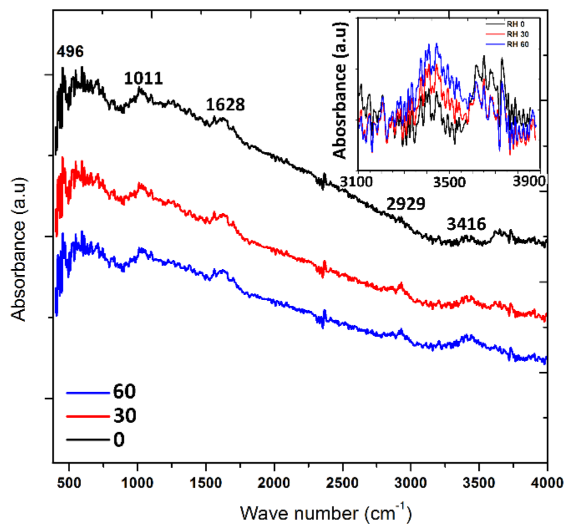

Figure 6.17 FTIR spectra of wear track and Ternary Phase diagram

Tribological test of uncoated steel substrate with steel countersphere at varying relative humidity is done to evaluate the efffect of substrate modification on the coefficient of friction evolution. Figure 6.18(a) shows average coefficient of friction with increasing number of cycles at different relative humidity. At RH0, the coefficient of friction is 0.85 and as the relative humidity of the the atmosphere is increased to RH 30 and RH 60, the coefficient of friction decreased to 0.57 and 0.45 respectively. Chemical analysis of the wear track by Raman spectroscopy is done to detect presence of Iron oxides and hydroxides. Characteristics peaks shown in Figure 6.18 (b) corresponds to Fe_20_3 with overlap of FeOOH, Fe_3O_4 and FeO peaks [145], [146].

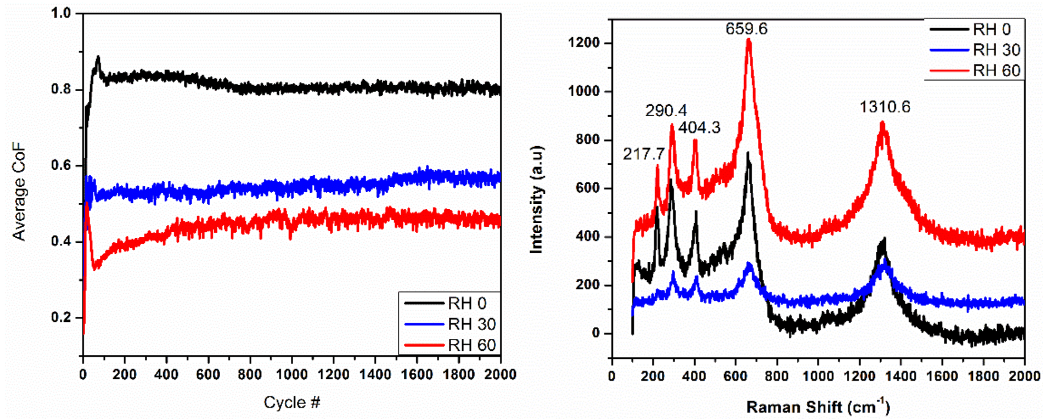

Figure 6.18 (a) Average coefficient of friction with cycle at varying relative humidity, (b) Raman Spectra of uncoated steel substrate wear track

6.4 Discussion

Sliding test of Cd coating using triboscopy method at varying relative humidity is studied and correlated with third body morphology. The difference in average coefficient of friction with progress of the test is due to the modification in third body morphology at the contact interface. Tribological behaviour evaluated for LHE Cd coating at RH 60 has four distinct regions of average friction coefficient as shown in Figure 6.19. Regime I is associated with high coefficient of friction due to formation of transfer film by adhesive wear, increasing the area of contact and friction force, observed as temporal features in triboscopic image (studied in Chapter 5). When the bulk layer of Cd is removed, the average coefficient of friction decreases due to mixed mode (Regime II). In Regime II, presence of wear debris and Cd coating acting as lubricant decreases the average coefficient of friction. In this region, the asperities of the steel substrate are at similar to that of Cd pockets. As the islands of Cd is depleted, the average coefficient of friction increases, termed as transition region. Regime III is associated with the depletion of the Cd pockets leading to increased lateral force due to increase in shear strength by steel on steel contact. Similar features was also observed by Sriraman et al. [72], they observed initial smoothening of the wear track due to adhesive wear with appearance of substrate steel during later cycles. The change in relative humidity modifies the contact conditions, leading to decrease in steady state friction regimes as shown in Figure 6.19.

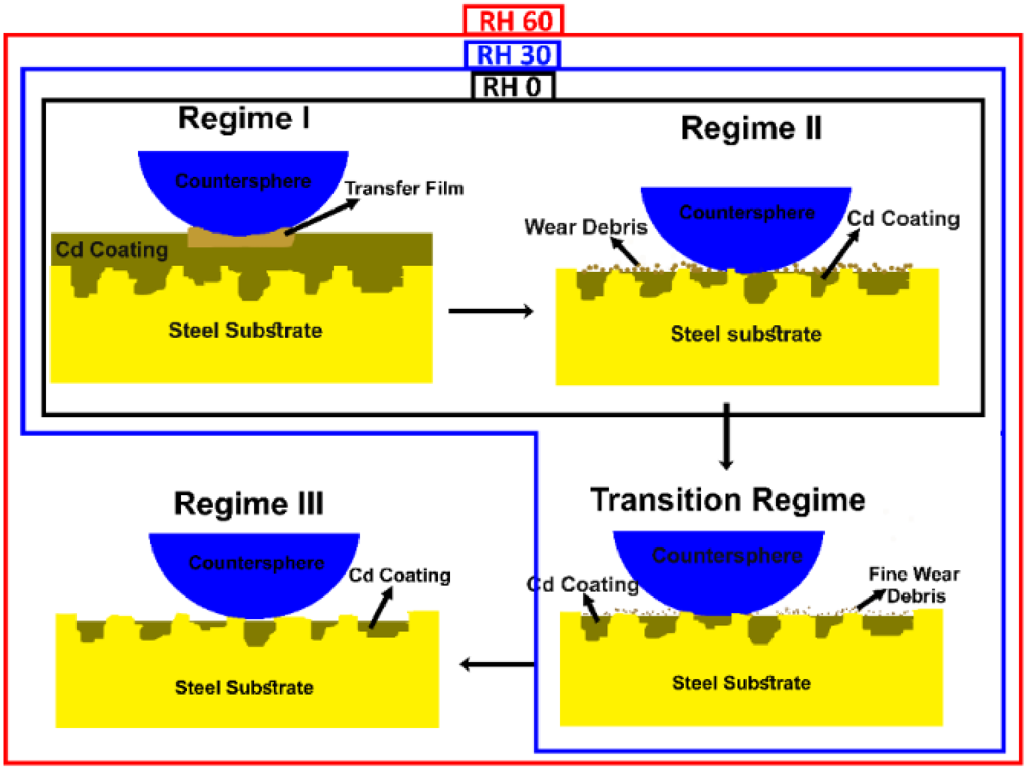

Figure 6.19 Schematic representation of change in average coefficient of friction with change in relative humidity

Spatial features observed from triboscopic image at the end of the test helped in better understanding of the evolution of instantaneous coefficient of friction. At RH 60, the increase in instantaneous coefficient of friction at Regime III is associated with presence and absence of Cd coating at the contact interface. The increase in instantaneous coefficient of friction is associated with depletion of Cd at the contact interface and protuberance of steel substrate. The regions with dominant Cd islands decreases this instantaneous coefficient of friction due to lubricating properties. At end of RH30, the average coefficient of friction is in Transition regime where the low instantaneous coefficient of friction is associated with presence of Cd layer at an elevated point on the wear track where as the presence of steel substrate increases the average coefficient of friction. At end of RH0, the average coefficient of friction is at Regime II where the wear debris is scattered throughout the contact interface with predominant steel countersphere with mixed mode of Cd and steel, leading to more uniform instantaneous coefficient of friction as compared at RH30 and RH60.

Spectral analysis of the triboscopic images used to compare the temporal features associated with transfer film morphological change at varying relative humidity helped in better understanding the effect of humidity. When the relative humidity is increased to higher percentage, the attachment of wear debris in the contact region decreases (seen by less frequent occurrence of temporal features in triboscopic image). Comparing Regime I at different relative humidity, it can be observed that the maximum relative frequency distribution is 0.6 at RH 60 which increases to 0.75-0.8 at RH 30 and to 0.8-0.9 at RH 0 indicating a change in third body morphology. Similar trend is also observed in Regime II. Shockley et al. [27] showed similar trend of variation in friction distribution due to third body variation from morphological difference in the first body. From the wear track analysis by FTIR and Raman spectroscopy, it was found that presence of oxides and hydroxides groups formed during the tribological test can modify the tribological properties. With change in relative humidity, faster on set of steel-steel contact at higher relative humidity was observed.

6.5 Conclusions

The current study helped in better understanding the tribological behavior of Cd coating at varying relative humidity. Combining triboscopy method with wear track morphology helped in understanding the spatial evolution of the instantaneous coefficient of friction. spectral analysis of the temporal features helped in understanding the difference in third body morphology with change in relative humidity.

Tribological test at higher relative humidity for Cd coating revealed four distinct regions of average coefficient of friction at RH60. High coefficient of friction at Regime I was associated formation of transfer film by adhesion. Low average coefficient of friction at Regime II is associated with a mixed mode contact of steel countersphere with Cd and steel substrate. The gradual depletion of Cd coating at the contact interface leads to initiation of Transition regime and subsequent transition to a high coefficient of friction (Regime III) associated contact of steel countersphere with steel substrate. With decrease in relative humidity, the no. of regimes decreases due to change in third body morphology. Spatial features studied from the triboscopic image revealed that the presence of steel and Cd coating at the contact interface modifies the instantaneous coefficient of friction. The presence of elevated Cd as compared to steel substrate decreases the instantaneous coefficient of friction. Spectral analysis done on the temporal features of the triboscopic images signifies difference in third body morphology at varying relative humidity.

Acknowledgments

The authors like to thank Salim Brahimi for their inputs in this work. We would also like to thank Natural Science and Engineering Research Council Canada (NSERC), Boeing Research and Technology, Pratt and Whitney Canada, Héroux Devtek, Canadian Fastener Institute and Messier-Bugatti-Dowty for their financial support.

Chapter 7

7. Effect of Relative Humidity on Tribological Behavior of IVD and Electrodeposited Al Coating

P. Behera, L. Lee, K. R. Sriraman, R. R. Chromik & S. Yue

This chapter is a manuscript prepared for journal publication. In the 5th chapter, effect of transfer film morphology on evolution of friction coefficient with a sapphire and steel countersphere is correlated for Cd coating. The next chapter focused on effect of varying relative humidity and its effect on the third body morphology for Cd coating; detailed study of the wear track is done to correlate the changes in instantaneous coefficient of friction with wear track morphology. This chapter focuses on effect of Al coating morphology on the third body evolution and friction coefficient studied by *in situ* and blind test.

Department of Mining & Materials Engineering

McGill University, Montreal, QC, Canada H3A 0C5

7.1 Introduction

Bulk metallic materials withstand sliding motion due to space constraints in aerospace application. Most often, the use of metallic coating is necessary to optimise properties like sacrificial corrosion protection, torque tension behavior (specific to fastener application), friction and wear modification requirements that are not delivered by the bulk substrate [84], [47]. Soft metallic coating like Al forms transfer film [27], [47] at the contact interface, acting as an shear accommodation site. This chemically or mechanically altered material different from the first bodies is known as third bodies, a concept formulated by Godet [45] which alters the friction coefficient. The formation of third bodies helps in accommodating the velocity difference between the sliding first bodies at the interface [23], affecting the friction coefficient.

The dynamic nature of third body [22] formation and its circulation at the interface makes the friction coefficient correlation more complex. Blau [118] described that the formation of transfer film by gradual build up or sudden attachment at the interface can significantly alter the friction coefficient. To correlate these changes, *in situ* examination of either or both of the sliding surface is necessary. The study of these dynamic third body evolution at the contact interface can be done using a transparent counterbody to record the third body evolution with friction coefficient. Various *in situ* studies has been done recently to correlate the evolution of third bodies with friction coefficient [24], [27], [46], [50] signifying the importance of *in situ* method. One of the other method to monitor instantaneous coefficient of friction is by generating triboscopic image [53]. Triboscopy method proposed by Belin [29] uses a numerical imager to produce the data recorded for the full test, which has been used in combination with electrical contact resistance to understand non-metallic coating [30], diamond like coating [29], duplex coatings [54] and solid lubricants [32]. By combining the real-time imaging of the third bodies (*in situ*) with features formed on triboscopic image, a better correlation between transfer film morphology and friction coefficient can be established.

In situ studies done by Shockley et al. [28] on cold sprayed pure Al coating with a pin on disk tribometer observed change in coefficient of friction from 0.55 to 1.4 in dry atmosphere with frequent increase in friction coefficient at intermittent intervals. The sudden change in friction coefficient is attributed to stochastic nature of the transfer film formed during the tribological test. Kim et al. [95] observed variation in sliding time to attain steady state friction coefficient with change in relative humidity. The change in steady state friction coefficient was due to formation of hydrated Al at higher relative humidity, observed with X-ray photoelectron spectroscopy (XPS), energy dispersive X-ray spectroscopy (EDS), differential scanning calorimetry (DSC) and annealing methods. They also observed the reduction in debris size with increase in relative humidity and higher oxygen content due to the formation of amorphous hydrated material.

Commercially pure Al coatings [84], [102], [147] applied on high strength substrate materials are potential replacement coatings and are viable alternatives for Cd coatings due to its carcinogenic properties [148] and cyanide plating solution. Cd coatings are soft coatings, forming transfer film [72] at the contact interface in addition to sacrificial nature [149]. Al coating is also relatively soft coating as compared to steel substrate with sacrificial properties, forming transfer film [27] during sliding test. The deposition of Al coating by traditional aqueous media is difficult due to dissociation of water molecule and is preferably deposited by vacuum evaporation [84] or electrodeposition [85] in non-aqueous media, making the coating morphology different. The difference in coating morphology due to different deposition method [86] can form different third bodies, subsequently changing the velocity accommodation mechanism.

The current work focuses on studying the effect of different plating procedure and relative humidity on the tribological properties of Al coatings deposited on low carbon steel substrates. *In situ* method and triboscopy method are used to correlate the dynamic nature of the third bodies with the friction coefficient. A linearly reciprocating ball-on-flat tribometer equipped with an optical microscope is used to observe the transfer film morphology (*in situ* studies). A steel countersphere is used with the same equipment to perform blind test.

7.2 Experimental Methodology

7.2.1 Plating conditions and coating characterization

Ion Vapor Deposited (IVD) Al coatings [99] were prepared in a vacuum deposition chamber. AISI 1018 low carbon steel was used as substrate material, the substrate material is grit-blast [59] prior to the coating process. The steel substrate was kept at a negative bias, Al wires were melted by resistor heating at 800-840 ^{0}C and evaporated to get a coating thickness of 20-25 μm on substrates. Just after the coating, the surface of the Al coating was glass bead peened to close the surface pores. Finally a chemical conversion coating [100] was done to generate a passivation layer. The tribological test was performed on coupons of 50 mm x 50 mm.

The electrodeposition of Al coating was done in an aprotic (water free) organic plating solution using a patented process used by Alumiplate Inc. [101]–[103] on AISI 1018 low carbon steel substrate after grit-blasting [59]. After coating, a chemical conversion coating [100] was done to generate a passivation layer. The tribological test was performed on sheared coupons of 50 mm X 50 mm.

Scanning electron microscopy (SEM) investigation of the surface and cross-section of the coating was done using a field emission gun of Philips FEI Inspect F-50 SEM equipped with EDS detector. X-ray diffraction of Al coatings was done by Bruker discover D8 diffractometer with 2D HISTAR area detector, source of Co Kα radiation (1.79 Å) at 35 kV and 45 mA and indexed from ICDD JCPDS Standards.

7.2.2 Tribological Test Parameters

The tribological tests were carried out with a linearly reciprocating ball on a flat tribometer [52]. For *in situ* tests, the counterface was a sapphire hemisphere (3.175 mm radius) with a track length of 10 mm and sliding velocity of 3 mm/s, while for standard tribology tests (blind test) a 440C steel countersphere (3.175 mm radius) was used with track length of 20 mm and sliding velocity of 14 mm/s. The normal load applied at the contact was set with dead weights applied on the arm. For *in situ* test, 0.871 N was applied, while for blind test 1.3 N was used. This led to an initial maximum Hertzian contact stress of 370 MPa for *in situ* test and 440 MPa for blind test. The friction force was measured with a piezoelectric sensor at a sampling rate of 800 Hz. The spatial resolution of the friction measurements was on the order of 20 μm, which was smaller than theoretical contact radius calculated according to Hertzian [44] two body contact theory (sapphire countersphere – 33.8 μm and steel countersphere – 38.2 μm). The coefficient of friction value was plotted as a color coded map as a function of track position and cycle number to generate what is often termed a “triboscopic image” [30], representing the spatial and temporal evolution of the friction coefficient.

For *in situ* tests, a video camera attached to an optical microscope with 10x optical zoom objective was used to record video of the contact through the sapphire hemispherical counterfaces and to study the third body evolution during the test. The video of the test was paused at the desired cycle number and track position, a snapshot was captured describes as *in situ* micrograph.

The relative humidity during *in situ* test was maintained at RH0 (0% relative humidity). For blind test, the relative humidity was varied as RH0, RH30 and RH60 by passing dry air and humidified air to the instrument enclosed within a high-density polyethylene bag. The relative humidity for both test was within the standard deviation of ±5% at 23 °C. The total number of cycles for *in situ* test was 1600 cycles leading to total sliding distance of 32 meters whereas for blind test the total number of cycles was 2000 cycles leading to a total sliding distance of 80 meters. Sampling rate (800 Hz) and spatial resolution (20 µm) was same for both *in situ* and blind test.

7.3 Results

7.3.1 Coating Characterization

XRD phase analysis of coatings shown in Figure 7.1 correspond to FCC Al phase. The cross-section and surface morphology of Al coating deposited by ion vapor method and electrodeposition method is shown in Figure 7.2. The cross-section of IVD Al coating is uniform with few through thickness cracks, the cross-section also indicates a columnar microstructure of the coating. The surface morphology of IVD Al coating is porous structure as observed from the cross-section morphology. The cross-section of electrodeposited Al coating is uniform with no cracks; the surface morphology of the electrodeposited Al coating has bright particles scattered over the surface. Spot analysis of these bright particles (not shown in this article) was found to be oxygen rich particles formed during the electrodeposition process. The platelet size of IVD Al coating is much smaller than the platelet size of electrodeposited Al. The average thickness of IVD Al coating is 25 ± 2 µm and average thickness of electrodeposited Al coating is 20 ± 2 µm.

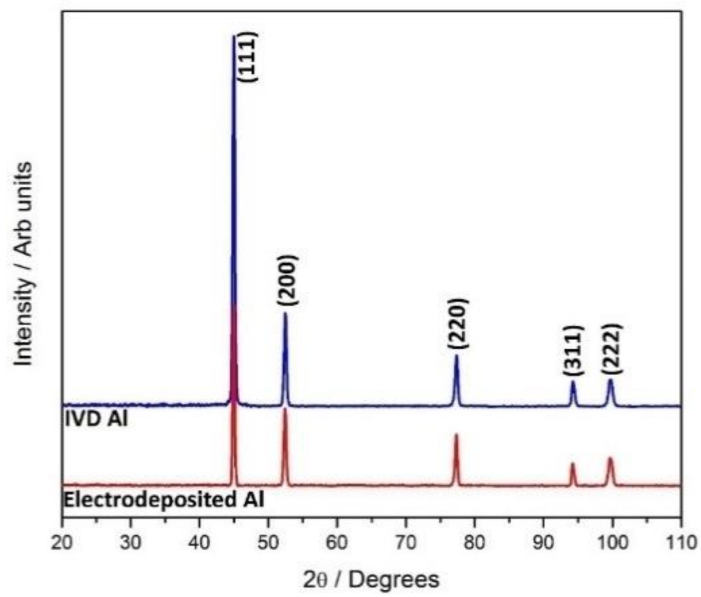

Figure 7.1 XRD Characterization of Al coatings indicating pure Al coating after deposition process

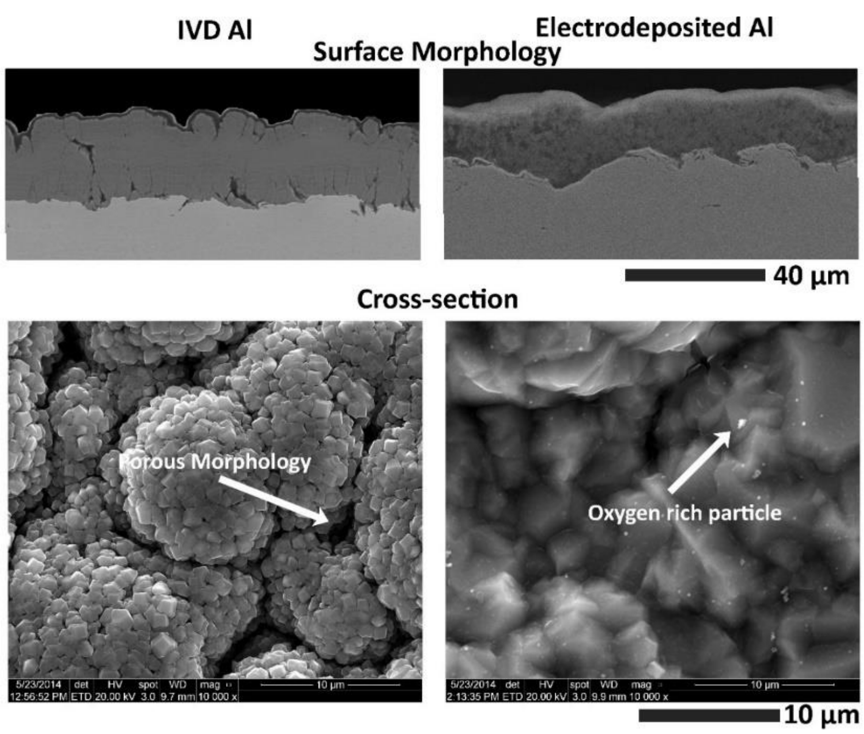

Figure 7.2 Surface and cross-section morphology of Al coating

7.3.2 In situ and Triboscopic study

7.3.2.1 IVD Al

In situ images of transfer film at cycles 20 and 40 for IVD Al coating is shown in Figure 7.3. With increase in no. of cycles, the transfer film area increases and the wear track widens. Cycle 20 indicates a bright patch of transfer film formed at the contact interface, which increases in size at 40 cycles. In addition to increase in transfer film size, formation of wear debris at periphery of the contact area is also observed.

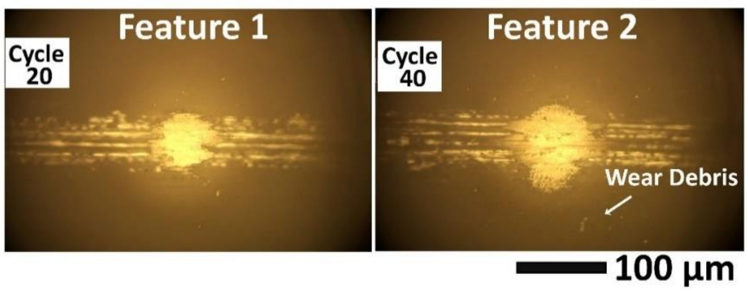

Figure 7.3 Transfer film morphology observed by in situ test at 20 and 40 cycles

The *in situ* image at 1000 cycles indicate replenishment of some previously formed holes seen at 830 cycles with formation of new holes as shown in Figure 7.4. At 1060 cycles, the *in situ* micrograph of transfer film indicates replenishment of holes present previously at 1000 cycles by adhesion leading to transfer film replenishment. The formation of holes and its subsequent replenishment shows the dynamic nature of transfer film with increase in sliding cycles.

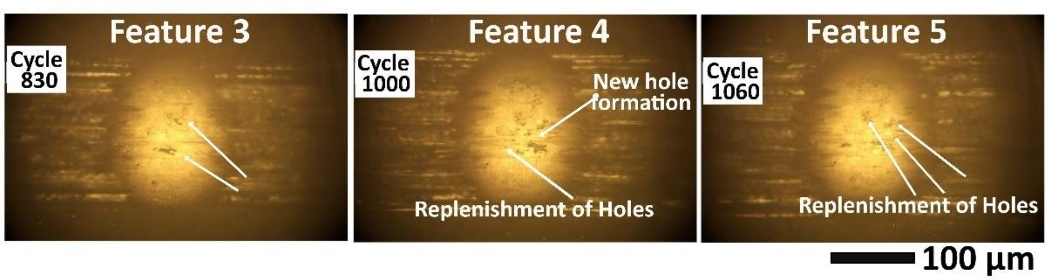

Figure 7.4 Transfer film morphology observed by in situ test at 830, 1000 and 1060 cycles

The *in situ* micrograph investigated at 1160 cycles has formation of scoring marks (characterized as horizontal scratches) on the transfer film as shown in Figure 7.5. The scoring marks increases at 1180 cycles. Some of the scoring marks visible at 1180 cycles is replenished at 1305 cycle, characterized as sudden increase in average coefficient of friction as shown in Figure 7.6. At 1305 cycles, the replenishment of the transfer film and decrease in hole and scoring marks can be attributed to formation of new transfer film and subsequent increase in average coefficient of friction (shown in Figure 7.6). The disintegration of bulk transfer film is observed at 1400 cycles with decrease in friction coefficient (shown in Figure 7.6 as feature 9). Though the bulk of transfer film is removed, the presence of transfer film at the top portion of contact interface modifies the friction coefficient. At the end of the test (1600 cycles), most of the transfer film is removed with exception at the sides of the contact interface.

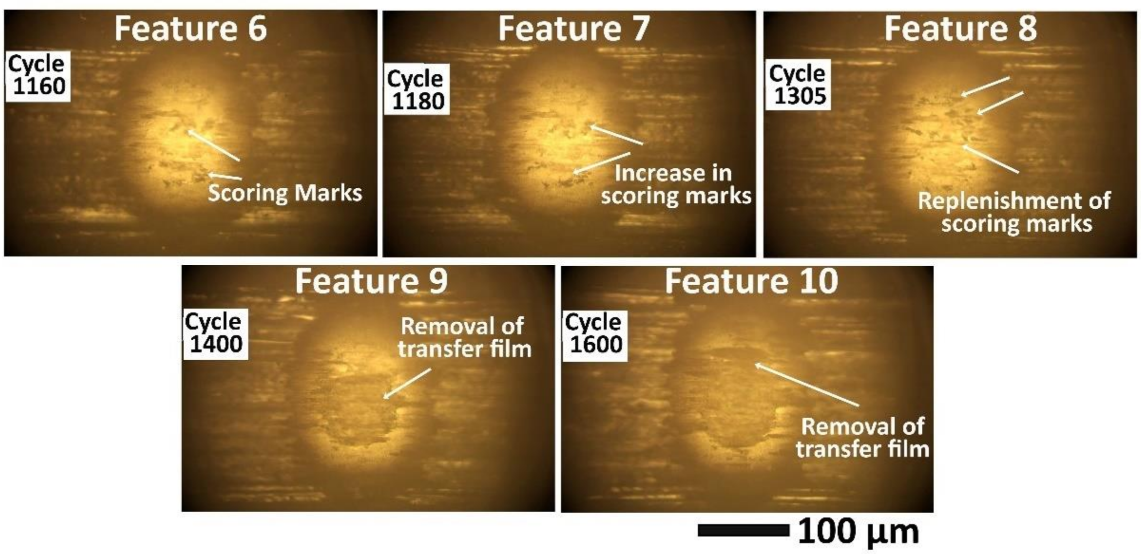

Figure 7.5 Transfer film morphology observed by in situ test at 1160, 1180, 1305, 1400 and 1600 cycles

The formation of transfer film on the sapphire countersphere conceals the contact region making it difficult to correlate the change in instantaneous coefficient of friction identified from the triboscopic image with corresponding track position. Thus, the transfer film morphology evaluation is done by correlating the features identified for few cycles associated with formation and removal. The triboscopic image of full cycle superimposed with the average friction coefficient with corresponding features identified from *in situ* test is shown in Figure 7.6. At cycle 20 and 40, both features correspond to high coefficient of friction region in the triboscopic image (shown as feature 1 and 2 in Figure 7.6). The abrupt increase in average coefficient of friction at 830 cycles can be associated with hole formation and subsequent replenishment of transfer film (shown as feature 3 in Figure 7.6). The triboscopic image investigated at 1000 cycles (shown as feature 4) has low average coefficient of friction due to higher number of holes as compared to 830 cycles. At 1060 cycles, the *in situ* micrograph of transfer film (shown in Figure 7.4) indicates replenishment of holes present previously at 1000 cycles indicating increase in coefficient of friction due to replenishment of transfer film (shown as feature 5). The scoring marks increases at 1160 and 1180 cycles leading to a decrease in average coefficient of friction (shown as feature 6 and 7). The replenishment of some scoring marks and holes at 1305 cycles increases the average coefficient of friction, observed as feature 8. At 1400 and 1600 cycles, the removal of the transfer film is associated with low average coefficient of friction observed as feature 9 and 10. By comparing the features from *in situ* imaging and triboscopy, the formation of hole, scoring marks and its replenishment is associated with temporal features in triboscopic image. Due to the concealment of buried interface, all the features identified from triboscopic image are not related to the transfer film morphology.

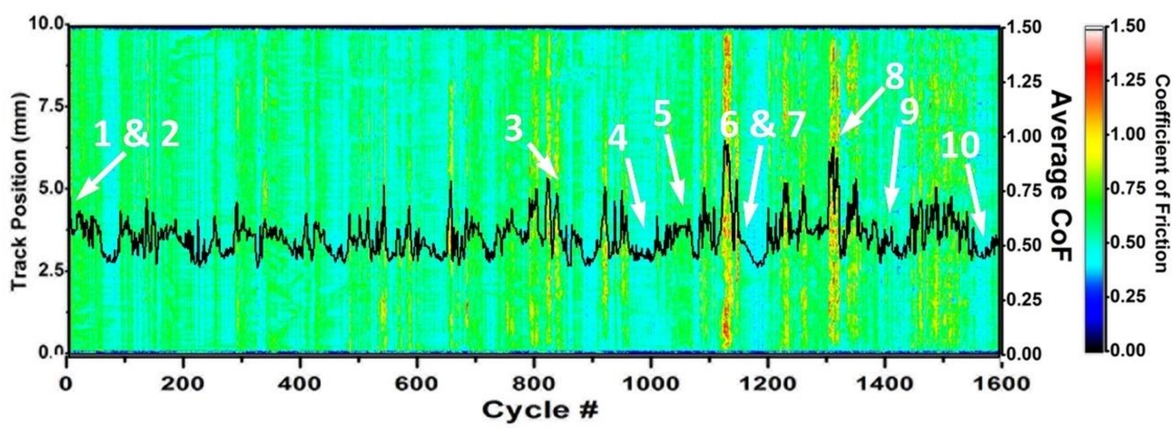

Figure 7.6 Triboscopic image of the full test and corresponding features identified from Figure 7.3, Figure 7.4 and Figure 7.5

7.3.2.2 Electrodeposited Al

The formation of extensive transfer film with sapphire countersphere for electrodeposited Al is similar to IVD Al. Similar concealment of contact interface makes it difficult to investigate and correlate the changes in transfer film morphology within one cycle from the triboscopic image. The *in situ* image of the transfer film formed at the interface is shown in Figure 7.7, more stochastic change in morphology of the transfer film was observed for electrodeposited Al compared to IVD Al coating. At 8 cycles, the transfer film becomes unstable and patches of transfer film were removed as shown in Figure 7.7. At cycle 14, the transfer film area is increased with replenishment of the hole observed at 8 cycles with additional new hole formation. At 80 cycle, the transfer film area has increased with a few holes present on the periphery of the transfer film.

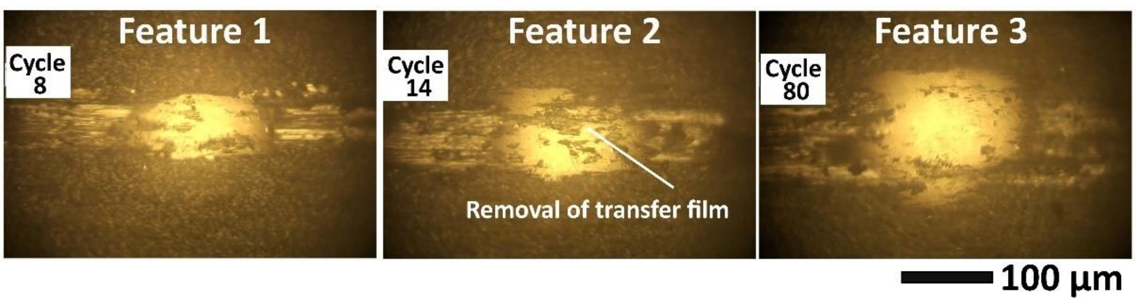

Figure 7.7 Transfer film morphology observed by in situ test at 8, 14 and 80 cycles

At 243 cycles, the transfer film became unstable with formation of scoring marks as shown in Figure 7.8. Some of the previously formed scoring marks at 243 cycles are replenished with formation of new scoring marks at 280 cycles. Similar features are also observed at 493 cycles. The scoring marks formed at 493 cycles is replenished at 506 cycles. At 520 cycle, the transfer film formed at the interface is again removed but the replenishment is gradual (not shown). At 955 cycle, the transfer film is again replenished.

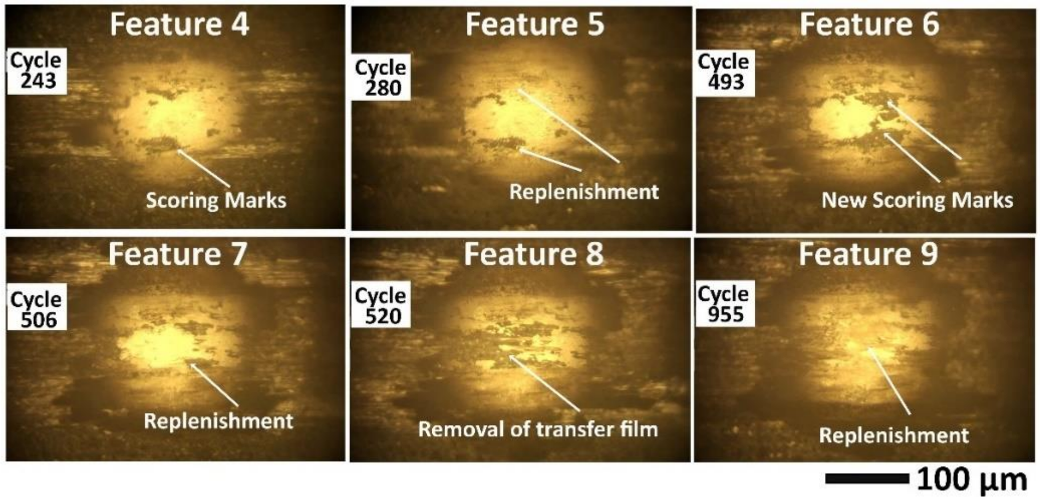

Figure 7.8 Transfer film morphology observed by in situ test at 243, 280, 493, 506, 520 and 955 cycles

The third body morphology observed at 1050 and 1350 cycles have extensive scoring, with removal of the transfer film as shown in Figure 7.9. At the end of test (1600 cycles), the transfer film is completely removed with sapphire contact.

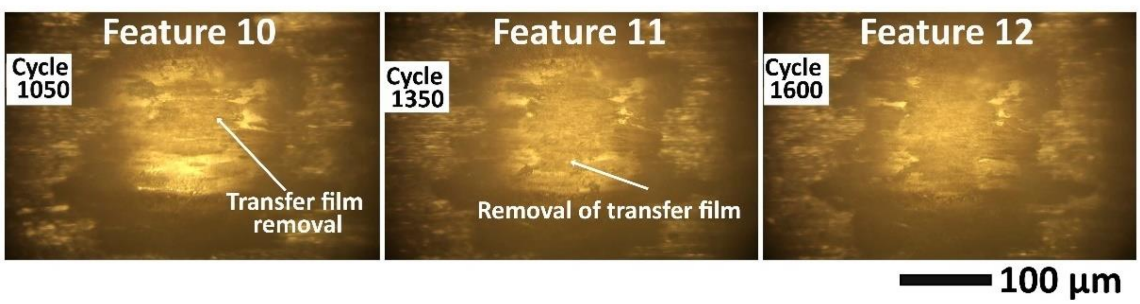

Figure 7.9 Transfer film morphology observed by in situ test at 1050, 1350 and 1600 cycles

The triboscopic image overlapped with the average coefficient of friction is shown in Figure 7.10. Some of the temporal features observed from triboscopic image can be correlated with the *in situ* features observed. The high coefficient of friction associated with the transfer film removal and replenishment at the initial part (upto approx. 20 cycles) is shown as feature 1 and 2. The temporal feature associated with high average coefficient of friction at 80 cycles is due to replenishment of transfer film at the contact interface. The temporal features associated with high coefficient of friction for 8-10 cycles (at approx. 250 cycles) is difficult to interpret because of the concealed contact interface. At 280 cycle, it can be observed that the hole formed at 243 cycle is partially replenished after sudden increase in average coefficient of friction, associated with formation of new transfer film and replenishment of previously formed scoring marks (shown as feature 4 and 5). The replenishment of scoring marks at 493 cycle and 503 cycles is associated with increase in average coefficient of friction shown as feature 6 and 7. At 520 cycle, the transfer film formed at the interface is again removed (with lower average coefficient of friction shown as feature 8) but the replenishment is gradual with no distinct temporal features visible upto 950 cycles (feature 9 is identified as high average coefficient of friction due to formation of transfer film). At 955 cycle, the hole is again replenished (feature 9 in Figure 7.9) with formation of temporal feature on the triboscopic image. The subsequent removal of this transfer film is associated with low average coefficient of friction shown as feature 10 (1050 cycles). At 1350 and 1600 cycles, the removal of the transfer film is associated with low average coefficient of friction, shown as feature 11 and 12.

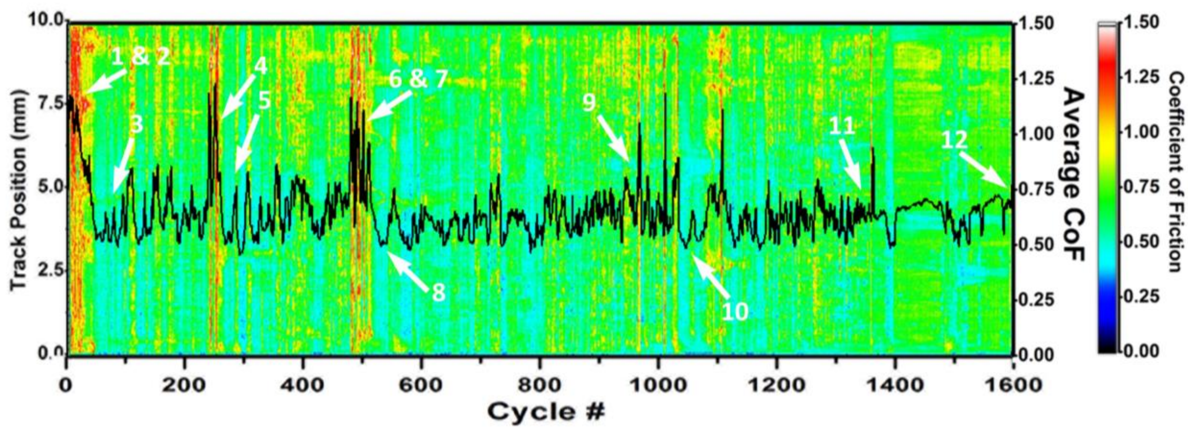

Figure 7.10 Triboscopic image of the full test and corresponding features identified from Figure 7.7, Figure 7.8 and Figure 7.9

7.3.3 Blind Test

In situ test performed on both coatings showed formation of transfer film at the contact interface. A dissimilarity in transfer film morphology was observed between IVD and electrodeposited Al coatings. In this section, tribological evaluation of both IVD and electrodeposited Al coating is done with a steel countersphere to simulate engineering contact conditions. The tribological test is performed at three different relative humidity to observe the change in third body morphology and its effect on the tribological behavior of coating.

7.3.3.1 RH 60

The tribological test for IVD and electrodeposited Al coating is done at RH60. Average coefficient of friction overlapped with triboscopic image for IVD Al coating and electrodeposited Al coating is shown in Figure 7.11. Comparing the triboscopic image, IVD Al coating has no discrete temporal features formed whereas electrodeposited Al coating has discrete temporal features formed. The variation in the temporal features can be attributed to formation of transfer film and its removal and replenishment observed more frequent for electrodeposited Al coating as compared to IVD Al. The high average coefficient of friction for IVD Al coating at initial cycle is due to initial run-in period with transfer film formation by adhesion. At 100 cycles the decrease in the average coefficient of friction continuing upto 1000 cycles is due to change in contact conditions. In comparison to IVD Al coating, electrodeposited Al coating has distinct temporal features at the start of the tribological test with higher average friction coefficient than IVD Al coating, the transition from average CoF of 1.1 to 0.4 for electroplated Al coating takes place at later cycles (approx. 150 cycles for electroplated Al coating as compared to 100 cycles for IVD Al). Although the transition of average CoF from 1.1 to 0.4 for electrodeposited Al coating takes place at a much later stage, the transition from average CoF from 0.4 to 0.8 for electrodeposited Al coating takes place at earlier cycles (approx. 400 cycles) as compared to IVD Al coating. The difference in transfer film formation and stability at the contact interface for IVD and electrodeposited Al observed as temporal features from triboscopic image leads to a difference in average coefficient of friction.

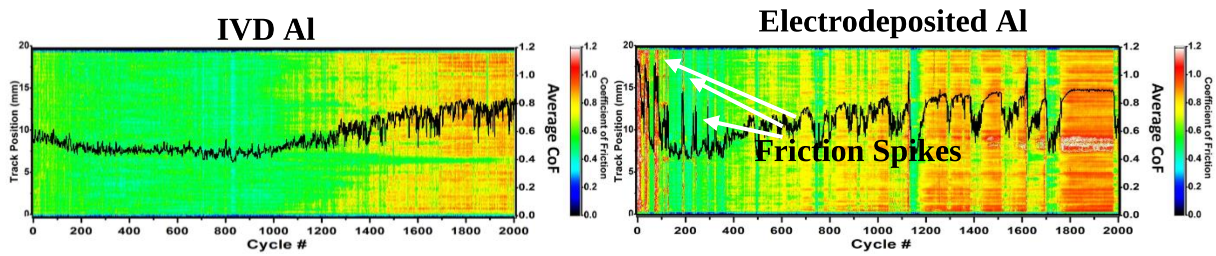

Figure 7.11 Average CoF overlapped with triboscopic image of IVD Al coating and Electrodeposited Al coating indicating the difference in tribological behavior of Al coatings deposited by different methods

The difference in triboscopic image and average coefficient of friction between IVD and electrodeposited Al coating is studied in detail and correlated with the wear track morphology of the coating after 50, 500 and 2000 cycles. EDS spot analysis of the wear track features done for qualitative analysis of different features is shown in Figure 7.12. At 50 cycles, both the coatings have adhesive wear due to plastic deformation and smearing of the soft Al coating. The wear track width of electrodeposited Al coating is larger as compared to IVD Al coating. At 500 cycles, the wear track morphology of both the coatings changes from adhesive feature (observed at 50 cycles) to wear debris scattered on the surface. The wear debris observed for IVD Al coating contains higher amount of oxygen as compared to 50 cycles (spot 3 and 4), few spots of adhesive features (spot 5) are also present. The wear track morphology of electrodeposited Al coating is similar to IVD Al coating at 500 cycles, but EDS analysis of the wear track indicates much difference in the chemical composition (Fe substrate peak observed for electrodeposited Al coating). At 500 cycles, the spot analysis of few morphologically different features on the wear track indicates presence of Fe peaks in addition to Al and O. Oxygen present in the wear track at 500 cycles is amorphous oxide of Al and doesn’t correspond to stoichiometric Al_2O_3 composition (determined from EDS spot analysis). At the end of the test (2000 cycles), the wear track morphology of IVD Al coatings has scattered fine wear debris on the surface as compared to electrodeposited Al coating with lower amount of wear debris. Wear track EDS spot analysis of IVD Al coating indicates the presence of Al and oxygen where as for electrodeposited Al coating, Fe substrate peak is also observed in addition to Al and O.

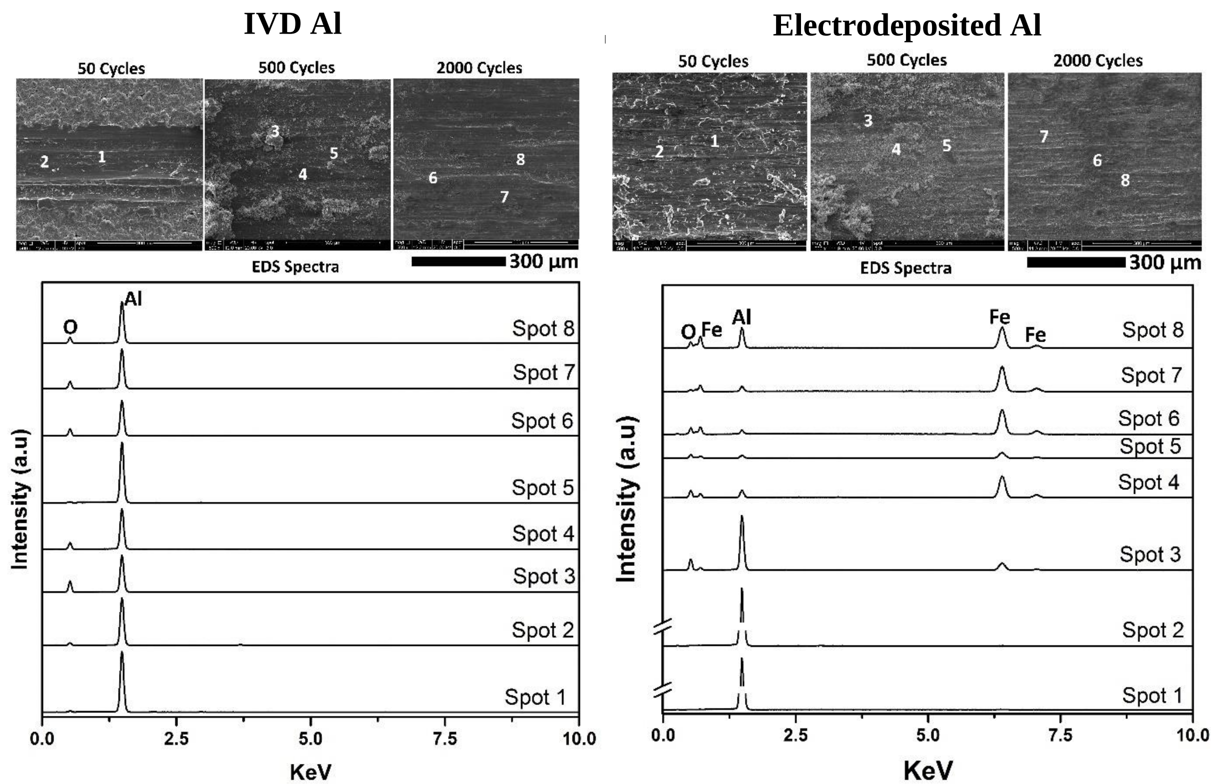

Figure 7.12 Wear Track Morphology and EDS analysis of IVD and electrodeposited Al coating. Additional Fe substrate peaks are observed for electrodeposited Al coating as compared to IVD Al coating with only Aluminum and oxygen

The countersphere observed after 2000 cycles sliding test at RH60 for IVD Al coating has wear scar at the contact interface (shown in Figure 7.13). Additional adherence of wear debris at the periphery of the contact region was observed. The diameter of the wear scar was measured to be 672 ± 33µm. The wear track morphology at 2000 cycles has fine wear debris scattered on the surface. The wear debris ejected out from the contact interface deposited at the end of wear track is collected and studied with SEM. Agglomeration of fine wear debris particles is observed.

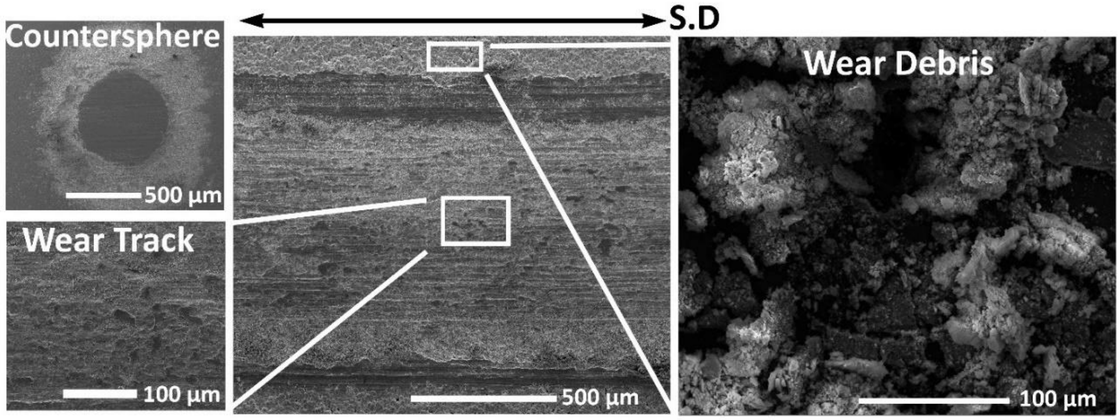

Figure 7.13 Countersphere, Wear track and Wear Debris at RH60 for IVD Al coating

The countersphere for electrodeposited Al coating has wear scar similar to IVD Al coating with fine particle type wear debris present at the contact interface as shown in Figure 7.14. The wear scar measured for electrodeposited Al coating is 709 ± 14 µm. The wear track morphology of electrodeposited Al coating has scattered wear debris at the contact interface, with some prominent dark patches indicating presence of Fe substrate (as observed from EDS analysis shown in Figure 7.12). The SEM image of the wear debris formed at the end of the test shows the presence of both fine and coarse wear debris. The wear debris observed for electrodeposited Al coating is flakier as compared to fine wear debris observed for IVD Al coating.

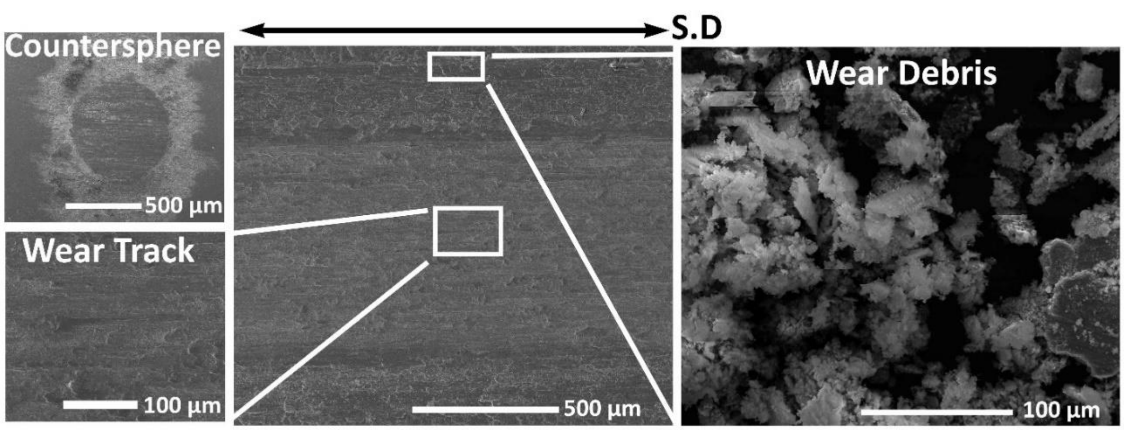

Figure 7.14 Countersphere, Wear track and Wear Debris at RH60 for Electrodeposited Al coating

Fine and agglomerated wear debris observed for IVD Al coating indicates extrusion of coating at the contact interface whereas the presence of flaky and coarse wear debris observed for electrodeposited Al coating indicates difference in average friction coefficient. The formation of fine wear debris for IVD Al coating has steady average coefficient of friction without any frequent fluctuation or spike whereas electrodeposited Al coating leads to frequent abrupt increase in average coefficient of friction till the end of the test.

7.3.3.2 RH 30

The average CoF vs cycle number for IVD Al coating and electrodeposited Al coating is shown in Figure 7.15. The abrupt increase in average friction coefficient was observed to be more frequent for electrodeposited Al as compared to IVD Al coating. The transition of average coefficient of friction to steady state of 0.8 is observed to be at lower cycles for electrodeposited Al coating as compared to IVD Al coating.

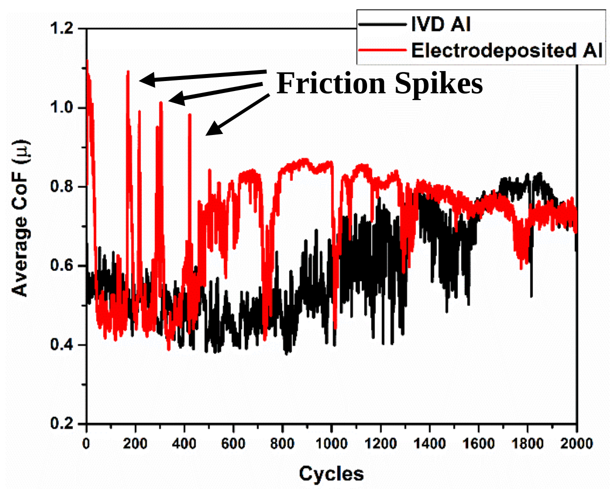

Figure 7.15 Average CoF vs Cycle of IVD and electrodeposited Al at RH30

SEM countersphere imaging has predominant contact of steel countersphere with the coating, the wear scar formed on the countersphere has fine wear debris sticking at the contact region in addition to scoring marks. Fine agglomerated wear debris are also present on the countersphere, formed by extrusion from the contact region. The wear track morphology shown in Figure 7.16 has fine wear present at the pockets. The wear debris deposited at the end of the wear track is coarser as compared at RH60 (shown in Figure 7.13).

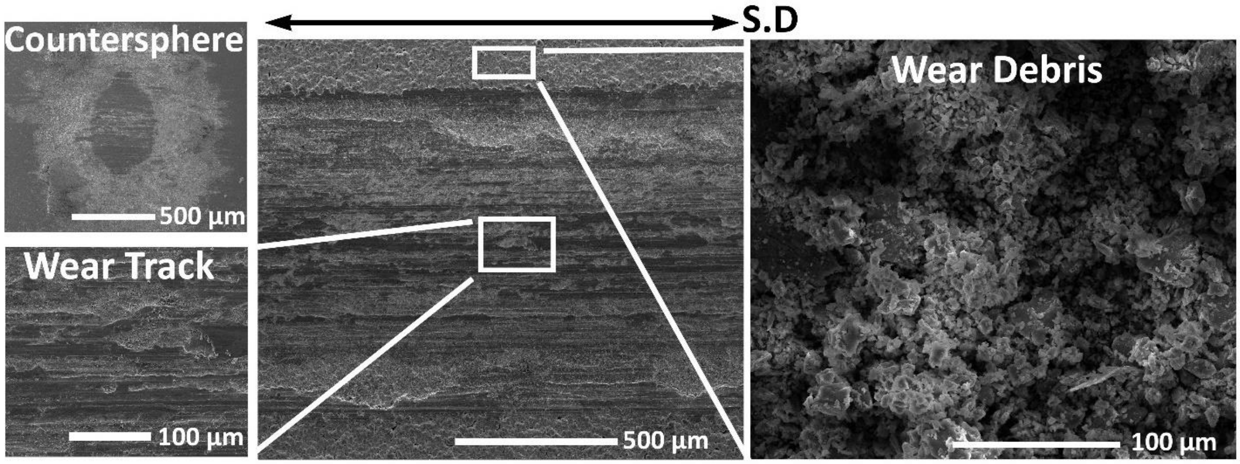

Figure 7.16 Countersphere, Wear track and Wear Debris at RH30 for IVD Al coating

SEM imaging of the countersphere shown in Figure 7.17 has similar morphology to that of IVD Al coating. The centre of the contact region has some fine wear debris with scoring marks. The wear track morphology has scoring marks formed in the sliding direction (Fe substrate peaks shown as dark patches) with Al coating present at the bright portion on the wear track. The wear debris morphology observed for electroplated Al has different morphology as compared to IVD Al at same relative humidity. The wear debris formed is flaky structure with features similar to the coating.

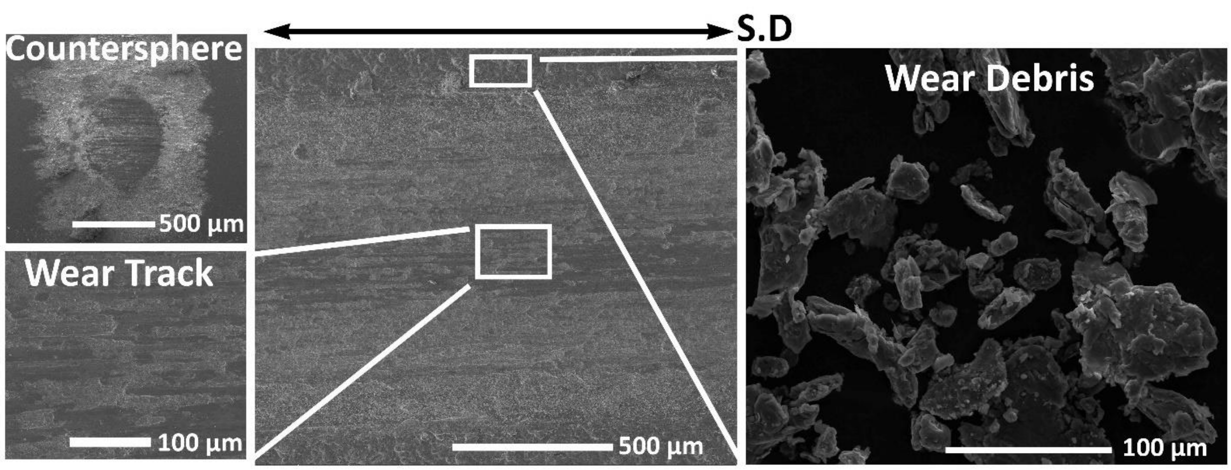

Figure 7.17 Countersphere, Wear track and Wear Debris at RH30 for electrodeposited Al coating

7.3.3.3 RH 0

The average CoF plotted with increasing cycle number for IVD and electrodeposited Al coating at RH0 (shown in Figure 7.18) is similar except at the initial run-in period. The abrupt increase in average coefficient of friction, characterized as friction spikes is similar for IVD and electrodeposited Al coatings.

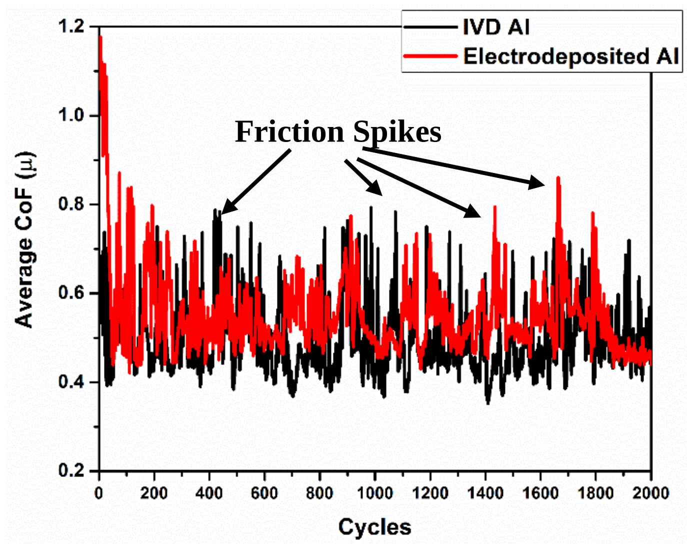

Figure 7.18 Average CoF vs Cycle of IVD and electrodeposited Al at RH0

The countersphere observed after 2000 cycles of sliding test by SEM has transfer film at the contact interface (shown in Figure 7.19) for IVD Al coating. The transfer film formed mostly consists of fine debris. Wear track has extensive scattered wear debris which are coarser as compared at RH30 and RH60, signifying a change in third body morphology. The wear debris obtained at the end of the wear track is flaky type with features of columnar IVD Al coating and delamination wear.

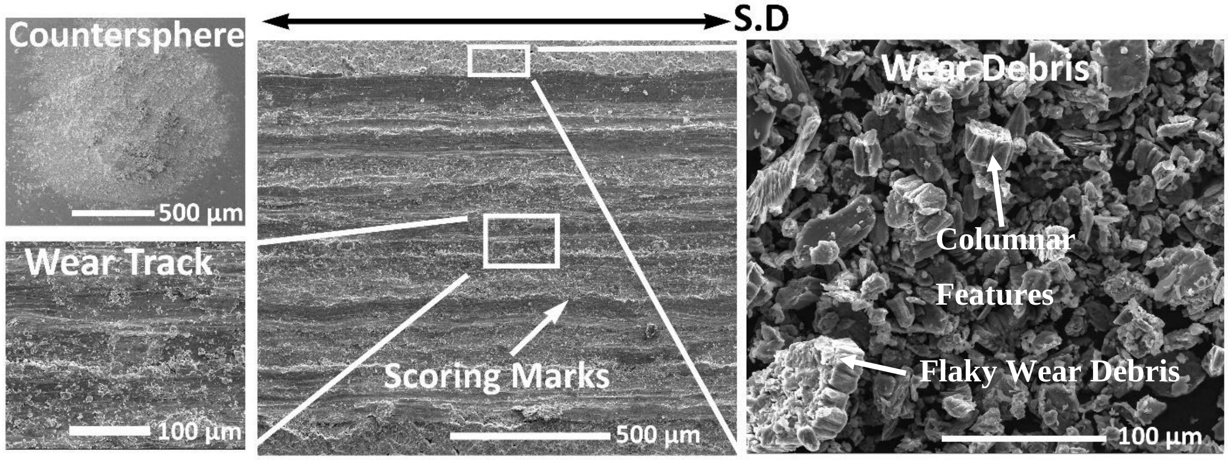

Figure 7.19 Countersphere, Wear track and Wear Debris at RH0 for IVD Al coating

The countersphere observed for electrodeposited Al coating has small patch of transfer film formed at the contact interface as shown in Figure 7.20. The wear track morphology is similar to that of IVD Al coating, coarse wear debris with presence of some adhesive features was observed on the wear track. The wear debris deposited at the end of the wear track is coarse with features similar to that of as-received coating.

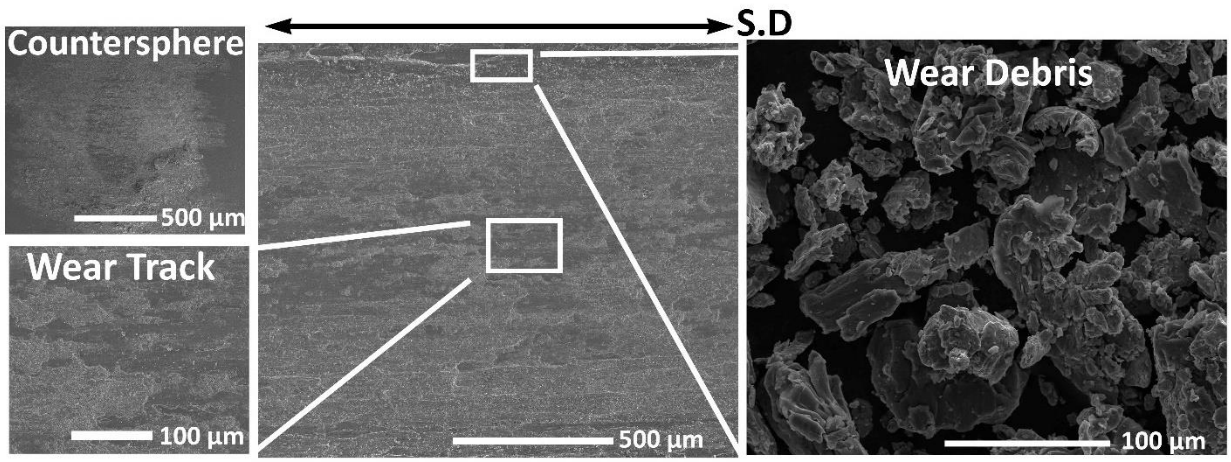

Figure 7.20 Countersphere, Wear track and Wear Debris at RH0 for electrodeposited Al coating

The average coefficient of friction for IVD and electrodeposited Al coating changes with change in relative humidity. The morphological difference between the wear track and wear debris formed after the sliding test indicates modification of third body morphology with change in relative humidity. Sliding test performed for IVD Al coating has a significant effect on the average coefficient of friction with change in relative humidity. At higher relative humidity, the formation of fine agglomerated wear debris with lesser wear debris present on the wear track indicates extrusion of the coating at the contact interface. At RH0, the wear debris formed is coarser with flaky structure. Electrodeposited Al coating shows the presence of both flaky and fine wear debris present at RH60, which changes to coarser morphology at RH0. The difference in wear debris morphology can be associated with frequent friction spikes observed for IVD Al coating at RH0, which decreases with increase in relative humidity. Electrodeposited Al coating has coarser wear debris present at varying relative humidity, showing friction spikes irrespective of the relative humidity.

7.4 Discussion

In this study, tribological behavior of Al coating deposited by two different processes and relative humidity was studied by *in situ* tribometry and blind test. *In situ* studies revealed metallic transfer film observed for both the coatings, the morphology of the transfer film was observed to be different for different coating method. Transfer film observed for IVD Al coating was more stable with less hole formation and scoring marks as compared to electrodeposited Al coating. The transfer film observed for electrodeposited Al coating was unstable at the initial stages of sliding test with frequent hole and scoring mark formation and its subsequent replenishment. Similar formation of transfer film was also observed by Shockley et al. [27] due to plastic flow at the interface during initial cycles followed by hole formation and scoring with high average coefficient of friction.

The formation of extensive transfer film at the sapphire interface during initial stages by prow formation reported by Belin et al. [31] for polymeric varnish coating with the help of triboscopic image is associated with high coefficient of friction similar to this study. Triboscopic images used to correlate the changes in instantaneous coefficient of friction with transfer film formation and instability used for the current study revealed that the removal and replenishment of the transfer film is associated with discrete temporal features on the triboscopic image. Due to extensive transfer film formation at the contact interface, one to one correlation was not feasible for current study but can be used for other coating materials.

The third body morphology of Al coating manufactured by different method leads to difference in coefficient of friction. With change in relative humidity, the third body morphology was modified for IVD Al coating. The columnar microstructure of IVD Al coating leads to morphologically different type of wear debris formed with different relative humidity, similar behavior in average coefficient of friction was also observed by Dvorak [49] for Pb-Mo-S coating with change in relative humidity. Wear debris morphology observed by Kim et al. [73] for Al metal observed that the size of wear debris varies depending on at what point of time during sliding it is ejected from the contact interface. They found that the larger wear debris particle are formed at early cycles, with less oxygen content. XPS analysis done on wear debris by Kim et al. [73] found a shifting of peaks due to large strain applied on the wear debris particles, with formation of hydroxylated Al at higher humidity. The formation of hydroxylated Al was also confirmed by the author with XRD, annealing, TGA and *ab initio* modelling. Similar studies done by Kim et al. [95] to reveal tribochemical phenomena observed variation in average coefficient of friction with increase in humidity, it was also observed that the oxygen content increased with increase in relative humidity. They also observed variation in size of wear debris with change in sliding duration and oxygen content with change in relative humidity. Wear track morphology of IVD Al coating and electrodeposited Al coating was observed to be different, presence of Fe substrate peaks for electrodeposited Al coating at same relative humidity signifies a difference in third body morphology. This difference in wear track morphology can be associated to better transfer film stability for IVD Al coating as compared to electrodeposited Al coating. With change in relative humidity, it was also observed that the wear debris morphology changes leading to a difference in average friction coefficient.

7.5 Conclusions

The current study helps in better understanding the evolution of third bodies for same chemical composition coating deposited by two different methods. *In situ* tribometry of two Al coatings revealed that the stability of the transfer film varies with change in the morphology of the coating. Occurrence of hole formation and scoring marks was observed to be more frequent for electrodeposited Al coating as compared to IVD Al coating signifying transfer film stability for IVD Al coating. Change in relative humidity studied with a steel countersphere indicates that the formation of wear debris at the contact interface changes with the change in relative humidity. At lower humidity level, the formation of coarser wear debris at the contact interface leads to abrupt increase in friction coefficient for IVD Al coating. The wear debris becomes finer in size with increase in relative humidity. Electrodeposited Al coating is less sensitive to change in relative humidity as compared to IVD Al coating. Coarser morphology of wear debris was observed for electrodeposited Al irrespective of variation in humidity.

Acknowledgments

The authors like to thank Salim Brahimi for their inputs in this work. We would also like to thank Natural Science and Engineering Research Council Canada (NSERC), Boeing Research and Technology, Pratt and Whitney Canada, Héroux Devtek, Canadian Fastener Institute and Messier-Bugatti-Dowty for their financial support.

Chapter 8

8. Influence of Cd and Al coating on modification of substrate steel wear rate

P. Behera, R. R. Chromik & S. Yue

This chapter is a manuscript prepared for journal publication. Chapter 5 to 7 focused on evolution of third bodies and its subsequent effect on friction coefficient at varying relative humidity for Cd and Al coatings on steel substrate. The variation in third body evolution with change in relative humidity can modify the velocity accommodation mechanism, modifying the wear rate of substrate. This chapter focuses on the study of modification in steel substrate wear rate with Cd and Al coating at varying relative humidity.

Department of Mining & Materials Engineering

McGill University, Montreal, QC, Canada H3A 0C5

8.1 Introduction

The majority of load bearing and high strength components in aerospace and industries are metallic materials. Among the wide variety of high strength materials available, the most common material used for advantage of its specific strength application is high strength steel. Though steel is mostly used for high strength application, other properties like corrosion resistance, friction, wear in different environmental conditions cannot be delivered by the bulk metal. To overcome this shortcoming of high strength steel, coatings are applied, modifying the surface properties. In specific to sliding conditions, the application of metallic coatings on steel substrate can modify the tribological behavior.

During sliding test, the formation of chemically and mechanically altered layer different than first bodies at the contact interface is defined as third bodies [22]. The formation of third bodies at the contact interface can significantly modify the friction coefficient and wear rate [123], [150]. The application of chemically and morphologically different coating material to the same substrate can modify third body formation at the contact interface [45], leading to a difference in velocity accommodation mechanism [23]. Cd coatings used as sacrificial coatings on high strength steel substrate withstand sliding motion in variety of applications like landing gear, fasteners etc. The presence of Cd coating at the contact interface can modify the friction coefficient as well as the wear rate as compared to bulk substrate material. Moreover, Cd coatings are specifically used for their lubricating properties and melting at the interface [70], acting as a solid lubricant. Recent regulations due to carcinogenic and work hazardousness of Cd coating on high strength steel material has limited its application. Al coating on the other hand also acts as a sacrificial coating, are relatively soft coating compared to the substrate material and can prove to be a potential replacement for Cd coating.

Many studies have been done on reduction of substrate wear with application of coating material [151], [152], [153]. In specific to Cd coated steel substrate, Jahanmir et al. [69] observed that the presence of 0.1 µm Cd coating on steel substrate reduces the wear rate by three order when tested in Ar atmosphere. The magnitude of reduction in wear rate was less in air than Ar atmosphere due to oxidation of the coating. It was found that the formation of cadmium oxide particle (harder than

Cd metal) can act as abrasive particle, increasing the wear rate as compared to Ar atmosphere. When the steel sample was coated with Cd thickness higher than 0.1 µm, delamination of the coating takes place to reach a steady state thickness of 0.1 µm. Ruggeri et al. [70] observed that soft Cd metal on the surface acts as solid lubricant, which becomes semi fluid enhancing the lubrication and decreasing the wear.

Application of Al coating on high strength steel substrate acts as an viable alternative for Cd coating. Due to excessive production of hydrogen at the steel interface during plating process of Al in aqueous solution, aprotic or vapor deposition process is generally employed for Al coating. This difference in plating process can lead to different microstructure [86], modifying the tribological properties. Kumar et al. [87] observed that the wear of Al coating predominantly takes place by adhesion and plastic deformation of bulk metal. Dry sliding test performed on Al after high pressure torsion (HPT) method has an effect on wear rate [88]. The formation of fine grain structure after HPT process reduces the wear due to decrease in adhesion as compared to coarse grain structure. In addition to morphology of Al, effect of relative humidity during sliding test can also affect the tribological properties. Modification of wear debris morphology [73], [95] with change in relative humidity was also observed for Al metal.

The current work focuses on measurement of steel substrate wear rate when Cd and Al are present. The wear rate of uncoated and coated steel substrate was measured by applying similar normal load at varying relative humidity. Linearly reciprocating ball-on-flat tribometer is used to measure the wear rate of the steel substrate in dry air, 30% and 60% relative humidity.

8.2 Experimental Methodology

8.2.1 Steel Substrate

Coupons of 5 cm X 5 cm were hand sheared from AISI 1018 steel, commercially available with dimension of 30 cm X 90 cm X 0.8 cm plates. Commercially available plates have oil on the surface to prevent corrosion during storage and transportation, this oil on the surface is removed by acetone just before the start of the tribological test and named as as-received steel substrate for this study.

Uncoated grit blast sample were not available with the industrial sponsors; the samples were prepared by removing Al coating in alkaline solution. Before the IVD Al coating process, the surface of the steel coupons was cleaned by immersing the coupons in acetone followed by grit blasting of the surface with Al_2O_3 of 80-320 size. The samples were prepared by dissolving commercially available electrodeposited Al coatings deposited on AISI 1018 steel coupons of 150 mm X 150 mm. After receiving the electrodeposited Al plates, the coated panel was sheared to 50 mm X 50 mm coupons followed by dissolving the coupons in 5% KOH solution to remove the Al coating. The AISI 1018 steel panels thus obtained were used for tribological test.

8.2.2 LHE Cd Coating

The Cd plating on steel substrate is done in an industrial facility by immersing the steel plates in an alkaline cyanide based bath solution with CdO – 20-30 g/l, NaCN – 90-135 g/l, Na_2CO_3 – 0-60 g/l and NaOH – 11-30 g/l. The substrate is acid pickled before immersion, current density applied for plating is 118-120 mA/cm^2 to generate a coating thickness of 15 µm in 5 minutes. After plating, the Cd coating is immersed in trivalent chromate conversion solution to generate a passivation layer.

8.2.3 Al Coatings

Ion Vapor Deposited (IVD) Al coating [99] was done in a vacuum deposition chamber with nitrogen gas purging. The steel substrate was kept at a negative bias, Al wires were melted by resistor heating at 800-840 ^{0}C and evaporated to get a coating thickness of 20-25 µm on substrates. Just after the coating, the surface of Al coating was glass bead peened to close the open pores present on the surface. Finally a chemical conversion coating [100] was done to generate a passivation layer in nm range. The tribological test was performed on sheared coupons of 50 mm X 50 mm.

The electrodeposition of Al coating is done in an aprotic (water free) organic plating solution using a patented process used by Alumiplate Inc. [101]–[103]. After coating, a chemical conversion coating [100] was done to generate a passivation layer in nm range. The tribological test was performed on sheared coupons of 50 mm X 50 mm.

8.2.4 Tribological Test Parameters

Tribological test on steel substrates and coatings was carried out by a the linearly reciprocating 440C 1/4" diameter spherical countersphere sliding on the AISI 1018 steel coupons. The load is applied on the arm to provide a constant normal force is 1.3 N, corresponding to initial maximum Hertzian stress as shown in Table 8-1. The total track length was 20 mm with sliding velocity of 14 mm/s for 2000 cycles corresponding to a total sliding distance of 80 metres. The relative humidity during the experiment was controlled by enclosing the setup in a high-density polyethylene (HDPE) bag with a provision to pass dry or humidified air to maintain humidity at 0, 30 and 60% with a standard deviation of 5% at 23 ˚C.

Table 8-1 Hertzian Stress Calculation [44]

Hertzian Stress Calculation – Similar Load of 1.3 N		
Sample	Initial Maximum Hertzian Stress (MPa)	Contact Radius (µm)
Low Carbon Steel	670	30.1
Cd	390	40.3
Al	440	38.2

8.2.5 Wear Rate Measurements

Stripe test with a decrease in track length by 2 mm at 1, 5, 10, 20, 50, 100, 200, 300 cycles and 300, 500, 850, 1000, 1250, 1500, 1750, 2000 cycles at same relative humidity are done in two set of experiment to measure the wear volume by using Optical profilometer (Zygo NewView 8000 Series 3D optical profilometer, USA). The full track length of test was 20 mm.

The wear rate of coating is determined by measuring the volume below the wear scar with the reference plane as the coating surface adjacent to the wear scar. After the bulk surface layer of the coating is removed, the wear rate of the steel substrate is measured by elevating the reference (unworn coating surface) to the thickness of the coating and measuring the wear volume below the wear scar by masking method. This method is a modified version of the ASTM G99 [154] method where an area scan is done instead of a line scan. Minimum of 1/3rd wear scar surface is scanned for the measurement of wear volume.

8.3 Results

8.3.1 Surface Morphology

The surface morphology of the steel substrate and the coatings is shown in Figure 8.1. The average surface roughness of as-received steel was observed to be 1.684 µm, the surface finish of the as-received steel sample is smooth due to rolling process. As compared to as-received steel substrate, the grit-blast steel substrate has a higher average surface roughness of 1.92 µm. All the three coatings are formed by platelet agglomeration on the substrate. LHE Cd coating is formed by agglomeration of spherical platelets with an average surface roughness of 4.28 µm, this agglomeration of spherical platelets leads to porous morphology of the coating. The surface morphology of IVD Al coating is formed by agglomeration of finer platelets as compared to LHE Cd coating. IVD Al coatings are generally glass bead peened to increase the compaction and to close the surface pores. The average surface roughness of IVD Al coating was measured to be 2.08 µm. Electrodeposited Al coating is also formed by agglomeration of fine platelets with better compaction and less porosity. The average surface roughness of electrodeposited Al was measured to be 1.97 µm.

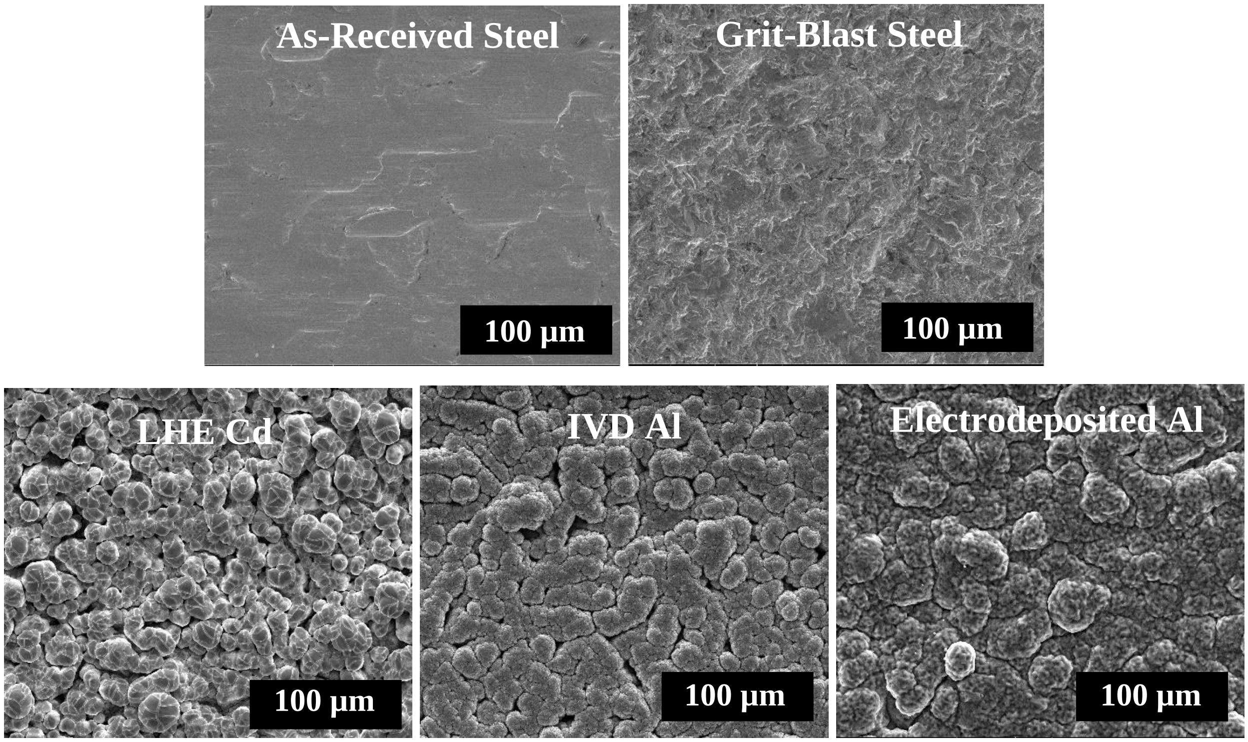

Figure 8.1 Surface morphology of as-received steel, grit-blast steel, LHE Cd coating, IVD and electrodeposited Al coating

8.3.2 Cross-section Assembly

Cross-section of LHE Cd, IVD Al and electrodeposited Al coating is shown in Figure 8.2. LHE Cd coating has globular morphology with surface roughness inherent to the steel substrate, few through thickness crack is also observed from the cross-section. IVD Al coating has higher density of cracks as compared to LHE Cd coating. Vacuum deposition method makes IVD Al coating porous although glass bead peening is done after the coating process. This process of glass bead peening only makes the surface layer more compact. Electrodeposited Al is defect free coating with surface roughness inherent to the steel substrate. The average thickness of LHE Cd coating is 11 ± 2 µm, IVD Al coating thickness is 25 ± 2 µm whereas the average thickness of electrodeposited Al coating is 20 ± 2 µm.

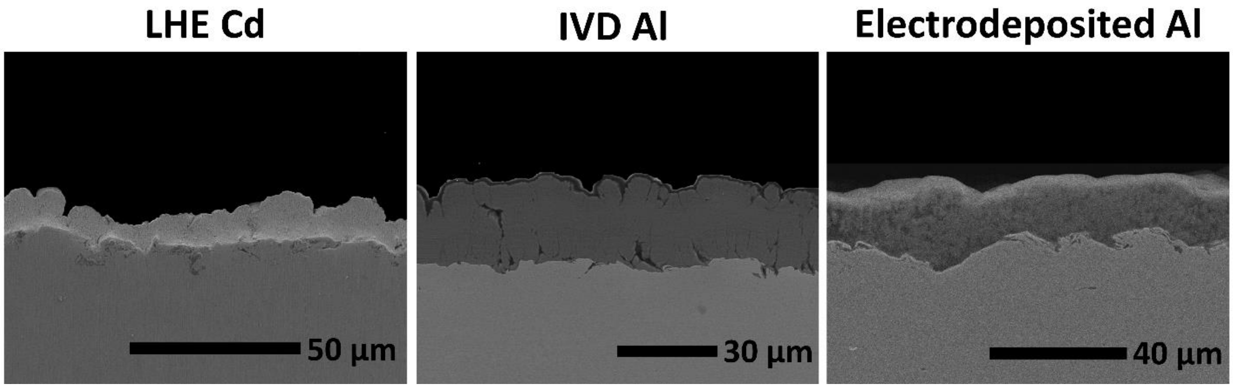

Figure 8.2 Cross-section assembly of the coatings

8.3.3 Average Friction Coefficient

The average coefficient of friction of as-received steel substrate, grit blast steel substrate, LHE Cd coating, IVD Al coating, electrodeposited Al coating with relative of 0% (RH0), 30% (RH30), 60% (RH60) at 23 ˚C is evaluated to identify the difference in friction coefficient with change in relative humidity.

8.3.3.1 Steel substrate

8.3.3.1.1 Average CoF

With change in relative humidity, the average coefficient of friction of steel substrate changes as shown in Figure 8.3. Increase in relative humidity decreases the average coefficient of friction. At the end of the tribological test, the average coefficient of friction is similar for both as-received and grit blast steel although the cycles required to reach steady state is different. The average coefficient of friction at steady state for RH60 is 0.45 which increases to 0.55 at RH30 and 0.8 at 2000 cycles. The average surface roughness for as-received sample is 1.568 µm where as after grit blasting, the surface roughness of sample has increased to 1.919 µm.

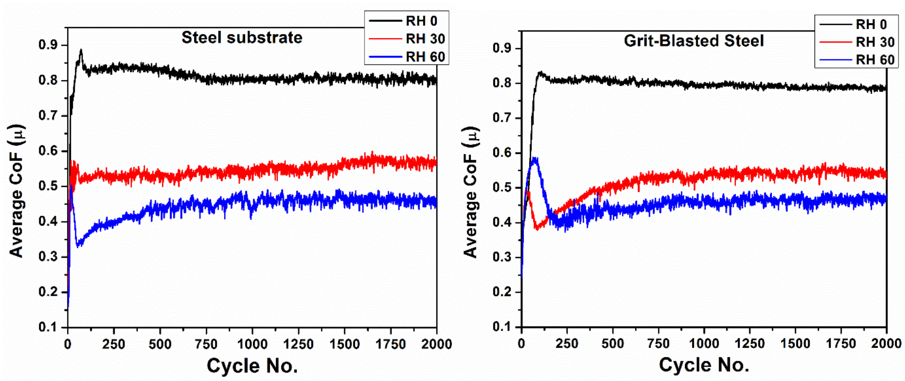

Figure 8.3 As-received and grit-blasted steel substrate tribological behavior at varying relative humidity

8.3.3.1.2 As-Received Steel Wear Track Morphology

The wear track morphology can vary with varying relative humidity. Wear track morphology of as-received steel at varying relative humidity is shown in Figure 8.4. At RH 0, formation of wear debris and asperity deformation is observed on the wear track. With increase in relative humidity to RH 30, the amount of wear debris decreases. The wear track formed at RH 30 is irregular with some unworn area present on the wear track. At RH 60, the amount of wear debris further decreases as compared to RH 0 and RH 30 with asperity deformation. The unworn area was observed to be higher as compared to RH 30 and RH 0. The variation in wear debris and asperity deformation with increase in relative humidity signifies the change in third body morphology.

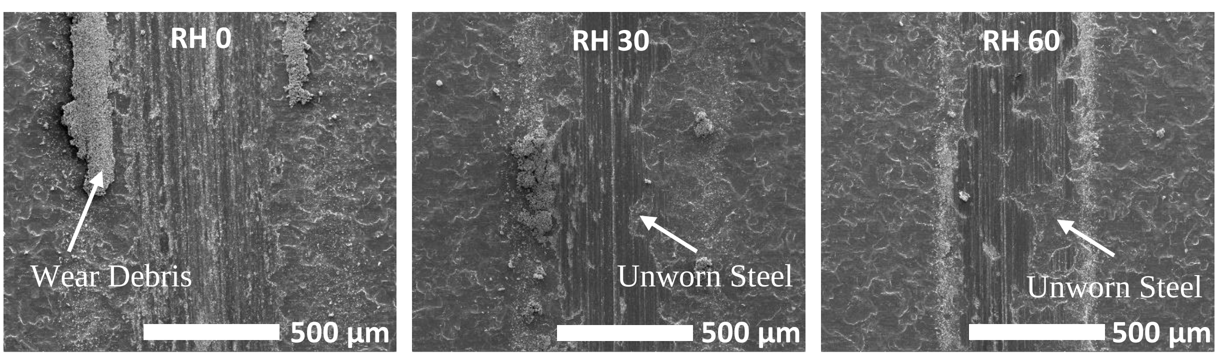

Figure 8.4 Wear Track morphology of as-received steel at RH 0, RH 30 and RH 60 showing wear debris particle and asperity deformation at 2000 cycles

8.3.3.1.3 Grit-Blast Steel Wear Track Morphology

The grit-blast steel at varying relative humidity is shown in Figure 8.5. Similar features are observed for grit-blast steel to that of as-received steel. The wear debris observed for grit-blast steel at RH 0 was finer in size as compared to as-received steel. The wear track at RH 0 is well defined as compared to RH 30 and RH 60. The amount of wear debris at RH 30 and RH 60 was observed to be lower with irregular wear track morphology. Similar to as-received steel, the wear track morphology at RH 30 and RH 60 for grit-blast steel has unworn wear surface present within the wear track.

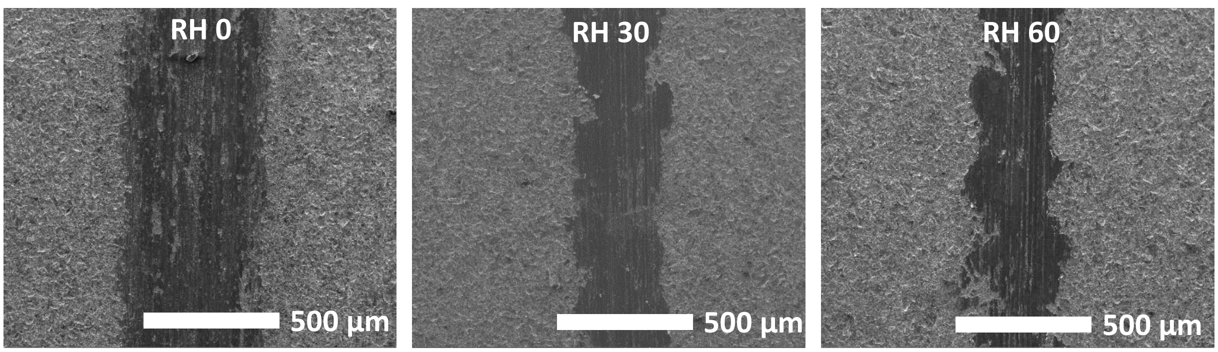

Figure 8.5 Wear Track morphology of grit-blast steel at RH 0, RH 30 and RH 60 showing wear debris particle and asperity deformation at 2000 cycles

8.3.3.2 LHE Cd Coating

8.3.3.2.1 Average CoF

With change in relative humidity, the friction coefficient evolution was observed to be different at varying relative humidity (shown in Figure 8.6). At RH0, the average friction coefficient at the end of test is lower as compared to RH30 and RH60. The change in average friction coefficient is due to change in third body morphology (chapter 6) at varying relative humidity. The decrease in average coefficient of friction at RH0 was due to the difference in formation of hydroxide and oxide compounds in Regime II (Chapter 6). At RH0, the presence of fine wear debris at the contact interface also modifies the velocity accommodation mechanism [23], modifying the friction coefficient. The average coefficient of friction with Cd coating was observed to be following a opposite trend as compared to steel substrate. With increase in relative humidity the average coefficient of friction is lower (compared to RH0 and RH30) for steel substrate as opposed to LHE Cd coating with higher CoF.

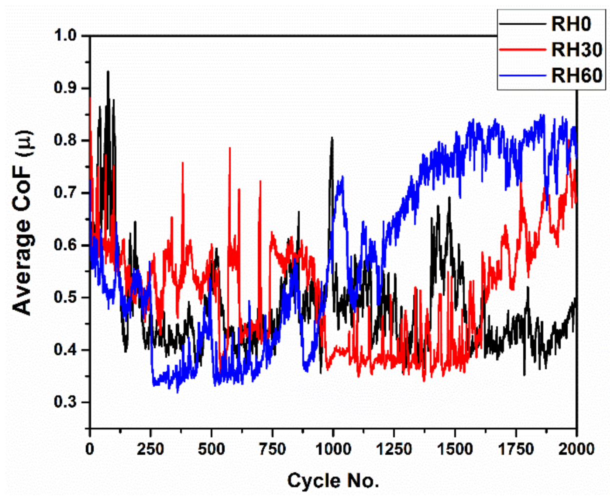

Figure 8.6 Tribological behavior of LHE Cd at varying relative humidity

8.3.3.2.2 Wear Track Morphology of LHE Cd Coating

The wear track morphology of LHE Cd coated steel substrate after 2000 cycles at varying relative humidity is shown in Figure 8.7. At RH 0, the wear track has significant wear debris present. The presence of dark patches at RH 0 is due to the protuberance of the steel substrate as shown in section 6.3.2.3 along with patches of Cd coating. With increase in relative humidity to RH 30, the protuberance of the steel substrate at the centre of the wear track is visible but with a decrease in amount of wear debris. At RH 60, the wear debris is lower compared to RH 30 with protuberance of steel substrate at the surface (shown in section 6.3.2.1). The decrease in amount of wear debris and protuberance of steel substrate indicates modification of third body morphology with change in relative humidity.

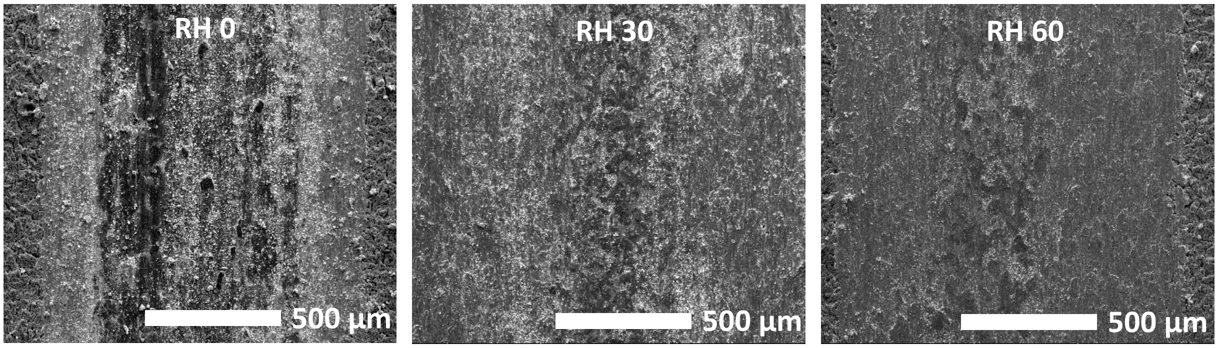

Figure 8.7 Wear Track morphology of LHE Cd coated steel at RH 0, RH 30 and RH 60 showing wear debris particle and steel substrate at 2000 cycles

8.3.3.3 Al Coating

8.3.3.3.1 Average CoF

The average CoF for IVD Al coating changed with change in relative humidity (shown in Figure 8.8). The average coefficient of friction at RH0 was observed to be relatively lower compared to RH 30 and RH 60 for IVD Al coating. In addition to difference in average CoF, the abrupt friction spikes at RH0 was observed to be higher and more frequent as compared to RH30 and RH60. The average CoF for electrodeposited Al coating was also different with change in relative humidity. The abrupt increase in average CoF was observed at all three relative humidity for electrodeposited Al coating.

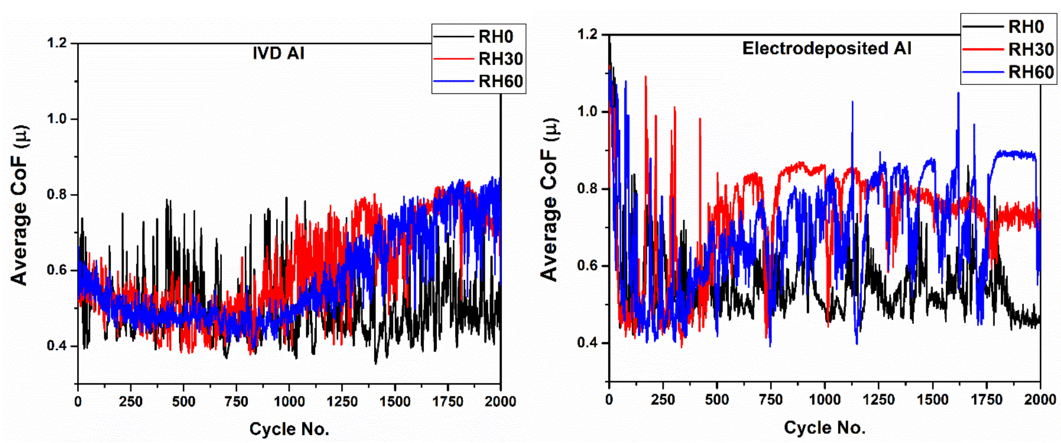

Figure 8.8 IVD Al and Electrodeposited Al coating tribologocial behavior at varying relative humidity

8.3.3.3.2 Wear Track Morphology of IVD Al Coating

The wear track morphology of IVD Al coating after 2000 cycles at varying relative humidity (shown in Figure 8.9) has a difference in wear debris present on the wear track. The wear debris was observed to be more at RH 0 and decreases with increase in relative humidity. At RH 0, there is visible fracturing of the coating with fine wear debris scattered on the surface. The wear track morphology at RH 30 has scoring marks at the centre of the wear track. With increase in relative humidity to RH 60, the wear track is irregular in shape with visible scoring marks.

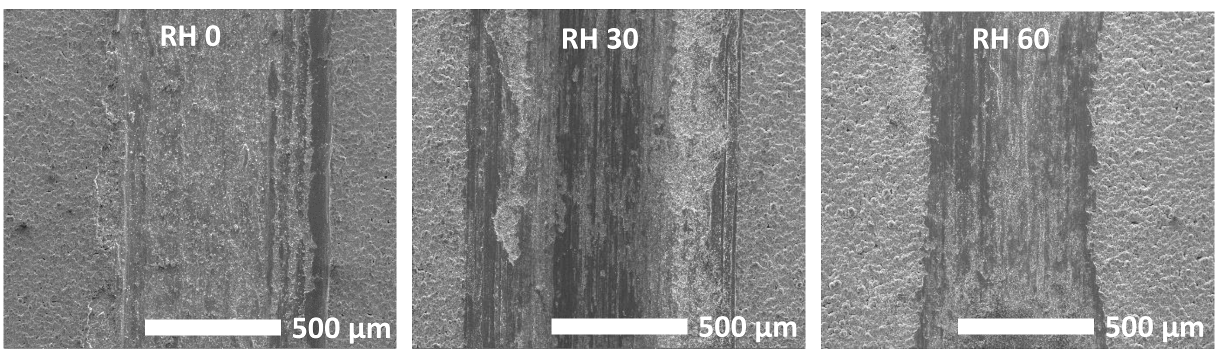

Figure 8.9 Wear Track morphology of IVD Al coated steel at RH 0, RH 30 and RH 60 showing wear debris particle and steel substrate at 2000 cycles

8.3.3.3.3 Wear Track Morphology of Electrodeposited Al Coating

The wear track morphology of electrodeposited Al coating after 2000 cycles at varying relative shown in Figure 8.10 has extensive wear debris scattered on the wear track. At RH 30, few scoring mark and protuberance of steel substrate can be observed. The wear track morphology was observed to be different than IVD Al coating (shown in Figure 8.9) where a decrease in wear debris with increase in relative humidity was observed.

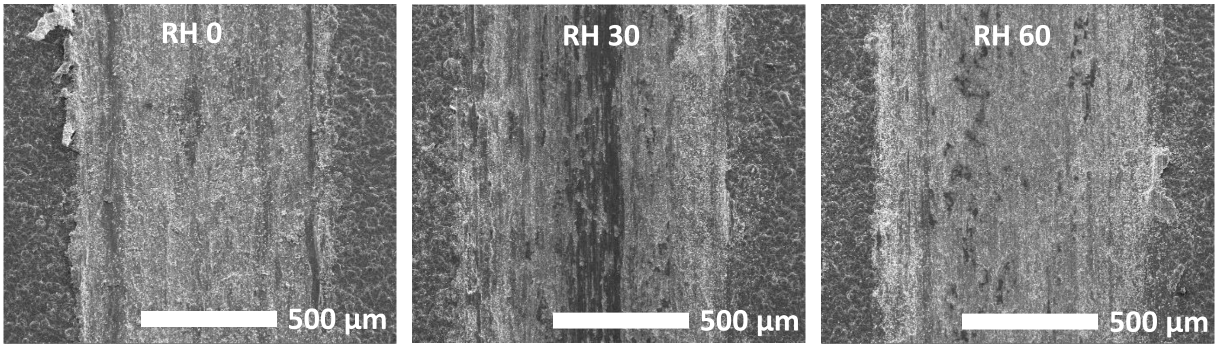

Figure 8.10 Wear Track morphology of electrodeposited Al coated steel at RH 0, RH 30 and RH 60 showing wear debris particle and steel substrate at 2000 cycles

Studies done on steel substrates and coatings indicates that the change in relative humidity affects the evolution of CoF. The average CoF for both type of steel substrate decreased with increase in relative humidity. The wear track morphology for both as-received steel and grit blast steel was different with change in relative humidity (section 4.1). This change in relative humidity can be linked to change in third body morphology at the contact interface due to variation in relative humidity. Formation of transfer film at the initial cycles observed for LHE Cd coating (section 6.3.2.1) and subsequent change of contact condition to mixed mode modifies the friction CoF. It was observed that with change in relative humidity, the third body formed at the interface was different (section 6.3.4). The presence of wear debris and dominant Cd or steel features can significantly modify the friction coefficient (section 6.3.2). For Al coating, abrupt increase in average friction for IVD Al coating was due to formation of coarse wear debris sticking to the interface at lower relative humidity. With increase in relative humidity, the wear debris became finer in morphology and the friction spikes was observed to be lower (Section 7.3.3). In contrast to IVD Al coating, friction spikes were independent of relative humidity for electrodeposited Al coating (Section 7.3.3). The wear debris morphology was similar for all three-relative humidity for electrodeposited Al coating.

8.3.4 Wear Rate

The wear rate measurements are divided into two sections. The first section focuses on the wear rate measurement of the coatings at varying relative humidity. The second section will focus on wear rate measurement of uncoated steel and substrate wear when bulk surface layer of coating is removed.

8.3.4.1 Wear of Coatings

8.3.4.1.1 RH0

The wear volume of electrodeposited Al coating shown in Figure 8.11 (a) is higher as compared to LHE Cd and IVD Al coating. The wear volume of IVD Al and LHE Cd coating was measured to be similar up to 100 cycles, after which the wear volume of LHE Cd coating decreases as compared to IVD Al coating. The wear rate of the electrodeposited Al coating (shown in Figure 8.11 (b)) is high followed by LHE Cd coating and and IVD Al coating. The high wear rate at initial cycles is due to prow formation of the coating as proposed by Antler [155]. The aprotic deposition method for electrodeposited Al coating leads to a higher wear rate as compared to ion vapor deposition process for IVD Al coating. The hardness difference between Al and Cd coating leads to bulk surface coating removal at 300 cycles as compared to IVD Al and electrodeposited Al.

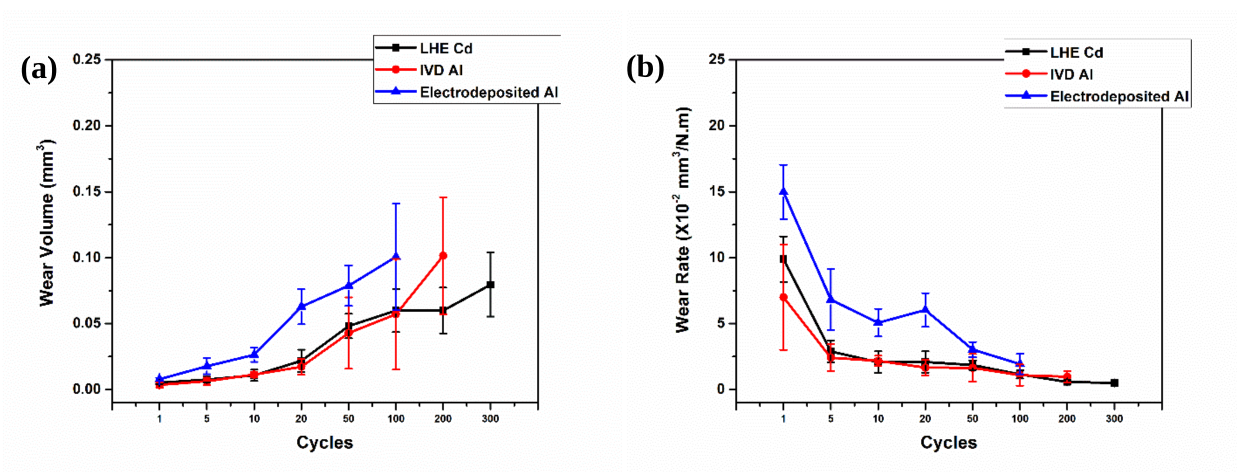

Figure 8.11 (a) Wear volume and (b) wear rate of coatings at RH0

8.3.4.1.2 RH30

Wear volume of electrodeposited Al coating was higher as compared to LHE Cd and IVD Al coating shown in Figure 8.12 (a). The wear volume of LHE Cd and IVD Al was measured to similar. The wear rate of electrodeposited Al coating was measured to be higher as compared to

IVD Al and LHE Cd coating as shown in Figure 8.12 (b). The wear rate of the coatings decreased with increase in sliding distance.

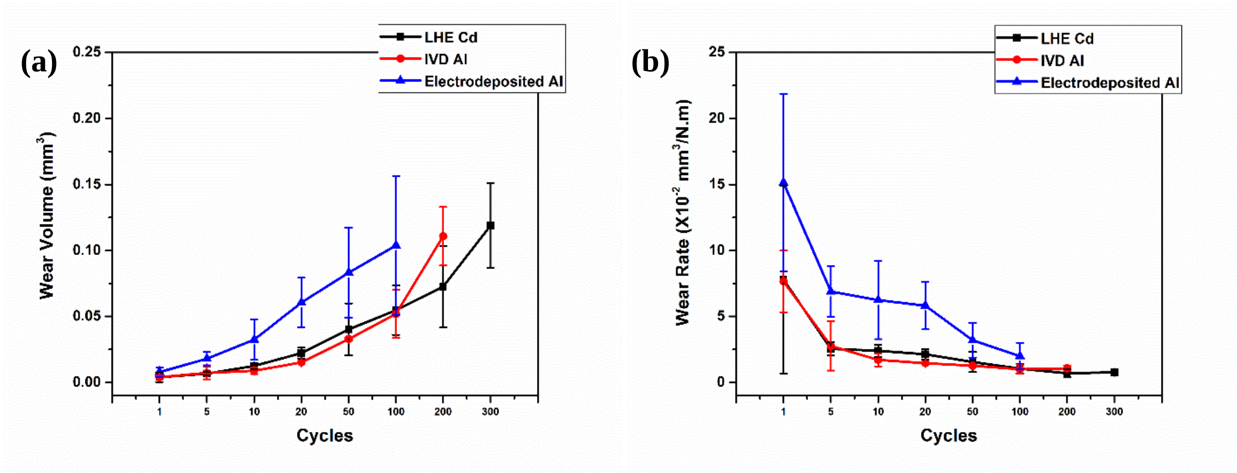

Figure 8.12 (a) Wear volume and (b) wear rate of coatings at RH30

8.3.4.1.3 RH60

The wear volume measured at RH60 for the coatings (shown in Figure 8.13 (a)) indicates removal of electrodeposited Al coating at a faster rate as compared to LHE Cd and IVD Al coatings. The wear volume of coatings is similar to that at RH0 and RH30. The wear rate of coatings decreases with increasing cycles. The wear rate of electrodeposited Al coating was measured to be highest and the wear rate of LHE Cd and IVD al coating was similar.

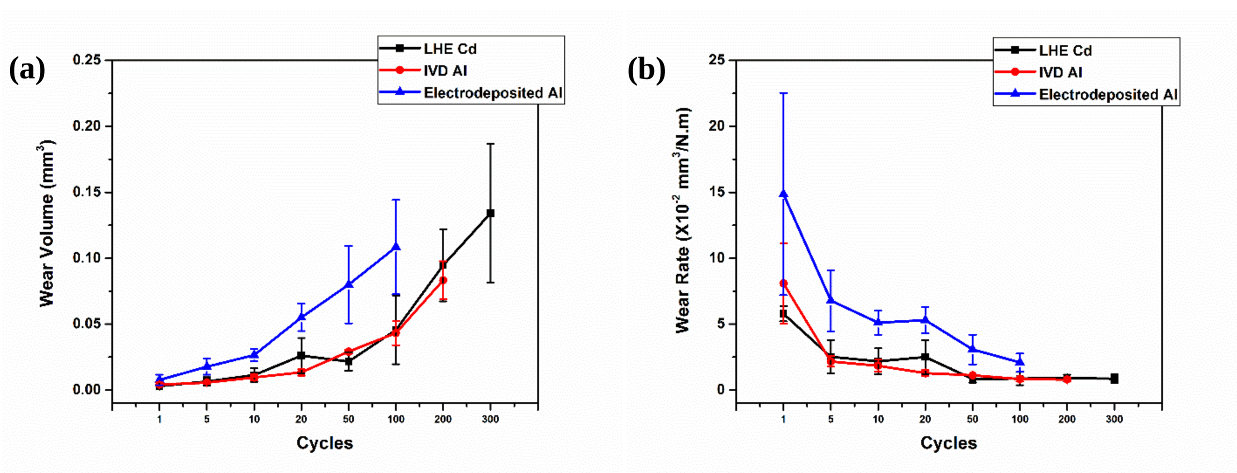

Figure 8.13 (a) Wear volume and (b) wear rate of coatings at RH60.

8.3.4.2 Wear of Substrate

8.3.4.2.1 RH0

The wear volume of steel substrate is shown in Figure 8.14 (a), the wear volume of Al coated steel substrate was measured to be higher as compared to LHE Cd and uncoated steel substrate. The onset of steel substrate wear takes place at earlier cycle for electrodeposited Al as compared to IVD Al coating. Both the Al coating has wear volume higher than the steel substrate. The process of grit blasting increases the wear rate of the uncoated steel substrate at RH0. Application of Cd coating to the steel substrate decreases the wear volume of the steel substrate, this might be attributed to the lubricating nature of Cd. The wear rate of steel substrate after the bulk surface of coating is removed at RH0 is shown in Figure 8.14 (b). The wear rate of as-received steel and grit-blast steel was measured to be higher at 5 cycles due to error associated with measurement of asperity deformation. With increase in sliding cycles, the formation of demarcated wear track decreases the error. The wear rate of LHE Cd coated steel substrate with Cd coating present at the pockets of steel substrate (section 6.3.2) roughness reduces the wear rate. The application of Al coating on the other hand during sliding test increases the substrate wear due to formation of predominant non-stochiometric oxide [73] abrasive particles (section 7.3.3). The zoomed in section of the wear rate measurement for steel substrate at the end of the test is shown in Figure 8.14 (c). The wear rate of electrodeposited Al was measured to be highest, followed by IVD Al coated steel. The process of grit blasting for uncoated steel substrate increases the wear rate of steel. The application of Cd coating to the steel substrate reduces the wear rate, acting as an beneficial coating.

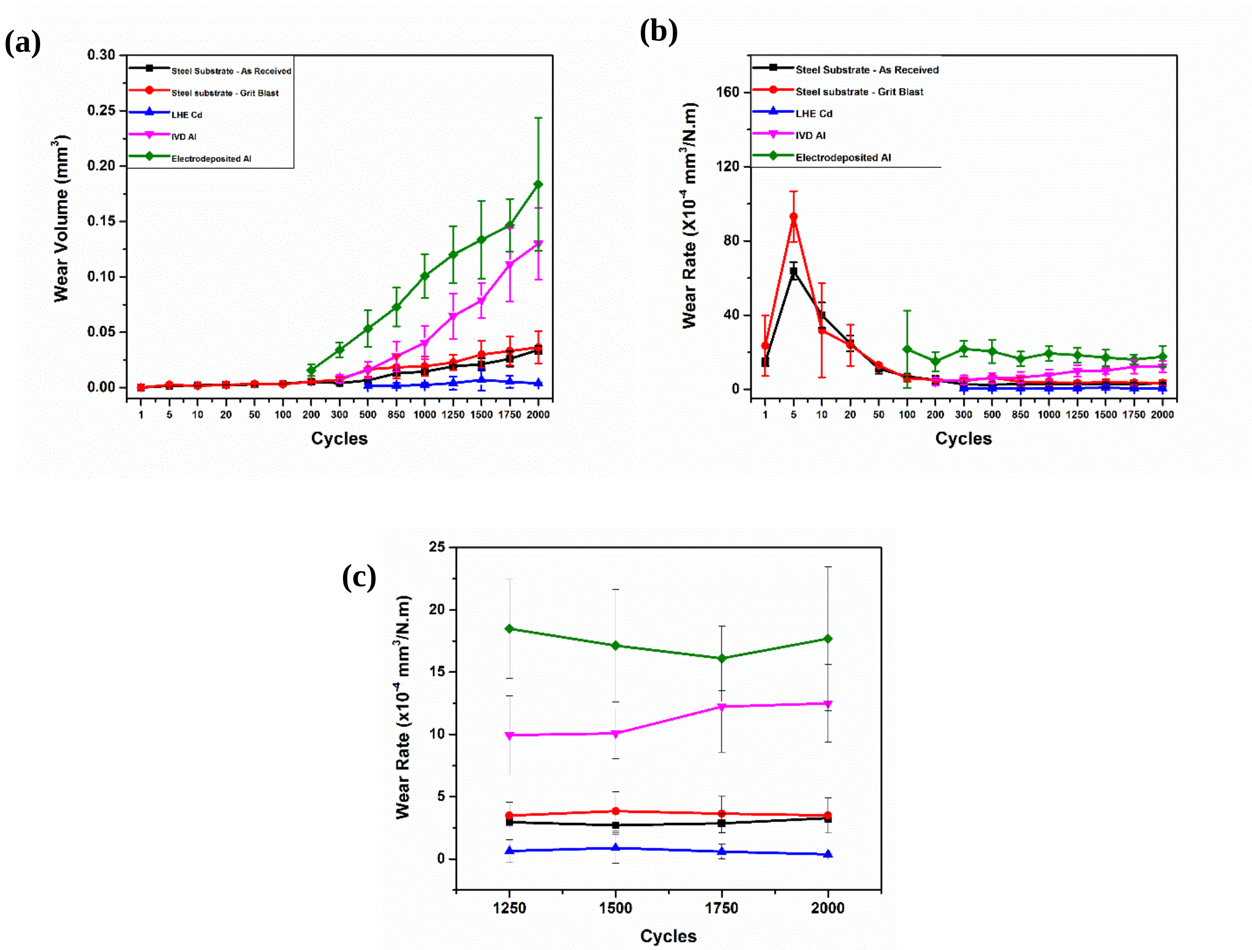

Figure 8.14 (a) Wear volume of substrate at RH0 (b) wear rate of substrate at RH0 (c) Zoomed in section of wear rate at RH0

8.3.4.2.2 RH30

The wear volume measured at RH30 (shown in Figure 8.15 (a)) is similar to RH0, the wear volume of Al coating was measured to be higher as compared to uncoated steel substrate and LHE Cd coating. The wear rate of coating shown in Figure 8.15 (b) indicates higher wear rate of grit-blast steel substrate as compared to as-received steel substrate. The wear rate of as-received steel and grit-blast steel was measured to be higher at initial cycles due to error associated with measurement of asperity deformation. The zoomed section shown in Figure 8.15 (c) near the end cycles indicate that Al coatings are detrimental to the steel substrate. Sliding test performed at RH30 indicates that LHE Cd present at the contact interface reduces the wear rate of steel substrate.

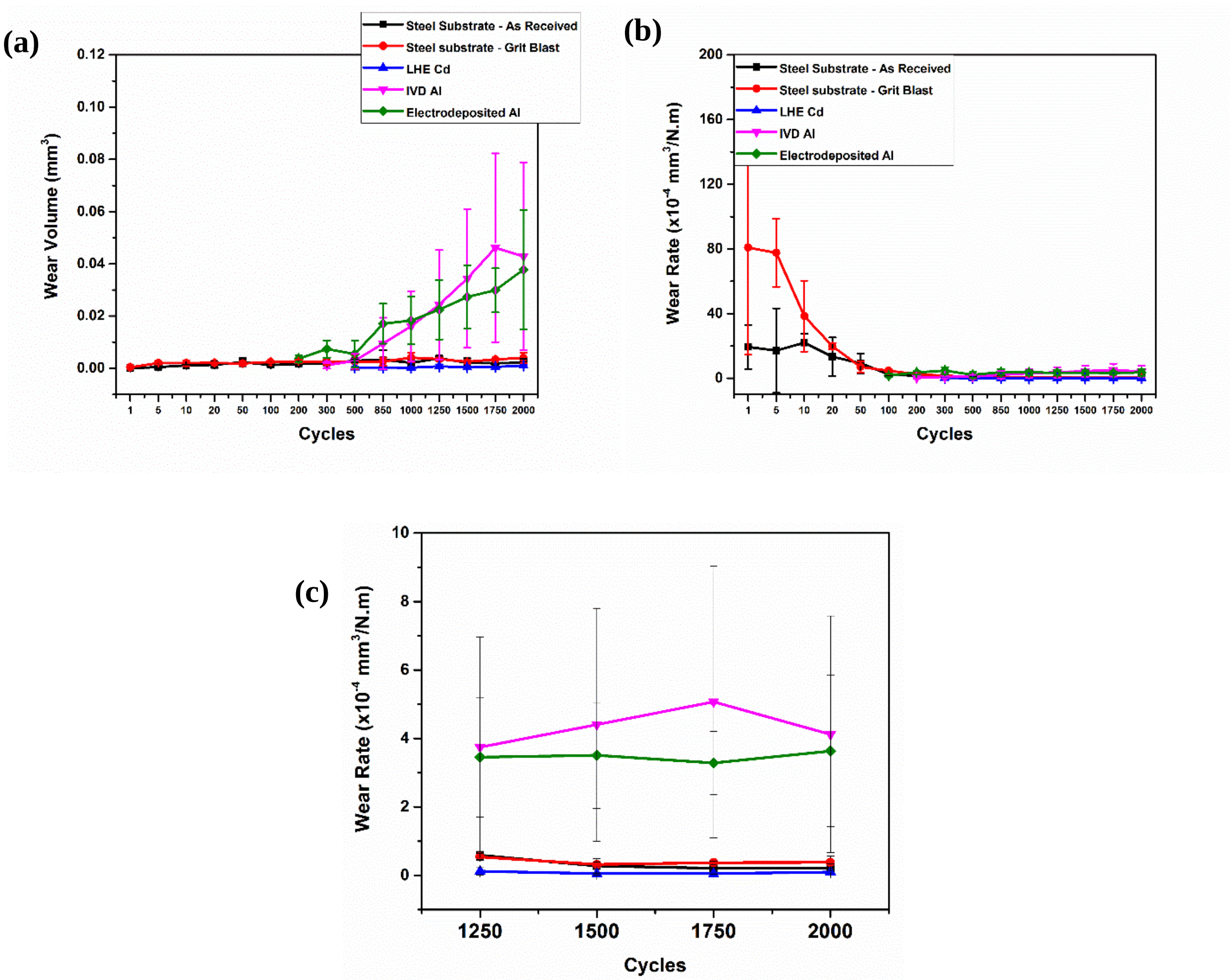

Figure 8.15 (a) Wear volume of substrate at RH30 (b) wear rate of substrate at RH30 (c) Zoomed in section of wear rate at RH30

8.3.4.2.3 RH60

The wear volume of steel substrate measured at RH60 is shown in Figure 8.16 (a). The wear volume of electrodeposited Al coating was measured to be higher as compared to steel substrate. The wear volume of steel substrate with IVD Al coating and LHE Cd coating was measured to be lower as compared to as-received and grit-blast steel substrate. With increase in relative humidity, predominant asperity deformation increased the error associated at initial cycles for as-received and grit-blast steel. The wear rate of the substrate measured at RH60 (shown in Figure 8.16 (b)) indicates that the with increase in relative humidity, the wear rate of steel substrate decreases for

IVD Al and LHE Cd coating whereas increases for electrodeposited Al coating as shown in Figure 8.16 (c).

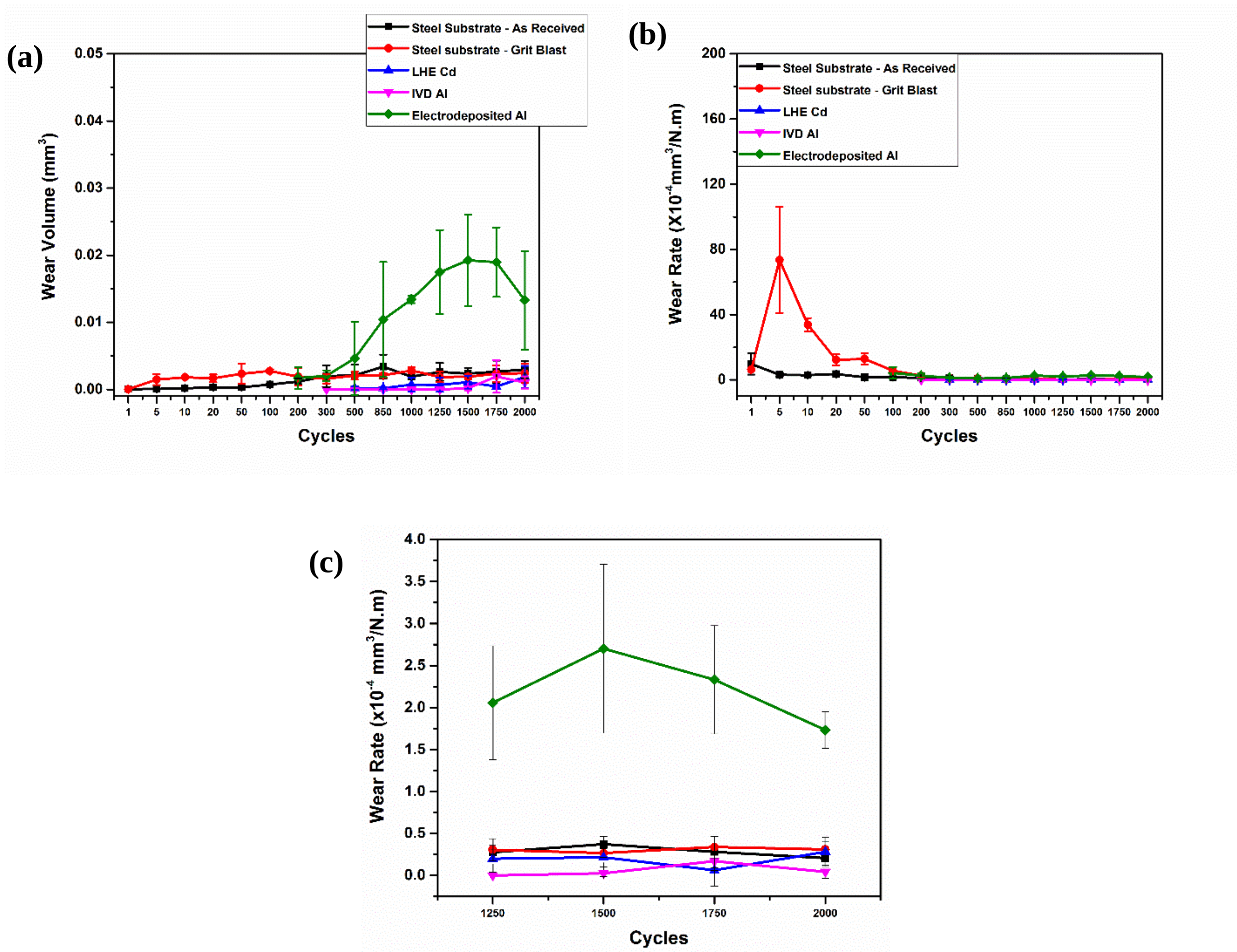

Figure 8.16 (a) Wear volume of substrate at RH60 (b) wear rate of substrate at RH30 (c) Zoomed in section of wear rate at RH60

8.4 Discussion

The wear rate of the steel substrate with Cd and Al coatings and varying relative humidity after 2000 cycles of sliding test is shown in Figure 8.17. With increase in relative humidity, the wear rate of uncoated and grit-blast steel substrate decreased. Similar behavior of decrease in steel substrate wear was also observed by Mercer et al. [67]. At RH0, the formation of abrasive wear debris particles at the contact interfaces increases the wear rate of substrate as compared to RH30 and RH60. Increase in relative humidity modifies the third bodies at contact interface leading to decrease in CoF and wear rate of coating. The process of grit-blasting is detrimental to the wear resistance of steel substrate, increasing the wear rate as compared to as-received steel. The morphological difference between electroplated Al and IVD Al coating has significant effect at varying relative humidity. Kim et al. [73], [95] studied that with variation in relative humidity significant modification in wear debris morphology and friction coefficient was observed. At RH60, the wear rate of steel substrate with IVD Al coating decreases as compared to increase in wear rate for electrodeposited Al coating. At RH0 and RH30, the application of IVD and electrodeposited Al coating increased the substrate wear due to formation of non-stochiometric aluminium oxide as observed by Kim et al. [73], due to increase in abrasiveness. LHE Cd coating on the other hand reduces the wear rate of the steel due to formation of cadmium oxide particles acting as lubricant during sliding test at RH0 [69]. With increase in relative to RH30 and RH60, the formation of $Cd(OH)_2$ modifies the contact conditions, leading to a decrease in wear rate (section 5.4) as well.

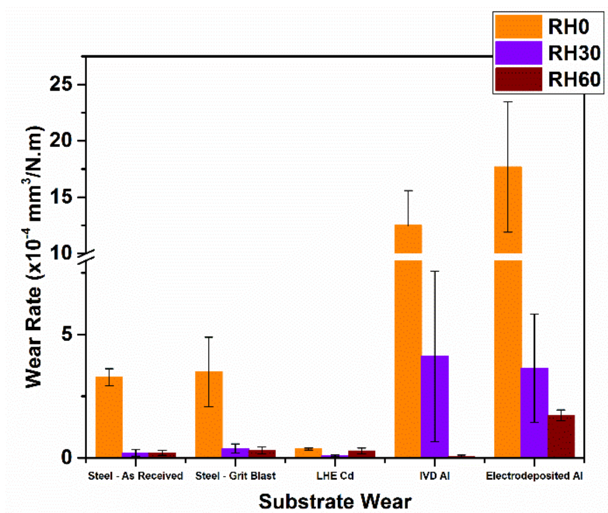

Figure 8.17 Comparison of steel substrate wear rate with different coatings and varying relative humidity after 2000 sliding cycles

The abrasive wear of steel substrate can be quantified by using Siniawski method [37] (Equation 8.1)

$$A(n) = \frac{V(n)}{d} = A_1 n^{\beta} \tag{8.1}$$

where A(n) is the abrasion rate averaged for n cycles, V(n) is the volume of the steel removed, d is the total sliding distance for test including wear of the coating and substrate, A_1 is the volume of material removed normalised by sliding distance and β is the cycle dependant abrasion rate. The value of β commonly lies between -1 to 0 for abrasion rate decreasing with time, β = -1is associated with no abrasiveness after first sliding cycle, β = 0 corresponds to constant abrasion rate and β > 0 corresponds to increase in abrasion rate with time.

Table 8-2 shows the β parameter for determination of abrasion rate. At RH0, the grit-blast process has higher abrasion rate. The abrasion rate for LHE Cd and IVD Al at RH0 is greater than 1, signifying increase in abrasion rate with sliding cycles. The abrasion rate determined for electrodeposited Al coating is -0.05 signifying a constant abrasion rate (considering approx. 0 as constant abrasion rate). With increase in relative humidity, initiation of other wear mechanism in addition to abrasive wear significantly modifies the β parameter. The range of β parameter determined for the current study varies from -0.8 to 2, typical for metal-metal sliding contacts [37].

Table 8-2 Siniawski method [37] for calculation of abrasion rate

Relative	Substrate	A1	β
RH0	As-Received	0.114	-0.40
	Grit-Blast	0.121	-0.39
	LHE Cd	0.011	0.11
	IVD Al	0.013	0.455
	Electrodeposited Al	0.085	-0.05
RH30	As-Received	0.122	-0.68
	Grit-Blast	0.202	-0.81
	LHE Cd	0.037	-0.51
	IVD Al	0.001	1.06
	Electrodeposited Al	0.022	0.14
RH60	As-Received	0.061	-0.45
	Grit-Blast	0.135	-0.69
	LHE Cd	0.006	0.16
	IVD Al	0.000006	2.12
	Electrodeposited Al	0.037	0.09

8.5 Conclusions

The current study on wear rate measurement helped in understanding the modification of steel substrate wear rate after grit-blasting and plating process. The following conclusions can be made from the current study

- Grit-blasting process increases the wear rate of the coating
- With increase in relative humidity, the wear rate of steel substrate decreases.
- Coating method significantly modifies the wear rate of substrate
    - Cd coating reduces the wear rate of substrate.
    - IVD Al coating increases the wear rate of substrate at RH0 and RH30
    - Electrodeposited Al coating increase the wear rate of the coating irrespective of the change in relative humidity.

Acknowledgments

The authors like to thank Lisa Lee, Sriraman Rajagoplan, Salim Brahimi for their inputs in this work. We would also like to thank Natural Science and Engineering Research Council Canada (NSERC), Boeing Research and Technology, Pratt and Whitney Canada, Héroux Devtek, Canadian Fastener Institute and Messier-Bugatti-Dowty for their financial support.

Chapter 9

9. Synopsis

9.1 Summary and Conclusions

The tribological behavior of uncoated steel was compared with Cd and Al coatings using *in situ*, blind test and triboscopy method at varying relative humidity. The difference in coating material influences the evolution of friction coefficient and third body morphology. Soft Cd and Al coatings modify the friction and wear behavior due to their difference in chemical and mechanical properties. Both the coatings form transfer film at initial cycles, the rheology of third bodies at the contact interface varies with change in relative humidity.

The average friction coefficient of steel substrate decreases with increase in relative humidity. Grit-blasting done prior to the coating process increases the average surface roughness of the steel substrate, the average coefficient of friction is similar to as-received steel at steady state. At low humidity of RH0, the evolution of average friction coefficient was due to combination of asperity deformation and formation of abrasive particles. With increase in relative humidity, the amount of abrasive particle decreased with predominant asperity deformation, decreasing the average coefficient of friction.

Tribosocopic method coupled with *in situ* tribometry helped in better understanding the friction coefficient evolution with change in third body morphology for Cd coating. By coupling *in situ* tribometry with triboscopy method, it was observed that initial run-in period during coating removal is associated with high coefficient of friction, removal of stable transfer film is associated with low coefficient of friction, the attachment of wear debris at the contact interface leads to increase in friction coefficient. Specifically, for Cd coating, the change in countersphere from sapphire to steel has similar third body morphology (observed from spectral analysis).

Sliding test performed with steel countersphere revealed change in average CoF with change in relative humidity. Four distinct regimes with different third body morphology was observed at RH60. The first regime with high coefficient of friction was associated with bulk Cd surface layer removal, the second regime was associated with a mixed mode contact of Cd pockets and steel substrate, gradual removal of the Cd pocket was associated with the transition regime, the fourth regime was associated with steel on steel contact and high coefficient of friction. As the relative humidity was decreased, the number of regimes decreased due to change in third body morphology. Changes in spatial coefficient of friction evaluated from triboscopic image was observed due to the presence of predominant steel or Cd coating at the contact interface. The changes in third body morphology with change in relative humidity was identified using statistical analysis of instantaneous friction coefficient distribution.

In situ studies done on Al coating showed transfer film formation with sapphire countersphere. Triboscopy method coupled with *in situ* tribometry showed formation of temporal features associated with transfer removal and replenishment. Electrodeposited Al coating has higher instability in transfer film morphology as compared to IVD Al coating due to the difference in coating process. Tribological test done on IVD Al coating revealed more frequent spikes in average coefficient of friction due to change in third body morphology (wear debris morphology) at RH0. With increase in relative humidity, the wear debris morphology changed leading to a decrease in abrupt spike in average coefficient of friction for IVD Al coating. Tribological evaluation of electrodeposited Al coating revealed less dependency of humidity on the average coefficient of friction fluctuation.

Wear measurements done on bulk surface layer of coating revealed a higher wear rate for electrodeposited Al coating and similar wear rate for IVD Al and LHE Cd coating. Grit-blasting process increases the wear rate of uncoated steel substrate as compared to as-received steel substrate. With increase in relative humidity, the wear rate of uncoated steel substrate decreases. Wear rate of LHE Cd coated steel substrate is lower than the uncoated steel substrate irrespective of relative humidity. Electrodeposited Al and IVD Al coating increased the wear rate of steel substrate as compared to uncoated steel substrate at RH0 and RH30. At RH60, the electrodeposited Al coating increased the wear rate of steel substrate where as IVD Al coating decreased the wear rate.

The formation of transfer film at the contact interface modifies the friction coefficient as compared to uncoated steel substrate. With increase in sliding distance, the average coefficient of friction regime changes for both Cd and Al coatings whereas a steady state friction was observed for uncoated steel substrate. LHE Cd coating decreases the wear rate of steel substrate irrespective of the relative humidity. The wear rate of IVD Al coated steel at RH60 is lower than uncoated steel substrate but this effect is diminished with increase in relative humidity to RH30 and RH0. Electrodeposited Al coating has detrimental effect, the wear rate of steel substrate increases than uncoated steel irrespective of the relative humidity.

9.2 Contributions to Original Knowledge

1. Though triboscopy method was previously used for studying non-metallic coating, the combination of *in situ* with triboscopy was first done in this thesis work. The combination of these two-method helped in understanding the change in instantaneous coefficient of friction with change in third body morphology.

2. Effect of relative humidity on steel substrate, Cd coating and two different type of Al coating by sliding test was first time correlated with the change in third body morphology. Similar tribological conditions used for the current study helped in direct comparison of different types of coating.

3. Statistical analysis of instantaneous coefficient of friction distribution (spectral analysis) done on coatings was first time utilized to study the change in third body morphology with change in relative humidity.

4. The selection of countersphere for a tribological test is a critical factor in simulating conditions in practical application. In this study, first time a direct comparison between different counterpshere was studied with the help of spectral analysis.

5. IVD Al and electrodeposited Al coating are potential replacement for Cd coating, the difficulty in manufacturing the coating limits its knowledge resource. In this study, IVD Al and electrodeposited Al coatings were first time evaluated for their difference in tribological properties with change in coating morphology and relative humidity.

9.3 Suggestions for Future Work

1. Further chemical characterization by integrating other spectrochemical analysis tool like Raman spectroscopy with *in situ* and post analysis of the transfer film and wear track will help in better understanding the chemical nature of third bodies formed.

2. Specific correlations between *in situ* and triboscopic image was done for current study but all the interesting features on the triboscopic images were not fully explored. The third morphology change at the buried interface often leads to a friction change but there is no direct correlation to something observable by *in situ* tribometry. The 'buried' interface problem remains for metals tribology as even with powerful *in situ* methods processes and third body flows directly at the interface are often unobservable.

3. Coupling of triboscopy method with other available tribometres like "on-line" tribometer [119] will help in better understanding the fundamentals of evolution of friction coefficient with surface roughness and other features formed by third morphology change.

4. For the current study, only ball on flat disk tribometer is used. The third body morphology can be significantly affected with change in tribometer geometry. A correlative study can be performed with different contact geometries.

5. FTIR, Nanoindentation, FIB and TEM of the wear track and transfer film can be performed to study the evolution of third body with change in relative humidity.

Bibliography

[1] K. R. Baldwin and C. J. E. Smith, "The Corrosion Behaviour of Zinc Alloy and Aluminium Alloy Coated Steel Panels in a Marine Environment," *Corros. Rev.*, vol. 12, no. 1–2, pp. 141–156, 1994.

[2] E. Cardilli and M. J. Robinson, "Aluminium based coatings for optimum sacrificial protection of high strength steel," *Corros. Eng. Sci. Technol.*, vol. 46, no. 7, pp. 782–789, 2011.

[3] G. Chalaftris and M. J. Robinson, "Hydrogen re-embrittlement of high strength steel by corrosion of cadmium and aluminium based sacrificial coatings," *Corros. Eng. Sci. Technol.*, vol. 40, no. 1, pp. 28–32, 2005.

[4] M. A. Baker, W. Gissler, S. Klose, M. Trampert, and F. Weber, "Morphologies and corrosion properties of PVD Zn-Al coatings," *Surf. Coat. Technol.*, vol. 125, no. 1–3, pp. 207–211, 2000.

[5] K. Chen and G. D. Wilcox, "Tin-manganese alloy electrodeposits II. Corrosion performacne studies," *J. Electrochem. Soc.*, vol. 155, no. 2, pp. C53–C61, 2008.

[6] Y.-S. Choi, D.-H. Shin, and J.-G. Kim, "Sacrificial anode cathodic protection of aluminum-coated steel for automotive mufflers," *Corrosion*, vol. 63, no. 6, pp. 522–528, 2007.

[7] A. Conde, M. A. Arenas, and J. J. de Damborenea, "Electrodeposition of Zn–Ni coatings as Cd replacement for corrosion protection of high strength steel," *Corros. Sci.*, vol. 53, no. 4, pp. 1489–1497, 2011.

[8] O. A. Fasuba, A. Yerokhin, A. Matthews, and A. Leyland, "Corrosion behaviour and galvanic coupling with steel of Al-based coating alternatives to electroplated cadmium," *Mater. Chem. Phys.*, vol. 141, no. 1, pp. 128–137, 2013.

[9] J. M. C. Mol, Z. F. Lodhi, A. Hovestad, H.-V. 't, H. Terryn, and W. de, "Electrodeposition and corrosion properties of Zn-Co and Zn-Co-Fe alloy coatings," in *Handbook of Material Science Research*, 2010, pp. 347–368.

[10] D. Pradhan, M. Manna, and M. Dutta, "Al-Mg-Mn alloy coating on steel with superior corrosion behavior," *Surf. Coat. Technol.*, vol. 258, pp. 405–414, 2014.

[11] M. Rahsepar and M. E. Bahrololoom, "Corrosion resistance of Ni/Zn-Fe/Zn and Ni/Zn/Zn-Fe compositionally modulated multilayer coatings," *Corros. Eng. Sci. Technol.*, vol. 46, no. 1, pp. 70–75, 2011.

[12] V. Ravindran, S. Jayakrishnan, R. Sridevi, R. Rajakumari, and V. S. Muralidharan, "Characterization of zinc-iron alloy electrodeposits for corrosion resistance," *Bull. Electrochem.*, vol. 20, no. 3, pp. 115–118, 2004.

[13] J. R. Scully, F. Presuel-Moreno, M. Goldman, R. G. Kelly, and N. Tailleart, "User-selectable barrier, sacrificial anode, and active corrosion inhibiting properties of Al-Co-Ce alloys for coating applications," *Corrosion*, vol. 64, no. 3, pp. 210–229, 2008.

[14] J. Sun, Y. Wang, M. Lu, L. Dong, and W. Liu, "Corrosion mechanism of arc spraying Aluminum coatings in marine environment," *Beijing Keji Daxue XuebaoJournal Univ. Sci. Technol. Beijing*, vol. 28, no. 11, pp. 1029–1033, 2006.

[15] K. Tani, M. Adachi, A. Nakahira, and Y. Takatani, "Aqueous Corrosion Behavior of Thermally Sprayed Coatings for Steel Substrate," Conference Proceedings of the International Thermal Spray Conference, 2000, pp. 1025–1031.

[16] Y. Yoon, L. Petry, and D. C. Hansen, "Corrosion protection of alternative coatings on high-strength 4130 steel," presented at the ECS Transactions, 2008, vol. 11, pp. 61–77.

[17] K.-B. Zhang, M.-M. Zhang, J.-F. Qiao, and S.-L. Zhang, "Enhancement of the corrosion resistance of Zinc-Aluminum-Chromium coating with cerium nitrate," *J. Alloys Compd.*, vol. 692, pp. 460–464, 2017.

[18] S. Jahanmir, E. P. Abrahamson II, and N. P. Suh, "Sliding wear resistance of metallic coated surfaces," *Wear*, vol. 40, no. 1, pp. 75–84, Oct. 1976.

[19] Z. Feng, L. Ren, J. Zhang, P. Yang, and M. An, "Influence of additives on microstructure, mechanical and tribological properties of nanocrystalline Zn-Ni coatings in a novel alkaline bath," *RSC Adv.*, vol. 6, no. 48, pp. 42029–42040, 2016.

[20] L. Lee, T. Régis, S. Descartes, and R. R. Chromik, "Fretting wear behavior of Zn-Ni alloy coatings," *Wear*, vol. 330–331, pp. 112–121, 2015.

[21] K. R. Sriraman, H. W. Strauss, S. Brahimi, R. R. Chromik, J. A. Szpunar, J. H. Osborne and S. Yue "Tribological behavior of electrodeposited Zn, Zn-Ni, Cd and Cd-Ti coatings on low carbon steel substrates," *Tribol. Int.*, vol. 56, pp. 107–120, 2012.

[22] Y. Berthier, "Maurice Godet's Third Body," in *Tribology Series*, vol. 31, Elsevier, 1996, pp. 21–30.

[23] Y. Berthier, M. Godet, and M. Brendle, "Velocity Accommodation in Friction," *Tribol. Trans.*, vol. 32, no. 4, pp. 490–496, 1989.

[24] R. R. Chromik, H. W. Strauss, and T. W. Scharf, "Materials Phenomena Revealed by In Situ Tribometry," *JOM*, vol. 64, no. 1, pp. 35–43, 2012.

[25] R. R. Chromik, C. C. Baker, A. A. Voevodin, and K. J. Wahl, "In situ tribometry of solid lubricant nanocomposite coatings," *Wear*, vol. 262, no. 9–10, pp. 1239–1252, 2007.

[26] T. W. Scharf and I. L. Singer, "Role of third bodies in friction behavior of diamond-like nanocomposite coatings studied by In Situ tribometry," *Tribol. Trans.*, vol. 45, no. 3, pp. 363–371, 2002.

[27] J. M. Shockley, H. W. Strauss, R. R. Chromik, N. Brodusch, R. Gauvin, E. Irissou and J. -G. Legoux, "In situ tribometry of cold-sprayed Al-Al_2O_3 composite coatings," *Surf. Coat. Technol.*, vol. 215, pp. 350–356, 2013.

[28] J. M. Shockley, S. Descartes, E. Irissou, J.-G. Legoux, and R. R. Chromik, "Third Body Behavior During Dry Sliding of Cold-Sprayed Al-Al_2O_3 Composites: In Situ Tribometry and Microanalysis," *Tribol. Lett.*, vol. 54, no. 2, pp. 191–206, 2014.

[29] M. Belin, "Triboscopy: A new quantitative tool for microtribology," *Wear*, vol. 168, no. 1–2, pp. 7–12, 1993.

[30] M. Belin and J. M. Martin, "Triboscopy, a new approach to surface degradations of thin films," *Wear*, vol. 156, no. 1, pp. 151–160, 1992.

[31] M. Belin, J. Lopez, and J. M. Martin, "Triboscopy, a quantitative tool for the study of the wear of a coated material," *Surf. Coat. Technol.*, vol. 70, no. 1, pp. 27–31, 1994.

[32] M. B. dos Santos, H. L. Costa, and J. D. B. De Mello, "Potentiality of triboscopy to monitor friction and wear," *Wear*, vol. 332–333, pp. 1134–1144, 2015.

[33] G. W. Stachowiak and A. W. Batchelor, "1 - Introduction," in *Engineering Tribology (Third Edition)*, Burlington: Butterworth-Heinemann, 2006, pp. 1–9.

[34] B. Bhushan, "Friction," in *Introduction to Tribology*, John Wiley & Sons, Ltd, 2013, pp. 199–271.

[35] B. Bhushan, "Wear," in *Principles and Applications of Tribology*, John Wiley & Sons, Ltd, 2013, pp. 447–544.

[36] J. F. Archard, "Contact and Rubbing of Flat Surfaces," *J. Appl. Phys.*, vol. 24, no. 8, pp. 981–988, 1953.

[37] M. T. Siniawski, S. J. Harris, and Q. Wang, "A universal wear law for abrasion," *Wear*, vol. 262, no. 7–8, pp. 883–888, 2007.

[38] P. Sainsot, J. M. Leroy, and B. Villechaise, "Effect of surface coatings in a rough normally loaded contact," in *Tribology Series*, vol. 17, C. M. T. and M. G. D. Dowson, Ed. Elsevier, 1990, pp. 151–156.

[39] K. Holmberg and A. Matthews, *Coatings Tribology: Properties, Mechanisms, Techniques and Applications in Surface Engineering*. Elsevier, 2009.

[40] "Tribometry: Test, Simulation and Control Methods," *Tribol. Ser.*, vol. 1, pp. 248–299, 1978.

[41] K. Holmberg, H. Ronkainen, and A. Matthews, "Tribology of thin coatings," *Ceram. Int.*, vol. 26, no. 7, pp. 787–795, 2000.

[42] A. Matthews, A. Leyland, K. Holmberg, and H. Ronkainen, “Design aspects for advanced tribological surface coatings,” *Surf. Coat. Technol.*, vol. 100, pp. 1–6, 1998.

[43] N. X. Randall, “Experimental Methods in Tribology,” in *Tribology for Scientists and Engineers*, P. L. Menezes, M. Nosonovsky, S. P. Ingole, S. V. Kailas, and M. R. Lovell, Eds. Springer New York, 2013, pp. 141–175.

[44] K. L. Johnson and K. L. Johnson, *Contact Mechanics*. Cambridge University Press, 1987.

[45] M. Godet, “Third-bodies in tribology,” *Wear*, vol. 136, no. 1, pp. 29–45, 1990.

[46] W. G. Sawyer and K. J. Wahl, “Accessing Inaccessible Interfaces: In Situ Approaches to Materials Tribology,” *MRS Bull.*, vol. 33, no. 12, pp. 1145–1150, 2008.

[47] T. W. Scharf and S. V. Prasad, “Solid lubricants: a review,” *J. Mater. Sci.*, vol. 48, no. 2, pp. 511–531, 2013.

[48] S. Descartes and Y. Berthier, “Rheology and flows of solid third bodies: background and application to an $MoS_{1.6}$ coating,” *Wear*, vol. 252, no. 7–8, pp. 546–556, 2002.

[49] S. D. Dvorak, K. J. Wahl, and I. L. Singer, “In Situ Analysis of Third Body Contributions to Sliding Friction of a Pb–Mo–S Coating in Dry and Humid Air,” *Tribol. Lett.*, vol. 28, no. 3, pp. 263–274, 2007.

[50] I. L. Singer, S. D. Dvorak, K. J. Wahl, and T. W. Scharf, “Third body processes and friction of solid lubricants studied by in situ optical and Raman tribometry,” in *Tribology Series*, vol. 40, M. P. G. D. and A. A. L. D. Dowson, Ed. Elsevier, 2002, pp. 327–336.

[51] M. R. de Figueiredo, C. Muratore, R. Franz, R. R. Chromik, K. J. Wahl, A. A. Voevodin, M. O'Sullivan, M. Lechthaler and C. Mitterer, “In Situ Studies of $TiC_{1-x}N_x$ Hard Coating Tribology,” *Tribol. Lett.*, vol. 40, no. 3, pp. 365–373, 2010.

[52] H. W. Strauss, R. R. Chromik, S. Hassani, and J. E. Klemberg-Sapieha, “In situ tribology of nanocomposite Ti-Si-C-H coatings prepared by PE-CVD,” *Wear*, vol. 272, no. 1, pp. 133–148, 2011.

[53] M. Belin and J. M. Martin, “Triboscopy, a New Approach to Study a Sliding Interface and the History of its Degradations,” in *Tribology Series*, vol. 21, C. M. T. D. Dowson T. H. C. Childs, M. Godet and G. Dalmaz, Ed. Elsevier, 1992, pp. 437–443.

[54] K. J. Wahl, M. Belin, and I. L. Singer, “A triboscopic investigation of the wear and friction of MoS_2 in a reciprocating sliding contact,” *Wear*, vol. 214, no. 2, pp. 212–220, 1998.

[55] H. Xiao, K. Wang, G. Fox, M. Belin, J. Fontaine, and H. Liang, “Spatial evolution of friction of a textured wafer surface,” *Friction*, vol. 1, no. 1, pp. 92–97, 2013.

[56] J. L. Loubet, M. Belin, R. Durand, and H. Pascal, “Triboscopic description of local wear phenomena under an AFM tip,” *Thin Solid Films*, vol. 253, no. 1, pp. 194–198, 1994.

[57] J. C. Sánchez-López, M. Belin, C. Donnet, C. Quirós, and E. Elizalde, “Friction mechanisms of amorphous carbon nitride films under variable environments: a triboscopic study,” *Surf. Coat. Technol.*, vol. 160, no. 2–3, pp. 138–144, 2002.

[58] J. Fontaine, M. Belin, T. Le Mogne, and A. Grill, “How to restore superlow friction of DLC: the healing effect of hydrogen gas,” *Tribol. Int.*, vol. 37, no. 11–12, pp. 869–877, 2004.

[59] “MIL-STD-1504 C ABRASIVE BLASTING,” 2007.

[60] “MIL-STD-870 C CHANGE-1 CADMIUM PLATING LOW EMBRITTLEMENT,” 2009.

[61] H. Begg, M. Riley, and H. de V. Lovelock, “Mechanization of the Grit Blasting Process for Thermal Spray Coating Applications: A Parameter Study,” *J. Therm. Spray Technol.*, vol. 25, no. 1–2, pp. 12–20, 2016.

[62] J. Day, X. Huang, and N. L. Richards, “Examination of a grit-blasting process for thermal spraying using statistical methods,” *J. Therm. Spray Technol.*, vol. 14, no. 4, pp. 471–479, 2005.

[63] J. A. E. Jr and N. S. E. Jr, “A Study of the Effect of Normal Stiffness on Kinetic Friction Forces Between Two Bodies in Sliding Contact,” *E Trans.*, vol. 12, no. 4, pp. 234–241, 1969.

[64] N. P. Suh and H.-C. Sin, “The genesis of friction,” *Wear*, vol. 69, no. 1, pp. 91–114, 1981.

[65] T. H. C. Childs, “The sliding wear mechanisms of metals, mainly steels,” *Tribol. Int.*, vol. 13, no. 6, pp. 285–293, 1980.

[66] D. Klaffke, “Influence of Normal Force and Humidity on the Friction and Wear of Unlubricated Reciprocating Sliding Steel/Steel Couples,” *Tribotest*, vol. 10, no. 4, pp. 311–325, 2004.

[67] A. P. Mercer and I. M. Hutchings, “The influence of atmospheric humidity on the abrasive wear of metals,” *Wear*, vol. 103, no. 3, pp. 205–215, 1985.

[68] M. A. Chowdhury and M. M. Helali, “The effect of frequency of vibration and humidity on the coefficient of friction,” *Tribol. Int.*, vol. 39, no. 9, pp. 958–962, 2006.

[69] S. Jahanmir, N. P. Suh, and E. P. Abrahamson II, “The delamination theory of wear and the wear of a composite surface,” *Wear*, vol. 32, no. 1, pp. 33–49, 1975.

[70] O. Ruggeri, G. Sambogna, C. P. Balboni, and G. A. Volpato, “Dry lubrication with soft metals: The tribological behaviour of a thin film of cadmium rubbing on carbon steel,” *Wear*, vol. 59, no. 2, pp. 433–446, 1980.

[71] V. Stepina and V. Vesely, *Lubricants and Special Fluids*. Elsevier, 1992.

[72] K. R. Sriraman, H. W. Strauss, S. Brahimi, R. R. Chromik, J. A. Szpunar, J. H. Osborne and S. Yue, “Tribological behavior of electrodeposited Zn, Zn–Ni, Cd and Cd–Ti coatings on low carbon steel substrates,” *Tribol. Int.*, vol. 56, pp. 107–120, 2012.

[73] H. J. Kim, W. Windl, and D. Rigney, “Structure and chemical analysis of aluminum wear debris: Experiments and ab initio simulations,” *Acta Mater.*, vol. 55, no. 19, pp. 6489–6498, 2007.

[74] D. Figueroa and M. J. Robinson, “The effects of sacrificial coatings on hydrogen embrittlement and re-embrittlement of ultra high strength steels,” *Corros. Sci.*, vol. 50, no. 4, pp. 1066–1079, 2008.

[75] K. G. Watkins, R. D. Jones, and K. M. Lo, “Electrochemical investigation of the corrosion rate of sacrificial coatings on steel,” *Mater. Lett.*, vol. 8, no. 1, pp. 21–25, 1989.

[76] M. Kwon, D. Jo, S. H. Cho, H. T. Kim, J.-T. Park, and J. M. Park, “Characterization of the influence of Ni content on the corrosion resistance of electrodeposited Zn–Ni alloy coatings,” *Surf. Coat. Technol.*, vol. 288, no. Supplement C, pp. 163–170, 2016.

[77] A. Tozar and İ. H. Karahan, “Structural and corrosion protection properties of electrochemically deposited nano-sized Zn–Ni alloy coatings,” *Appl. Surf. Sci.*, vol. 318, no. Supplement C, pp. 15–23, 2014.

[78] S. Ghaziof and W. Gao, “The effect of pulse electroplating on Zn–Ni alloy and Zn–Ni–Al2O3 composite coatings,” *J. Alloys Compd.*, vol. 622, no. Supplement C, pp. 918–924, 2015.

[79] Z. Feng, Q. Li, J. Zhang, P. Yang, and M. An, “Studies on the enhanced properties of nanocrystalline Zn–Ni coatings from a new alkaline bath due to electrolyte additives,” *RSC Adv.*, vol. 5, no. 72, pp. 58199–58210, 2015.

[80] S. Ghaziof and W. Gao, “Electrodeposition of single gamma phased Zn–Ni alloy coatings from additive-free acidic bath,” *Appl. Surf. Sci.*, vol. 311, no. Supplement C, pp. 635–642, 2014.

[81] M. Tafreshi, S. R. Allahkaram, and H. Farhangi, “Comparative study on structure, corrosion properties and tribological behavior of pure Zn and different Zn-Ni alloy coatings,” *Mater. Chem. Phys.*, vol. 183, no. Supplement C, pp. 263–272, 2016.

[82] C. N. Panagopoulos, K. G. Georgarakis, and P. E. Agathocleous, “Sliding wear behaviour of Zinc–Nickel alloy electrodeposits,” *Tribol. Int.*, vol. 36, no. 8, pp. 619–623, 2003.

[83] K. R. Sriraman, S. Brahimi, J. A. Szpunar, and S. Yue, “Hydrogen embrittlement of Zn-, Zn–Ni-, and Cd-coated high strength steel,” *J. Appl. Electrochem.*, vol. 43, no. 4, pp. 441–451, 2013.

[84] V. Lee Holmes and M. Bridger, "Aluminum coatings turn green: IVD process delivers environmentally friendly corrosion protection," *Met. Finish.*, vol. 102, no. 12, pp. 6–10, 2004.

[85] S. Grainger and J. Blunt, *Engineering Coatings: Design and Application*. Woodhead Publishing, 1998.

[86] K. H. and A. Matthews, Ed., "Chapter 2 Surface Coating Methods," in *Tribology Series*, vol. 28, Elsevier, 1994, pp. 7–32.

[87] A. N. Kumar, R. Srinivasu, and J. B. Rao, "Dry Sliding Wear Behavior of Pure Aluminium and Al-Cu Alloys," in *Advanced Tribology*, Springer, Berlin, Heidelberg, 2009, pp. 422–425.

[88] K. Edalati, M. Ashida, Z. Horita, T. Matsui, and H. Kato, "Wear resistance and tribological features of pure aluminum and Al–Al_2O_3 composites consolidated by high-pressure torsion," *Wear*, vol. 310, no. 1–2, pp. 83–89, 2014.

[89] M. Antler, "Processes of metal transfer and wear," *Wear*, vol. 7, no. 2, pp. 181–203, 1964.

[90] S. M. Kuo and D. A. Rigney, "Sliding behavior of aluminum," *Mater. Sci. Eng. A*, vol. 157, no. 2, pp. 131–143, 1992.

[91] C. T. Wang, N. Gao, R. J. K. Wood, and T. G. Langdon, "Wear behavior of an aluminum alloy processed by equal-channel angular pressing," *J. Mater. Sci.*, vol. 46, no. 1, pp. 123–130, 2011.

[92] C. T. Wang, N. Gao, R. J. K. Wood, and T. G. Langdon, "Wear behaviour of Al-1050 alloy processed by severe plastic deformation," *Mater. Sci. Forum*, vol. 667–669, pp. 1101–1106, 2011.

[93] M. Eizadjou, H. D. Manesh, and K. Janghorban, "Microstructure and mechanical properties of ultra-fine grains (UFGs) aluminum strips produced by ARB process," *J. Alloys Compd.*, vol. 474, no. 1–2, pp. 406–415, 2009.

[94] K. Lepper, M. James, J. Chashechkina, and D. A. Rigney, "Sliding behavior of selected aluminum alloys," *Wear*, vol. 203, pp. 46–56, 1997.

[95] H. J. Kim, S. Karthikeyan, and D. Rigney, "The structure and composition of aluminum wear debris generated by unlubricated sliding in different environments," *Wear*, vol. 263, no. 1–6, pp. 849–857, 2007.

[96] N. P. Suh, "The delamination theory of wear," *Wear*, vol. 25, no. 1, pp. 111–124, 1973.

[97] K. Endo and H. Goto, "Effects of environment on fretting fatigue," *Wear*, vol. 48, no. 2, pp. 347–367, 1978.

[98] "MIL-STD-1501 F E CHROMIUM PLATING LOW EMBRITTLEMENT," 2011.

[99] "MIL-DTL-83488 D COATING ALUMINUM HIGH PURITY," 1999.

[100] "MIL-DTL-5541 F CHEMICAL CONVERSION COATINGS ON ALUMINUM," 2006.

[101] T. E. G. Daenen and S. A. Stolk, "Electrolyte-liquid for the electrodeposition of aluminum," US4145261 A, 1979.

[102] S. Birkle and J. Gehring, "Electroplating apparatus particularly for electro-deposition of aluminum," US4759831 A, 1988.

[103] S. Birkle and K. Stoger, "Electrolyte for the electrodeposition of aluminum," US4417954 A, 1983.

[104] A. I. IAkushev, *Effect of manufacturing technology and basic thread parameters on the strength of threaded connexions*. Macmillan, 1964.

[105] I. A. Birger, "Distribution of load in a screw thread," *Bull. Mach. Engineeirng*, vol. 24, pp. 7–12, 1944.

[106] R. C. Weast, *CRC handbook of chemistry and physics: a ready-reference book of chemical and physical data*. Boca Raton, Fla.: CRC Press, 1986.

[107] M. Bauccio and American Society for Metals, *ASM metals reference book*. Materials Park, Ohio: ASM International, 1993.

[108] *Hysitron TI 950 Triboindenter User Manual Revision 9.3.0314*. Minneapolis USA.

[109] A. C. Fischer-Cripps, "Nanoindentation Testing," in *Nanoindentation*, Springer New York, 2011, pp. 21–37.

[110] W. C. Oliver and G. M. Pharr, "An improved technique for determining hardness and elastic modulus using load and displacement sensing indentation experiments," *J. Mater. Res.*, vol. 7, no. 06, pp. 1564–1583, 1992.

[111] A. C. Fischer-Cripps, "Analysis of Nanoindentation Test Data," in *Nanoindentation*, Springer New York, 2011, pp. 39–75.

[112] "ISO 25178-2:2012 - Geometrical product specifications (GPS) -- Surface texture: Areal -- Part 2: Terms, definitions and surface texture parameters.".

[113] A. W. Momber and Y. C. Wong, "Overblasting effects on surface properties of low-carbon steel," *J. Coat. Technol. Res.*, vol. 2, no. 6, pp. 453–461, 2005.

[114] M. Mellali, A. Grimaud, A. C. Leger, P. Fauchais, and J. Lu, "Alumina grit blasting parameters for surface preparation in the plasma spraying operation," *J. Therm. Spray Technol.*, vol. 6, no. 2, pp. 217–227, 1997.

[115] J. A. Greenwood and J. B. P. Williamson, "Contact of Nominally Flat Surfaces," *Proc. R. Soc. Lond. Math. Phys. Eng. Sci.*, vol. 295, no. 1442, pp. 300–319, 1966.

[116] D. H. Buckley, *Surface effects in adhesion, friction, wear, and lubrication*. Elsevier, 1981.

[117] K. Holmberg, "A concept for friction mechanisms of coated surfaces," *Surf. Coat. Technol.*, vol. 56, no. 1, pp. 1–10, 1992.

[118] P. J. Blau, "Mechanisms for transitional friction and wear behavior of sliding metals," *Wear*, vol. 72, no. 1, pp. 55–66, 1981.

[119] S. Korres and M. Dienwiebel, "Design and construction of a novel tribometer with online topography and wear measurement," *Rev. Sci. Instrum.*, vol. 81, no. 6, p. 063904, 2010.

[120] P. Stoyanov, J. M. Shockley, M. Dienwiebel, and R. R. Chromik, "Combining in situ and online approaches to monitor interfacial processes in lubricated sliding contacts," *MRS Commun.*, pp. 1–8, 2016.

[121] K. J. Wahl, D. N. Dunn, and I. L. Singer, "Wear behavior of Pb–Mo–S solid lubricating coatings," *Wear*, vol. 230, no. 2, pp. 175–183, 1999.

[122] K. R. Sriraman, P. Manimunda, R. R. Chromik, and S. Yue, "Effect of crystallographic orientation on the tribological behavior of electrodeposited Zn coatings," *RSC Adv.*, vol. 6, no. 21, pp. 17360–17372, 2016.

[123] J. M. Shockley, S. Descartes, P. Vo, E. Irissou, and R. R. Chromik, "The influence of Al2O3 particle morphology on the coating formation and dry sliding wear behavior of cold sprayed Al–Al_2O_3 composites," *Surf. Coat. Technol.*, vol. 270, pp. 324–333, 2015.

[124] Y. Zhang, J. M. Shockley, P. Vo, and R. R. Chromik, "Tribological Behavior of a Cold-Sprayed Cu–MoS_2 Composite Coating During Dry Sliding Wear," *Tribol. Lett.*, vol. 62, no. 1, p. 9, 2016.

[125] Y. Zhang, N. Brodusch, J. Michael Shockley, R. Gauvin, and R. R. Chromik, "Sliding-induced Microstructure of Cold-Sprayed Copper Coating Observed by Electron Channeling Contrast Imaging," *Microsc. Microanal.*, vol. 20, no. Supplement S3, pp. 2104–2105, 2014.

[126] A. Birkett and J. K. Lancaster, "Counterface effects on the wear of a composite dry-bearing liner," *Wear*, vol. 110, no. 3–4, pp. 345–357, 1986.

[127] R. Ramadoss, N. Kumar, R. Pandian, S. Dash, T. R. Ravindran, D. Arivuoli and A. K. Tyagi, "Tribological properties and deformation mechanism of TiAlN coating sliding with various counterbodies," *Tribol. Int.*, vol. 66, pp. 143–149, 2013.

[128] M. Cocks, "Interaction of Sliding Metal Surfaces," *J. Appl. Phys.*, vol. 33, no. 7, pp. 2152–2161, 1962.

[129] M. Antler, "Wear, Friction, and Electrical Noise Phenomena in Severe Sliding Systems," *E Trans.*, vol. 5, no. 2, pp. 297–307, Jan. 1962.

[130] Z. Rymuza, Ed., "3. Lubricants," in *Tribology Series*, vol. 13, Elsevier, 1989, pp. 33–72.

[131] L. Lee, É. Régis, S. Descartes, and R. R. Chromik, "Fretting wear behavior of Zn–Ni alloy coatings," *Wear*, vol. 330–331, pp. 112–121, 2015.

[132] P. Stoyanov, R. R. Chromik, D. Goldbaum, J. R. Lince, and X. Zhang, "Microtribological Performance of Au–MoS2 and Ti–MoS2 Coatings with Varying Contact Pressure," *Tribol. Lett.*, vol. 40, no. 1, pp. 199–211, 2010.

[133] H. A. N and H. L. C, "Solid lubricant film resistant to corrosion," US3051586 A, 28-Aug-1962.

[134] P. Stoyanov, R. R. Chromik, S. Gupta, and J. R. Lince, "Micro-scale sliding contacts on Au and Au-MoS_2 coatings," *Surf. Coat. Technol.*, vol. 205, no. 5, pp. 1449–1454, 2010.

[135] D. Klaffke, "On the repeatability of friction and wear results and on the influence of humidity in oscillating sliding tests of steel-steel pairings," *Wear*, vol. 189, no. 1, pp. 117–121, 1995.

[136] J. Larsen-Basse, "Influence of atmospheric humidity on abrasive wear—i. 3-body abrasion," *Wear*, vol. 31, no. 2, pp. 373–379, 1975.

[137] J. Larsen-Basse and S. S. Sokoloski, "Influence of atmospheric humidity on abrasive wear — II. 2-body abrasion," *Wear*, vol. 32, no. 1, pp. 9–14, Mar. 1975.

[138] F. P. Bowden and D. Tabor, *The Friction and Lubrication of Solids*. Clarendon Press, 2001.

[139] J. K. Lancaster, "A review of the influence of environmental humidity and water on friction, lubrication and wear," *Tribol. Int.*, vol. 23, no. 6, pp. 371–389, 1990.

[140] P. D. Cuong, H.-S. Ahn, E.-S. Yoon, and K.-H. Shin, "Effects of relative humidity on tribological properties of boron carbide coating against steel," *Surf. Coat. Technol.*, vol. 201, no. 7, pp. 4230–4235, 2006.

[141] D. Tabor, *The Hardness of Metals*. OUP Oxford, 2000.

[142] I. L. Singer, "Solid Lubrication Processes," in *Fundamentals of Friction: Macroscopic and Microscopic Processes*, I. L. Singer and H. M. Pollock, Eds. Springer Netherlands, 1992, pp. 237–261.

[143] P. J. Blau, *Friction Science and Technology: From Concepts to Applications, Second Edition*. CRC Press, 2008.

[144] B. Gu, J. Schmitt, Z. Chen, L. Liang, and J. F. McCarthy, "Adsorption and desorption of natural organic matter on iron oxide: Mechanisms and models," *Environ. Sci. Technol.*, vol. 28, no. 1, pp. 38–46, 1994.

[145] D. L. A. de Faria, S. Venâncio Silva, and M. T. de Oliveira, "Raman microspectroscopy of some iron oxides and oxyhydroxides," *J. Raman Spectrosc.*, vol. 28, no. 11, pp. 873–878, 1997.

[146] M. Esteves, A. Ramalho, and F. Ramos, “Fretting behavior of the AISI 304 stainless steel under different atmosphere environments,” *Tribol. Int.*, vol. 88, pp. 56–65, 2015.

[147] B. Navinšek, P. Panjan, and I. Milošev, “PVD coatings as an environmentally clean alternative to electroplating and electroless processes,” *Surf. Coat. Technol.*, vol. 116–119, pp. 476–487, 1999.

[148] M. P. Waalkes, “Cadmium carcinogenesis in review,” *J. Inorg. Biochem.*, vol. 79, no. 1–4, pp. 241–244, 2000.

[149] K. R. Sriraman, S. Brahimi, J. A. Szpunar, J. H. Osborne, and S. Yue, “Characterization of corrosion resistance of electrodeposited Zn–Ni Zn and Cd coatings,” *Electrochimica Acta*, vol. 105, pp. 314–323, 2013.

[150] L. Lee, P. Behera, K. R. Sriraman, and R. R. Chromik, “Effects of humidity on the sliding wear properties of Zn–Ni alloy coatings,” *RSC Adv.*, vol. 7, no. 37, pp. 22662–22671, 2017.

[151] R. Takagi and T. Liu, “Lubrication of Bearing Steels with Electroplated Gold under Heavy Loads,” *E Trans.*, vol. 11, no. 1, pp. 64–71, 1968.

[152] M. Antler, “The Wear of Electrodeposited Gold,” *E Trans.*, vol. 11, no. 3, pp. 248–260, 1968.

[153] E. Rabinowicz, “Variation of Friction and Wear of Solid Lubricant Films with Film Thickness,” *E Trans.*, vol. 10, no. 1, pp. 1–9, 1967.

[154] “ASTM International - G99-05(2010) Standard Test Method for Wear Testing with a Pin-on-Disk Apparatus.”.

[155] M. Antler, “Stages in the Wear of a Prow-Forming Metal,” *E Trans.*, vol. 13, no. 2, pp. 79–86, 1970.